The Insulin-like Growth Factor 2 (*IGF2*) mRNA Binding Protein p62/IGF2BP2-2 Amplifies Steatosis, Inflammation, and Fibrosis in Murine Non-Alcoholic Steatohepatitis (NASH)

Dissertation

zur Erlangung des Grades

des Doktors der Naturwissenschaften

der Naturwissenschaftlich-Technischen Fakultät III

Chemie, Pharmazie, Bio- und Werkstoffwissenschaften

der Universität des Saarlandes

von

Yvette Simon

Saarbrücken

Oktober 2013

Tag des Kolloquiums: 06. Dezember 2013

Dekan: Prof. Dr. V. Helms

1. Berichterstatter: Prof. Dr. Alexandra K. Kiemer

2. Berichterstatter: Assoz. Prof. Dr. Dr. Johannes Haybäck

Vorsitz: Prof. Dr. Claus-Michael Lehr

Akad. Mitarbeiter: Dr. Matthias Engel

CONTENTS

Abbreviations

[v/v]	volume per volume
[w/v]	weight per volume
µ	micro (10^{-6})
A	ampere
Actb	beta-actin
Akt	v-akt murine thymoma viral oncogene homolog
ALT	alanine aminotransferase
amp	ampicillin
ANOVA	analysis of variance
AP-1	activator protein-1
APS	ammonium persulfate
AST	aspartate aminotransferase
BHQ	black hole quencher
bp	base pair
BSA	bovine serum albumin
c	concentration
Ccl2	chemokine (C-C motif) ligand 2
cDNA	complementary DNA
Chrebp	carbohydrate responsive element binding protein
clo	clodronate liposomes
CoA	coenzyme A
Col1a1	collagen type I alpha 1
Cox	cyclooxygenase
Cpt	carnitine palmitoyltransferase
Ctgf	connective tissue growth factor
ctrl	control
CV	central vein
CYP2E1	cytochrom P450 family 2 subfamily E polypeptide 1
DAPI	4′,6-diamidine-2-phenylindol
DEN	diethylnitrosamine
DEPC	diethyl pyrocarbonate
d	deci (10^{-1})
DNA	desoxyribonucleic acid
dNTP	deoxynucleosid-triphosphate
doxy	doxycycline
E. coli	*Escherichia coli*
EDTA	ethylenediamine-N,N,N,N´-tetraacetic acid
Elovl6	ELOVL fatty acid elongase 6
Emr1	egf-like module containing, mucin-like, hormone receptor-like 1 (F4/80)
ERK	extracellular-activated kinase
FAM	6-carboxy-fluorescein
FAME	fatty acid methyl ester
Fasn	fatty acid synthase
FCS	fetal calf serum
g	gram
G6pc	glucose-6-phosphatase, catalytic subunit
GC-MS	gas chromatography - mass spectrometry
GWA	genome-wide association
H_2O	water
Hamp	hepcidin antimicrobial peptide

HBV	hepatitis B virus
HCC	hepatocellular carcinoma
HCV	hepatitis C virus
HDL	high density lipoprotein
HE	hematoxylin and eosin
Hmgcr	3-hydroxy-3-methylglutaryl-CoA reductase
HPC	hepatic progenitor cells
HSC	hepatic stellate cells
IF	immunofluorescence
IGF2	insulin-like growth factor 2
IGF2BP	insulin-like growth factor 2 mRNA binding protein
IHC	immunohistochemistry
IkB	inhibitor of kappa light polypeptide gene enhancer in B-cells
IKK	inhibitor of kappa light polypeptide gene enhancer in B-cells kinase complex
Il1b	interleukin 1 beta
Il6	interleukin 6
IMP	insulin-like growth factor 2 mRNA binding protein
ip	intraperitoneal
JNK	mitogen-activated protein kinase
k	kilo (10^3)
KC	Kupffer cell
KH	hnRNP K homology
Koc	KH domain-containing protein overexpressed in cancer
LAP	liver enriched activator protein
LB	lysogeny broth
l	litre
m	milli (10^{-3})
M	molar
MCD	methionine/choline deficient diet
Mcp1	monocyte chemoattractant protein-1
MDA	malondialdehyde
µ	micro (10^{-6})
min	minute
Mlxipl	MLX interacting protein-like (Chrebp)
mmHg	unit millimeter of mercury
MP	milk powder
mRNA	messenger RNA
mRNP	ribonucleoprotein complex
mTOR	mechanistic target of rapamycin (serine / threonine kinase)
MUFA	monounsaturated fatty acids
MW	molecular weight
n	nano (10^{-9})
NAFLD	non-alcoholic fatty liver diseases
NASH	non-alcoholic steatohepatitis
Nfkb	nuclear factor of kappa light polypeptide gene enhancer in B-cells
Nlrp3	NLR family, pyrin domain containing 3
Nos2	nitiric oxide synthase 2, inducible
OD	optical density
p	pico (10^{-12})

PAGE	polyacrylamide gel electrophoresis
PBS	phosphate buffered saline
PC	phosphatidylcholine
PCR	polymerase chain reaction
PE	phosphatidyl-ethanolamine
PI3-K	phosphatidylinositol 3-kinase
Pipa	peptidylprolyl isomerase A (cyclophilin A)
Ppara	peroxisome proliferator-activated receptor alpha
PT	portal triad
PTEN	phosphatase and tensin homolog
Ptgs2	prostaglandin-endoperoxidase 2 (Cox)
PUFA	polyunsaturated fatty acids
PVDF	polyvinylidene fluoride
Pycard	PYD and CARD domain containing (Asc)
Raf	v-raf murine leukemia viral onocogene homolog
Ras	rat sarcoma
RBB	Rockland Blocking Buffer
RNA	ribonucleic acid
ROS	reactive oxygen species
RRM	RNA recognition motif
RT	reverse transcriptase
RT	room temperature
s	second
Scd1	stearoyl-CoA desaturase
SDS	sodium dodecyl sulfate
SEM	standard error of mean
SFA	saturated fatty acids
Socs	supressor of cytokine signaling
sham	PBS liposomes
Srebf	sterol regulatory element binding transcription factor
TAA	tumor-associated antigen
TBARS	thiobarbituric acid reactive substances
TBE	Tris-boric acid-EDTA buffer
TE	Tris-EDTA buffer
tetO	operator sequences
Tfrc	transferrin receptor (p90, CD71)
tg	transgene
TG	triglycerides
Tgfb1	transforming growth factor, beta 1
Tnf	tumor necrosis factor
Tnfsf12	tumor necrosis factor (ligand) superfamily, member 12 (Tweak)
TRE-CMV_{min}	transrepressive responsive element cytomegaly virus
Tris	α, α, α-tris-(hydroxymethyl)-methylamine
tTA	tetracycline-controlled transactivator
U	unit
UV	ultra violet
V	volt
VLDL	very low density lipoprotein
Wnt	wingless-type MMTV integration site family
x g	fold gravitational fold

Abstract

The insulin-like growth factor 2 mRNA binding protein p62/IGF2BP2-2 is overexpressed in human cirrhotic nodules and in up to two thirds of hepatocellular carcinoma (HCC) tissue. Liver-specific overexpression of p62 induces steatosis. Aim of this study was to investigate the pathophysiological role of p62 in non-alcoholic steatohepatitis (NASH) and NASH-induced liver fibrosis.

MCD-induced steatosis was more pronounced in transgenic compared to wild-type animals and characterized by elevated levels of monounsaturated fatty acids and free cholesterol. p62 induced the expression of lipogenic regulators, most likely *via* elevated iron deposition. Despite no effect of p62 overexpression on transaminase levels, transgenic mice exhibited an aggravated inflammatory response as indicated by elevated leukocyte recruitment and lipid peroxidation. Also the activation of NFKB and the gene expression of its inflammatory downstream target cytokines were increased in hepatocytes of transgenic animals. We also observed an elevated activation of the inflammasome. Fibrosis development was accelerated with increased *procollagen 1* mRNA expression and confirmed by histological analyses. A TGF-beta-independent upregulation of collagen 1 is suggested due to upregulated *Ctgf* mRNA and serum IL-13. Most notably, a pronounced ductular reaction was observed in transgenic animals.

In summary, our data provide evidence that p62 acts as an active promotor in the progression of NASH and fibrosis.

Zusammenfassung

Die Expression des *IGF2* mRNA bindenden Proteins p62/IGF2BP2-2 ist in menschlichen Leberzirrhosen und -tumoren erhöht. Die Überexpression von p62 in Mäuselebern induziert eine Steatose. Ziel dieser Studie war es, die pathophysiologische Rolle von p62 in der nicht-alkoholischen Steatohepatitis und der dadurch induzierten Fibrose zu untersuchen.

In *p62* transgenen Tieren war die durch eine MCD-Diät induzierte Fettleber stärker ausgeprägt als im Wildtyp und durch erhöhte Spiegel einfach ungesättigter Fettsäuren und freiem Cholesterin gekennzeichnet. p62 induzierte die Genexpression lipogener Regulatoren, die im Zusammenhang mit einer erhöhten Eisen-Akkumulation steht. Obwohl keine erhöhten Leberwerte in den Transgenen gemessen wurden, zeigten diese eine verstärkte Entzündungsreaktion. Dies wurde durch eine gesteigerte Lipidperoxidation sowie eine lobuläre Entzündung bestätigt. Zudem wurde eine Aktivierung des Transkriptionsfaktors NFKB, die verstärkte Expression seiner Targetgene sowie eine Aktivierung des Inflammasoms beobachtet. Histologische Untersuchungen belegten die beschleunigte Entwicklung einer Fibrose. Hier ist aufgrund erhöhter *Ctgf* mRNA und IL-13 Spiegel von einer TGF-beta-unabhängigen Erhöhung der Kollagen-Produktion auszugehen. Besonders festzuhalten ist eine verstärkte duktuläre Reaktion in den *p62* transgenen Tieren.

Zusammenfassend zeigen diese Daten, dass p62 als aktiver Promotor in der Progression der Fettleberentzündung und der dadurch induzierten Fibrose agiert.

Für Mama

„Pleasure in the job

puts perfection in the work”

Aristotle

1 INTRODUCTION

1.1 **Non-Alcoholic Fatty Liver Disease (NAFLD)**

33 years ago Ludwig and colleagues described non-alcoholic steatohepatitis (NASH) in individuals whose liver biopsies showed findings similar to alcoholic hepatitis in the absence of significant alcohol intake (Ludwig et al., 1980). The broad term non-alcoholic fatty liver disease (NAFLD) has been adopted to cover the full spectrum of metabolic fatty liver disorders (Angulo, 2002). NAFLD encompasses a spectrum of conditions from simple steatosis to steatohepatitis, advanced fibrosis, and cirrhosis (Angulo, 2002). In addition, evidence suggests NASH as a reason for a large proportion of “cryptogenic” cirrhosis (cirrhosis without known origin) due to the fact that typical histological findings of NASH may be lost in the progression from NASH to cirrhosis (Bugianesi, 2007; Caldwell et al., 1999; Hashimoto & Tokushige, 2012; Powell et al., 1990; Struben et al., 2000; Van Der Poorten et al., 2012). Furthermore, NAFLD may progress to end-stage liver diseases such as hepatocellular carcinoma (HCC) or liver failure (Starley et al., 2010) (**Figure 1-1**).

For the general population in Western countries the prevalence of NAFLD was estimated as 6-33% with a median of 20% (Angulo, 2002; Vernon et al., 2011) and 2-12% for NASH (Bedogni et al., 2005; Neuschwander-Tetri & Caldwell, 2003; Vernon et al., 2011). The prevalence among obese patients (with BMI >30 kg/m^2) is referred to 70-95% for steatosis, 9-30% for NASH, and 7-16% for cirrhosis (Clark, 2006). A study about indications for liver transplantation in the United States revealed NASH as the third most common indication behind hepatitis C and alcoholic liver disease. Most importantly, it is the only indication with rising incidence (Charlton et al., 2011).

Many studies highlighted the association of features of the metabolic syndrome with NAFLD, some of them proposing NAFLD as hepatic manifestation of the metabolic syndrome (Gaggini et al., 2013). The metabolic syndrome is characterized by obesity (BMI >30 kg/m^2), hyperinsulinemia, peripheral insulin resistance, diabetes, hypertriglyceridemia (>150 mg/dL), and hypertension (systolic blood pressure >130 mmHg), from which three or more features need to be present (Marchesini et al., 2003; Milić & Stimac, 2012).

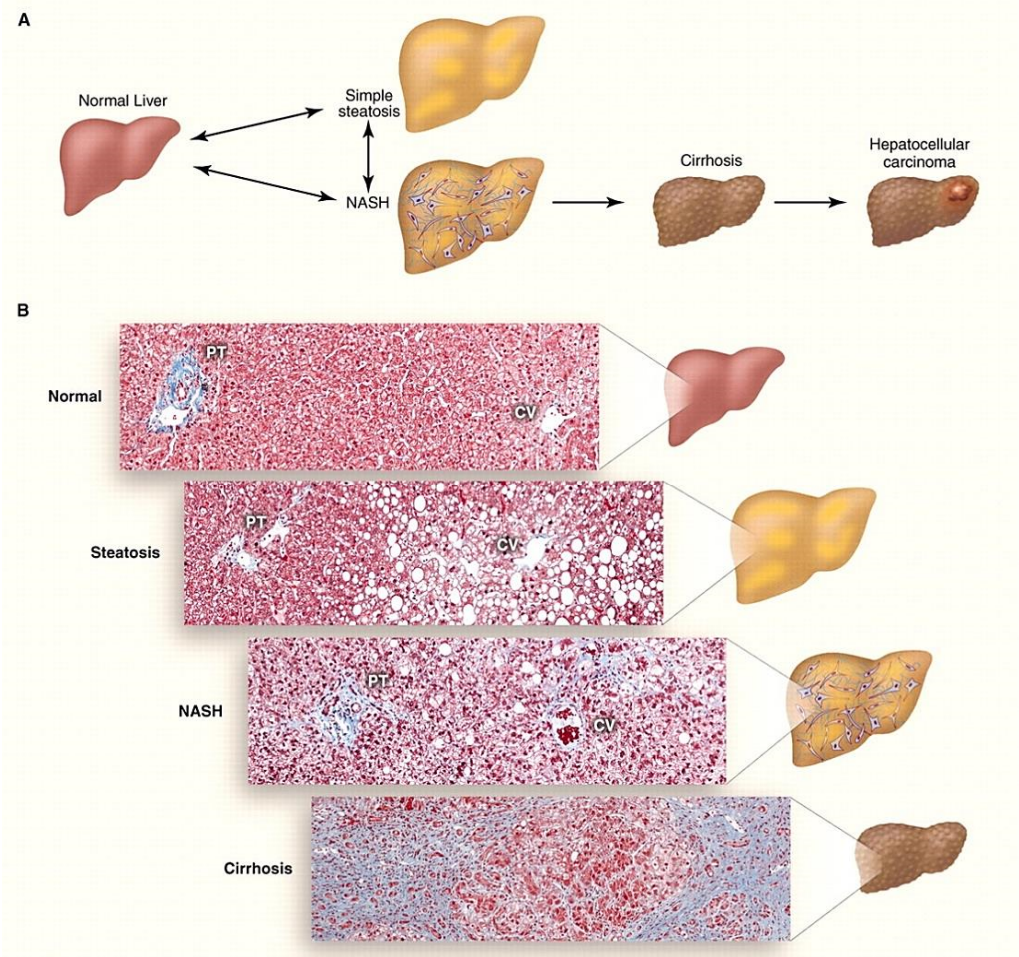

Figure 1-1: Spectrum of non-alcoholic fatty liver disease. (**A**) Progression of NAFLD. Triglycerides accumulation within lipid droplets in hepatocytes causes steatosis. Steatosis associated with inflammation leads to NASH, which can then progress to fibrosis and cirrhosis. Patients with cirrhosis have an increased risk to develop hepatocellular carcinoma. (**B**) Histological sections from normal liver, steatosis, NASH, and cirrhosis. Collagen fibers are stained blue with Massons´s trichrome stain. PT portal triad; CV central vein (Cohen et al., 2011).

Nevertheless, NAFLD/NASH is also diagnosed in patients without obesity or symptoms of the metabolic syndrome and was recently demonstrated as an independent manifestation of the metabolic syndrome (Smits, 2013). In this context, a recently published review suggested to reconsider the spectrum of NAFLD into simple steatosis and NASH as two independent conditions (Yilmaz, 2012).

However, the pathogenesis of NAFLD and in particular NASH was proposed in 1998 as so-called “two-hit” model (Day & James, 1998). Steatosis as first hit sensitizes the liver to the second hit, which leads to hepatocyte injury, inflammation, and subsequent fibrotic changes (Day, 2002; Day & James, 1998).

1.1.1 **Steatosis**

Steatosis without inflammatory changes is a very slow progressing disease. Several longitudinal studies have shown that patients with benign steatosis have a low risk for the development of more severe diseases (Dam-Larsen et al., 2004; Teli et al., 1995). Steatosis is defined as macrovesicular steatosis in more than 5% of hepatocytes in the absence of significant inflammation or fibrosis (Kleiner et al., 2005). Disruption of the normal mechanisms for synthesis, transport, and removal of fatty acids and triglycerides are the basis for the development of steatosis (Anstee & Goldin, 2006). In particular, fat accumulates within hepatocytes when the rate of import or fatty acid synthesis exceeds their degradation or export (Koteish & Diehl, 2001). The rate of fatty acid uptake can be increased due to excess dietary intake or release from adipose tissue (Day, 2002), whereas increased *de novo* hepatic fatty acid and triglyceride synthesis is due to impaired glucose and insulin sensitivity (Anstee & Goldin, 2006).

De novo lipogenesis is regulated by insulin and glucose through activation of the transcription factors sterol regulatory element binding transcription factor SREBF1 and carbohydrate responsive element binding protein (CHREBP), respectively (Cohen et al., 2011) (**Figure 1-2**). Either activation leads to the upregulation of lipogenic genes, whereby SREBF1 is activated by insulin and CHREBP by glucose (Cohen et al., 2011; Kawano & Cohen, 2013). Upon activation of *de novo* lipogenesis the following steps proceed: the first building block of lipogenesis is acetyl-CoA, which is catalyzed from glucose and then further converted to malonyl-CoA. Palmitic acid (C16) is generated by fatty acid synthase (FASN) through assembling of acetyl-CoA with 7 malonyl-CoAs. The long chain fatty acid elongase (ELOVL) 6 elongates and stearoyl-CoA desaturase (SCD) 1 desaturates saturated fatty acids as palmitic acid to form monounsaturated fatty acids, the major components of triglycerides (Kawano & Cohen, 2013).

Hepatic triglycerides are exported into the blood as very low-density lipoproteins (VLDL). Failure of VLDL synthesis is responsible for decreased fat elimination and is a cause of hepatic steatosis (Anstee & Goldin, 2006). In addition to export, hepatic triglyceride levels are controlled by mitochondrial and peroxisomal β-oxidation or microsomal ω-oxidation in hepatocytes. The activity of the carnitine

palmitoyltransferase (CPT) 1a, which is located in the outer mitochondrial membrane, is critical for the mitochondrial β-oxidation. CPT1a is responsible for the translocation of long-chain fatty acids across the mitochondrial membrane, and its activation provides substrates for the subsequent β-oxidation (Eaton et al., 1996). Increased levels of glucose as in the postprandial state lead to suppression of β-oxidation due to formation of Malonyl-CoA as inhibitor of CPT1a during lipogenesis (Sidossis et al., 1996). Another important mediator in catabolism is the transcription factor peroxisome proliferator-activated receptor (PPAR) alpha. PPARA regulates a range of genes related to fatty acid oxidation in mitochondria, peroxisomes, and microsomes (Fruchart, 2009) (**Figure 1-2**). Beside the regulation of lipid homeostasis, PPARA is further involved in a wide array of pathways, such as inflammation or gluconeogenesis, through regulation of different target genes or its regulation by other genes (Mandard et al., 2004). Impairment of mitochondrial activity is suggested to be the source for oxidative stress within the liver and to contribute to the progression towards NASH (Kawano & Cohen, 2013).

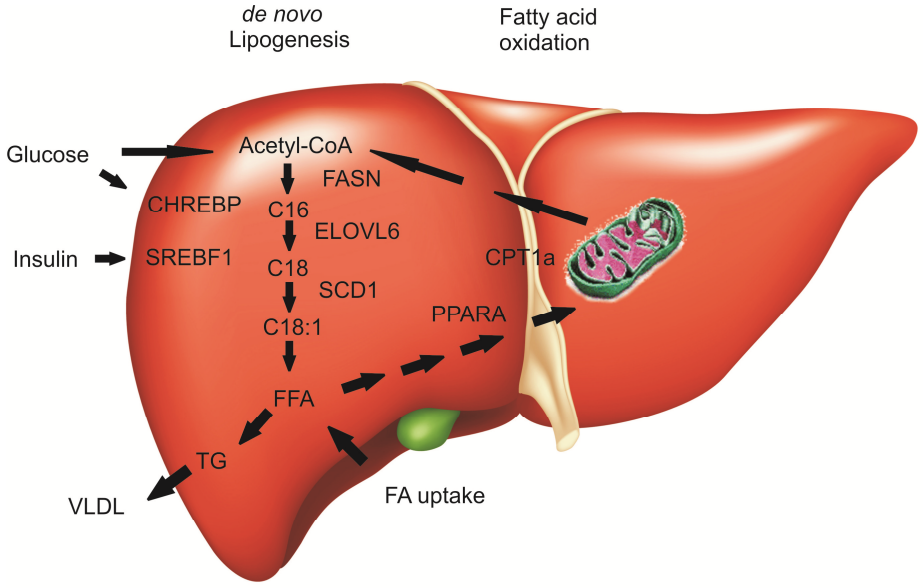

Figure 1-2: Hepatic fatty acid metabolism. Free fatty acids (FFA) can either be taken up by the liver or synthesized in response to insulin or glucose *via* the transcriptional regulation of SREBF1 and CHREBP. FFA can then be metabolized by β-oxidation in the mitochondria, esterified, and stored as triglycerides in lipid droplets, or packed and secreted as VLDL into the blood stream (adapted from (Cohen et al., 2011)).

1.1.2 **Inflammation**

The fatty liver is predisposed to the “second-hit”, which can involve oxidative stress (Farrell & Larter, 2006). Impaired mitochondrial β-oxidation is a hallmark for reactive oxygen species (ROS)-formation (Pessayre et al., 2001). In addition, excessive iron accumulation in the liver of NASH patients is recognized as further source for ROS. Thereby, the underlying reaction is the formation of hydroxyl radicals by ferrous iron (Fe^{2+}) in the presence of hydrogen peroxide known as Fenton´s reaction (a) (Fujita et al., 2009).

$$\text{(a) } 2\ Fe^{2+} + H_2O_2 \rightarrow 2\ Fe^{3+} + OH^- + OH^{\cdot}$$

ROS in turn trigger steatohepatitis *via* different mechanisms, among them lipid peroxidation and the induction of cytokines. Lipid peroxidation releases malondialdehyde and 4-hydroxynonenal, which both can crosslink proteins and therefore might be involved in the formation of Mallory Denk bodies, which contain cross-linked cytokeratin monomers (Pessayre et al., 2001). These events lead to cellular damage and hepatocyte stress inducing a pro-inflammatory state. The activation of several pro-inflammatory pathways leads to the production of an array of cytokines, which in turn promote the accumulation of immune cells within the liver. The activation of nuclear factor kappa light polypeptide gene enhancer in B-cells (NFKB) and the inflammasome pathway, both important regulators of genes involved in immunity and inflammatory response, are in the focus of this study and will therefore be discussed in more detail.

1.1.2.1 NFKB

NFKB is a family of dimeric transcription factors consisting of the five Rel subunits with the heterodimer of p65 and p50 being the most abundant of them. NFKB is found in all cell types in the uninitiated phase in the cytoplasm bound to the inhibitory protein inhibitor of kappa light polypeptide gene enhancer in B-cells (IκB). Upon stimuli, such as tumor necrosis factor (TNF) alpha or interleukin-1beta, IκB is degraded by phosphorylation by the catalytical activity of IκB kinase complex (IKK), leading to the nuclear translocation of the NFKB heterodimers, such as p65/p50, and their binding to the DNA. Here, it facilitates the transcription of an array of pro-

inflammatory cytokines such as TNF, IL-1beta, and others (He & Karin, 2011; Barnes & Karin, 1997; Robinson & Mann, 2010) (**Figure 1-3**).

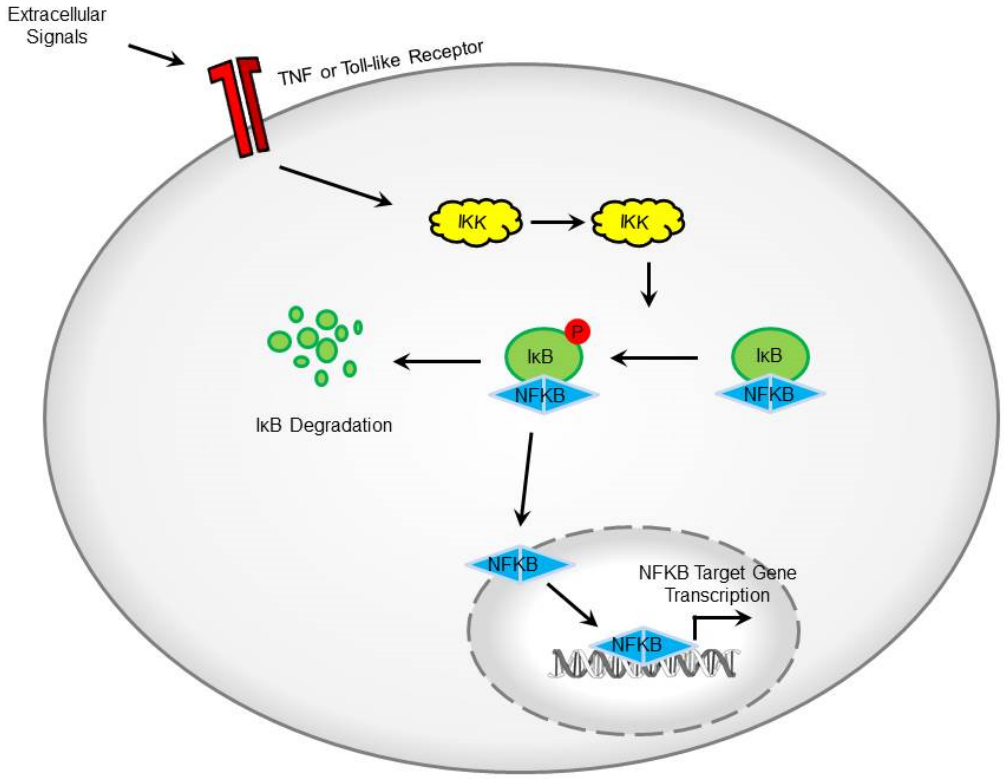

Figure 1-3: Pathway of NFKB activation. TNF (tumor necrosis factor) or toll-like receptor-mediated transduction of extracellular signals leads to activation of IKK (IκB kinase kinases complex) and thus, phosphorylation of IκB (inhibitor of NFKB). Ubiquitination of IκB and subsequent degradation by proteosome activity leads to liberation of NFKB from IκB and its nuclear translocation with subsequent NFKB targeted gene transcription.

1.1.2.2 Inflammasome

The role of inflammasomes and their product IL-1beta is obtaining rising attention in NASH (Szabo & Csak, 2012). Inflammasome activation was shown in NASH, but not in steatosis. Saturated fatty acids as well as ROS are a potential inducer for inflammasome activation (Csak et al., 2011; Tschopp & Schroder, 2010). The inflammasome is a multiprotein complex, which activates caspase-1 in response to cellular danger signals, and subsequently cleaves pro-IL-1beta into its mature form

(Szabo & Csak, 2012). Different subtypes of inflammasomes are known with the NLRP3-inflammasome as characterized member, containing the NLR family, pyrin domain containing (NLRP) 3, the PYD and CARD domain containing (PYCARD / ASC), and the effector molecule pro-caspase-1 (Szabo & Csak, 2012). IL-1beta production is transcriptionally regulated by NFKB and post-transcriptionally by NLRP3 inflammasome activation to facilitate the cleavage of pro-IL-1beta (**Figure 1-4**) (Bauernfeind et al., 2009).

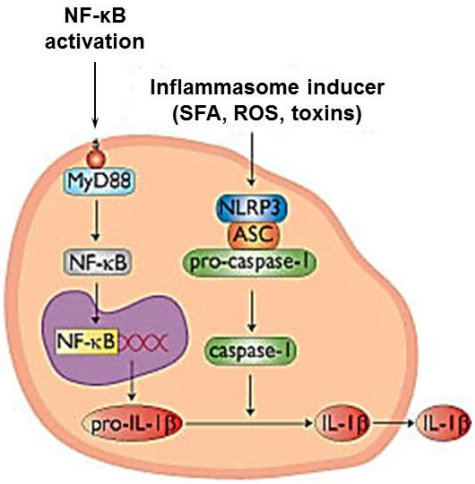

Figure 1-4: Inflammasome pathway. NFKB activation leads to transcriptional upregulation of pro-IL-1beta. Activation of the inflammasome complex facilitates the cleavage of pro-IL-1beta into its mature form and results in subsequent secretion into the blood stream (adapted from www.Invitrogen.com).

1.1.3 **Fibrosis**

Liver fibrosis represents a further progression of chronic liver diseases as one third of NASH patients progresses to fibrosis (Argo et al., 2009; Farrell & Larter, 2006). In NASH oxidative stress, chronic inflammation, and hepatocyte death are responsible for the activation of hepatic stellate cells (HSC) (Brenner, 2009). Activated HSCs are the major source for the production of collagen and the subsequent deposition of extracellular matrix leads to fibrosis (Rombouts & Marra, 2010). The profibrogenic transforming growth factor (TGF)-beta is considered to be the pivotal cytokine leading to fibrosis, as it triggers the transdifferentiation of HSCs and directly induces *collagen I* expression and alpha-smooth muscle actin stress fiber organization

(Gressner et al., 2002). However, numerous pathways are responsible for the initiation and perpetuation of HSC action (Friedman, 2008). Connective tissue growth factor (CTGF) is regarded as another important modulator of hepatic fibrogenesis as it is a downstream target gene of TGF-beta (Grotendorst, 1997). Interestingly, recent data demonstrate that CTGF is not uniquely induced by TGF-beta, but rather in a TGF-beta-independent pathway *via* interleukin 13, a T-cell-derived cytokine with profibrogenic actions (Gressner et al., 2007; Liu et al., 2011b; McKenzie et al., 1993; Weng et al., 2009; Wynn, 2004). Generally, lobular activation of HSCs causes perisinusoidal and zone 3 fibrosis as an early stage in NASH patients (Kleiner et al., 2005). Progression of the disease leads to portal fibrosis in stage 2, with increasing septal formations and bridging in the higher stages (Kleiner et al., 2005). A possible explanation for portal fibrosis is the activation of hepatic progenitor cells (HPC) (Roskams et al., 2003; Yang et al., 2004). These cells are the source for regenerating liver tissue, and as bipotential cells are located in the periportal area. They can differentiate into hepatocytes, cholangiocytes, and draining ductules (Libbrecht & Roskams, 2002). Misleading activation of HPC can result in a ductular reaction, which is a reactive lesion in the portal tract built from small biliary ductules and is accompanied by a complex stroma and inflammatory cells. Studies have shown that these ductular reactions can induce proinflammatory and profibrogenic mediators and that high NASH stages correlate with their occurrence in human samples (Richardson et al., 2007). Longstanding NASH and fibrosis can finally progress to cirrhosis, whereby fat deposition and inflammation can disappear (Rosmorduc & Fartoux, 2012). Cryptogenic cirrhosis accounts for around 10% of cirrhosis cases and the majority is probably related to NASH progression (Caldwell et al., 1999).

1.2 **HCC as a Complication of NAFLD**

Hepatocellular carcinoma (HCC) is the predominant primary liver cancer with rising incidence (**Figure 1-5**). HCC is considered the sixth most common malignancy worldwide and represents the third leading cause of cancer-related deaths (El-Serag, 2011; Mittal & El-Serag, 2013). Besides exposure to toxins as direct carcinogens and the infection with hepatitis B and C virus, the incidence of HCC is rising due to non-

viral causes (Van Thiel & Ramadori, 2011). HCC exhibits an interesting distribution pattern as it is associated with chronic liver diseases, geographic and ethnic variations, and gender differences (Hashimoto & Tokushige, 2012).

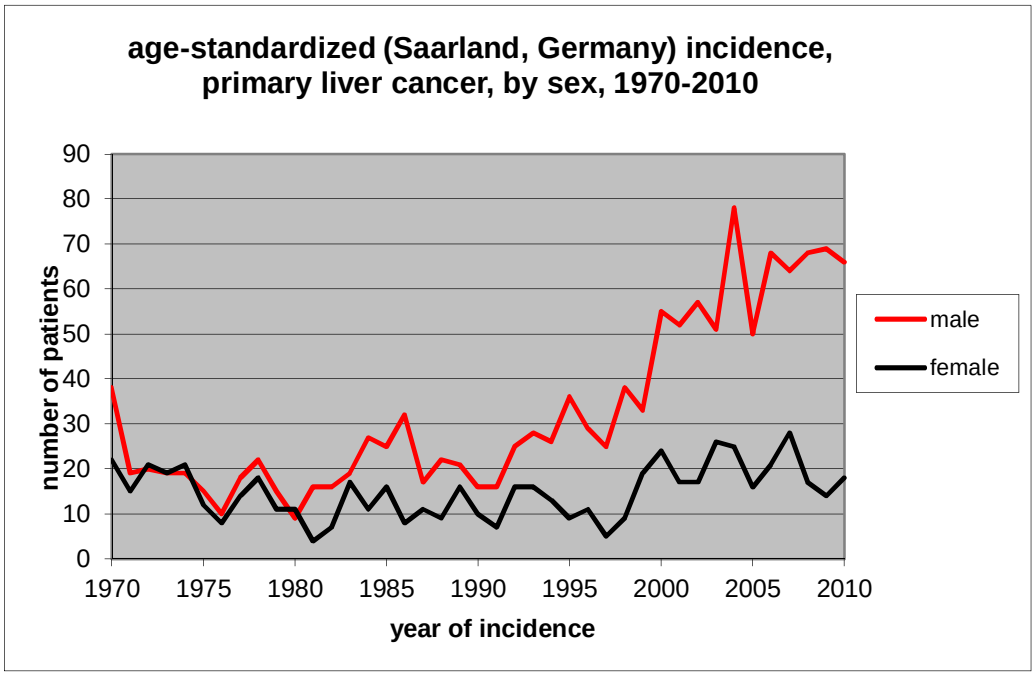

Figure 1-5: Incidence of liver cancer in Germany (Krebsregister Saarland)

Since cirrhosis is the main risk factor for HCC, and 15-50% of HCC cases occur in a context of cryptogenic cirrhosis, HCC represents a rare but severe complication of end-stage NAFLD (Stickel & Hellerbrand, 2010). Interestingly, the incidence of HCC is decreasing in high-prevalence areas, whereas its incidence in low-prevalence regions as Europe and United States has almost doubled (Stickel & Hellerbrand, 2010). This decrease of virus-associated HCC might be due to large-scale vaccination against HBV and the latter increase might attribute to the rising incidence of NAFLD, in particular NASH (Stickel & Hellerbrand, 2010).

During chronic hepatitis, liver cell proliferation is increased, whereas a decreased proliferation is detectable in the cirrhotic stage, indicating that the regenerative capacity of the liver is exhausted (Delhaye et al., 1996; El-Serag & Rudolph, 2007). Further features of chronic liver diseases, such as insulin resistance, oxidative

stress, inflammatory cytokines, and autophagy have a carcinogenic potential (Hashimoto & Tokushige, 2012). The deregulation of different oncogenic pathways, such as PI3K/Akt (Hu et al., 2003), m-TOR (Villanueva et al., 2008), Wnt/β-catenin (Chan et al., 2006; Micsenyi et al., 2004), Ras/Raf/AP-1/ERK (Mitsui et al., 2001), JNK (Czaja, 2010), or PTEN/Akt (Chen et al., 2009) are also associated with the development of NASH or hepatic carcinogenesis. However, the exact mechanisms leading to development of HCC in patients with NASH remain unclear.

1.3 The *IGF2* mRNA Binding Protein p62/IGF2BP2-2

The insulin-like growth factor 2 mRNA binding protein p62/IMP2-2/IGF2BP2-2 was first isolated by immunscreening of a cDNA library with autoantibodies from a patient with hepatocellular carcinoma (Zhang et al., 1999). In a subsequent cohort study of HCC patients, it was found that 21% of them had autoantibodies against p62 (Zhang et al., 1999). Furthermore, p62 was shown to be expressed in α-fetoprotein negative HCC and in cirrhotic nodules, as well as in other primary gastrointestinal carcinomas (Liu et al., 2013; Lu et al., 2001; Qian et al., 2005; Su et al., 2005), whereas it was not detectable in non-malignant liver tissue (Lu et al., 2001; Zhang & Chan, 2002). In accordance, p62 expression was found at high levels in fetal liver but was not detectable in adult livers (Lu et al., 2001). *De novo* appearance of antibodies to p62 in serum prior to or during the development of liver cancer indicates that auto-antibodies may be produced in response to the transformation process from chronic liver disease to malignancy (Zhang & Chan, 2002; Zhang et al., 2001). The highly specific antigen-driven autoantibody response of the immune system can be used as reporter for the transition to malignancy, and therefore serve as a monitor for tumor development (Li et al., 2012; Liu et al., 2013; 2011a). p62 was recognized as tumor-associated antigen (TAA), and serum autoantibodies against p62 were suggested as biomarkers in cancer immunodiagnostics (Li et al., 2012; Liu et al., 2013; 2011a).

The family of insulin-like growth factor 2 mRNA binding proteins (IGF2BPs/IMPs) was identified by Nielsen *et al.* at the same time as the discovery of p62 during studies on isolated proteins binding to a developmentally regulated, fetally expressed insulin-like growth factor 2 (*Igf2*) mRNA (Nielsen et al., 1999). p62 belongs to the family of IGF2BPs together with two other IGF2BPs, i.e. IGF2BP1 and IGF2BP3/Koc

(Nielsen et al., 1999). p62 represents a splice variant of IGF2BP2 lacking exon 10 with 43 amino acids between hnRNP K homology (KH) 2 and 3 (**Figure 1-6**) (Lu et al., 2001; Nielsen et al., 1999). The protein contains two types of RNA-binding motifs, i.e. the RNA recognition motif (RRM) and the KH motif organized in a characteristic arrangement (Burd & Dreyfuss, 1994; Kenan et al., 1991). In fact, IGF2BPs are almost exclusively observed in the cytoplasm where they form ribonucleoprotein complexes (mRNPs) with their target mRNA (Bell et al., 2013).

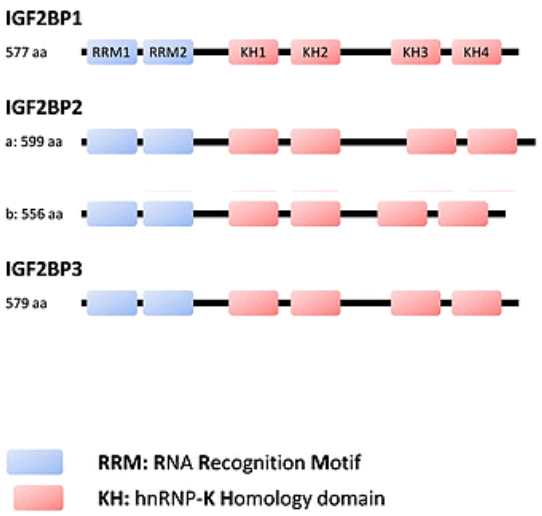

Figure 1-6: The IGF2BP protein family. Domain structure of human IGF2BPs. RNA-binding domains comprising RNA recognition motifs (*RRM*s, *blue*) and hnRNP-K homology domains (*KH*, *red*). The following proteins are shown: *IGF2BP1*, the longest IGF2BP1 protein isoform; *IGF2BP2-a*, the longest IGF2BP2 protein isoform; *IGF2BP2-b* (p62), spliced IGF2BP-a lacking exon 10; *IGF2BP3* (adapted from (Bell et al., 2013)).

The mRNPs are “stable” protein-RNA complexes causing a long half-life, allowing long-distance transports as well as transient storage of the target mRNA (Bell et al., 2013). Therefore, IGF2BPs control the target mRNA right after transcription and modulate the rate of its mRNA degradation, translation, or transport (Bell et al., 2013). In particular, IGF2BP1 has beta-actin (*Actb*) mRNA as target transcript suggesting a role in controlling cytoskeletal organization, cell adhesion, and cell migration (Hüttelmaier et al., 2005).

Phosphorylation of IGF2BP2 promotes the association with the leader 3 5´-UTR of IGF2 leading to elevated protein synthesis of IGF2 (Dai et al., 2011). Furthermore, IGF2BP2 is suggested to be involved in metabolic homeostasis and response to nutrients and it might play a role in type 2 diabetes (Christiansen et al., 2009).

1.4 **Effects of p62 on Fatty Acid Metabolism**

The first characterization of a functional implication of the oncofetal protein p62 was recently presented in *p62* transgenic mice. Histological fat staining revealed a fatty liver phenotype in mice overexpressing the human p62 protein specifically in the liver (Tybl et al., 2011). Due to the lack of spontaneous tumor formation in these transgenic animals, the phenotype of a fatty liver was suggested to be the benign “first hit“ towards the formation of NASH (Tybl et al., 2011).

Interestingly, a downregulation of the phosphatase and tensin homolog (PTEN), a known tumor suppressor, was found in *p62* transgenic mice (Tybl et al., 2011). PTEN expression was shown to be inhibited by fatty acids (Vinciguerra et al., 2009; 2008) and is frequently mutated in different kinds of cancer (Chow & Baker, 2006; Stickel & Hellerbrand, 2010). PTEN knockdown in mice was further demonstrated to lead to steatosis and ultimately to HCC, linking metabolism with hepatocarcinogenesis (Horie et al., 2004; Watanabe et al., 2005). Only recently, PTEN knockdown was shown to modulate fatty acid metabolism resulting in an altered fatty acid pattern similar to human NASH and NASH-induced HCC (Muir et al., 2013).

Furthermore, an activation of the pro-oncogenic extracellular signal-regulated kinase (ERK) pathway was seen upon p62 overexpression (Kessler et al., 2013), which was also upregulated in a mouse model of a high-fat diet promoted HCC (Park et al., 2010).

1.5 Methionine and Choline Deficient Diet

To investigate the effect of p62 on liver pathophysiology of NASH a methionine/choline-deficient (MCD) diet was fed to the *p62* transgenic animals. The MCD diet is the most common murine model of acquired NASH induced by a specific dietary intervention. The diet contains higher levels of sucrose and fat compared to standard chow (40% sucrose and 10% fat), and lacks the two components methionine and choline (Fan & Qiao, 2009). Mice fed the MCD diet develop measurable hepatic steatosis by two weeks, which progresses to inflammation (Weltman et al., 1996), inducing steatohepatitis by week four (Kirsch et al., 2003), and, in the long term, fibrosis or even cirrhosis and HCC (**Figure 1-7**) (Dobosy et al., 2008; Weltman et al., 1996). The observed histological features are comparable to human NASH (Wasmuth et al., 2007).

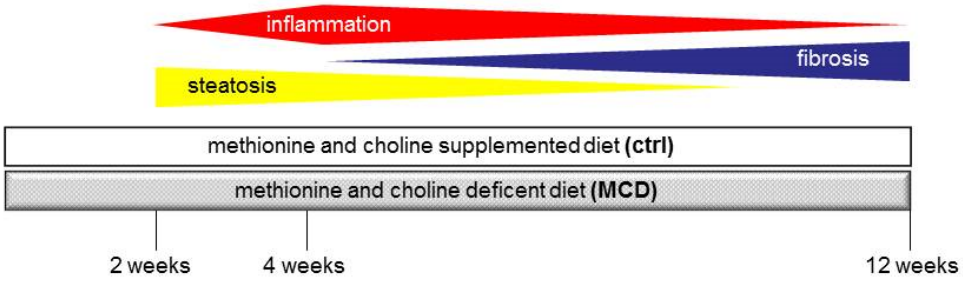

Figure 1-7: Time elapsed upon MCD treatment. 2 weeks representing the time point with the highest steatosis level, followed by the manifestation of NASH after 4 weeks with the peak of inflammation, and reaching the highest score for fibrosis after 12 weeks on MCD.

Choline is classified as an essential nutrient with roles in cell membrane integrity, transmembrane signalling, phosphatidylcholine synthesis, neurotransmission, and methyl metabolism (Anstee & Goldin, 2006). Lack of choline leads to impaired synthesis of phosphatidylcholine resulting in diminished VLDL assembly, secretion, and consequently to a reduced triglyceride (TG) clearance (Jamil et al., 1990). Deficiency in both choline and methionine additionally leads to an impaired mitochondrial β-oxidation and induction of alcohol-inducible cytochrom P450 (CYP) 2E1 expression, which is responsible for reactive oxygen species (ROS) production (Weltman et al., 1996). Thus, the MCD diet exerts to an accumulation of fatty acids in hepatocytes due to an increased uptake, and an impaired release and degradation

of fatty acids. Subsequently, hepatic lipid peroxidation and the formation of ROS results in the formation of oxidative stress and induction of a histological steatohepatitis (Leclercq et al., 2000; Weltman et al., 1996). Oxidative stress induces inflammatory cytokines, such as Il-1beta and TNF, followed by an infiltration of lymphocytes and neutrophils into the liver tissue and accompanied by apoptosis of hepatocytes (Fan & Qiao, 2009). The fibrogenic response is accompanied by a necroinflammatory state and is associated with an upregulation of mRNA levels of e.g. *collagen 1*, tissue inhibitor of metalloproteinases (*TIMP*) 1 / 2*,* and matrix metalloproteinase (*MMP*) 13 (Ip et al., 2004). NFKB activation displays an important link between oxidative stress, chronic inflammation, and hepatic fibrogenesis (Dela Peña et al., 2005).

The MCD NASH model is one of the best established models to study the evolution of steatosis, oxidative stress, inflammation, and fibrogenic changes associated with NASH (Fan & Qiao, 2009). However, this model features two drawbacks: mice fed the MCD diet lose significant amounts of muscle and fat weight (up to 40-50% loss in 12 weeks) and, unlike most human NASH cases, animals do not develop peripheral insulin resistance (Rinella & Green, 2004). However, NASH and peripheral insulin resistance as part of the metabolic syndrome are not observed in all NASH cases (Smits, 2013; Yilmaz, 2012). Still, despite differences to human NASH, the MCD diet represents one of the most important models to study steatosis-associated liver injury.

1.6 **Doxycycline Dependent Temporal Inhibition of *p62* Expression**

Transgenic systems are *per se* an interesting tool, but have several limitations. In the classical binary systems, the target gene is silent or activated upon crossing with a recombinase or transactivator. In such a system, the expression rate is irreversible and cannot be varied by changing experimental conditions; here the expression is directly dependent on the expression of the effector molecule (Furth et al., 1994; Kistner et al., 1996).

Using the tetracycline (Tet) regulatory system in the *p62* transgenic animals a conditional gene expression was achieved (Schönig et al., 2010; Tybl et al., 2011). The mouse model used within this study has a liver-specific overexpression of the

human p62. The human *p62* transgene was placed under control of the transrepressive responsive element cytomegaly virus (TRE-CMV_{min}) promotor to ensure that no constitutive *p62* mRNA expression occurs in these animals (**Figure 1-8A**). To induce the expression of the transgene, mice need to be crossed with liver transactivator (*LT2*) transgenic mice. These animals carry a liver-specific promotor, the liver enriched activator protein (LAP), controlling the expression of the tetracycline-controlled transactivator (tTA). In $p62^{+}$ *x* $LT2^{+}$ mice tTA activates the TRE-CMV_{min} promotor leading to the subsequent mRNA expression of the transgene (**Figure 1-8B**). Through this mechanism an inducible and liver-specific expression of human *p62* is achieved.

In the *p62* transgenic mice the presence of doxycycline inactivates tTA and prevents its binding to the TRE-CMV_{min} promoter, resulting in gene silencing of *p62* (**Figure 1-8C**). This system is also known as Tet-off system, since doxycycline inhibits the expression of the gene of interest (**Figure 1-8D**).

In contrast, in the Tet-on system, 4 amino acids are exchanged in the tetR moiety, which leads to a reverse phenotype to the repressor (rtetR). The resulting rtTA requires doxycycline for binding to the operator sequences (tetO) and the activation of transcription (Gossen et al., 1995) (**Figure 1-8E**).

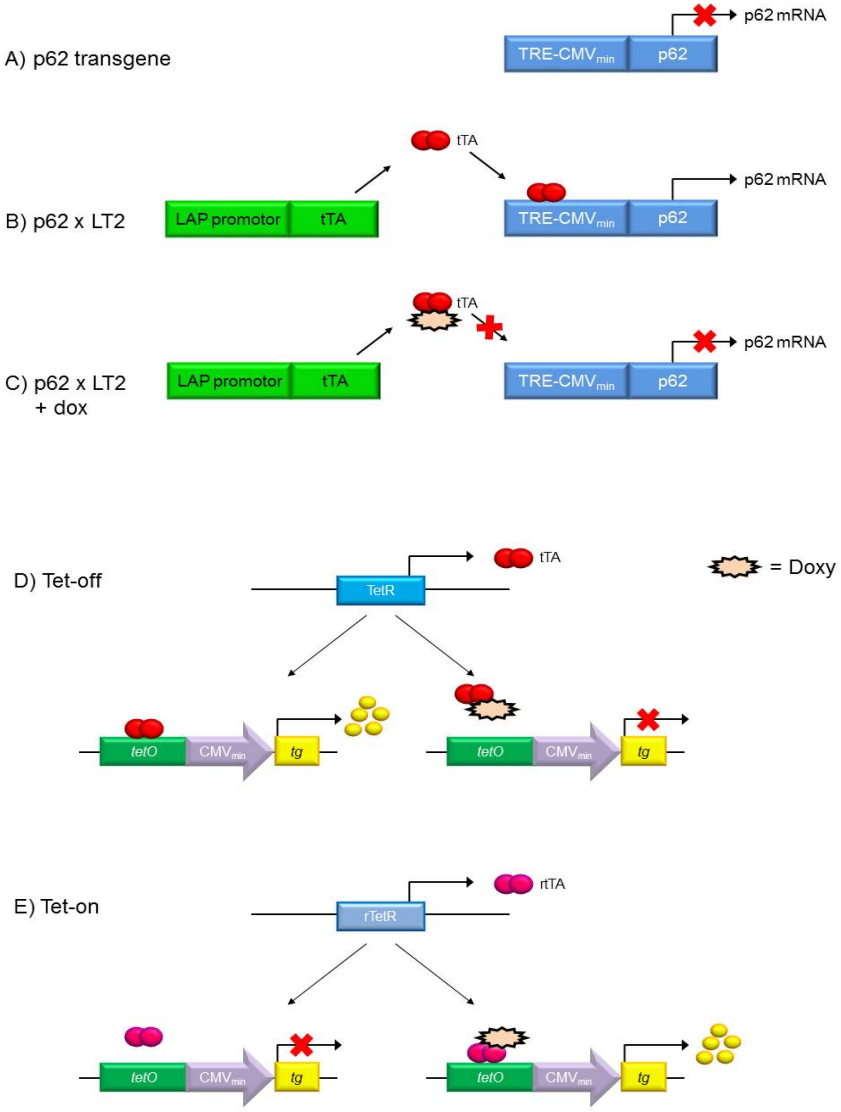

Figure 1-8: Generation of *p62* transgenic mice. (**A**) No expression of *p62* mRNA under TRE-CMV_{min} promotor control. (**B**) Liver-specific expression of *p62* mRNA in double positive $p62^{+}/LT2^{+}$ mice. (**C**) Application of doxycycline inhibits transgene expression. (**D**) Tet-off system (**E**) Tet-on system. TRE-CMV_{min}: transrepressor responsive element cytomegalovirus; tTA: tetracycline transactivator; LAP: liver enriched activator protein; tetO: operator sequences; tg: transgene

1.7 Selective Kupffer Cell Depletion

The major cell type of the liver is the hepatocyte. In addition, the liver contains numerous different cell types including parenchymal cells, stellate cells, sinusoidal endothelial cells, cholangiocytes, and Kupffer cells (Stienstra et al., 2010). Kupffer

cells are the liver-specific macrophages and represent the largest resident population of macrophages within an organ (Neyrinck et al., 2009). Recently, their origin as being myeloid-derived mononuclear cells has been challenged and updated. Now, Kupffer cells are proposed to derive from the yolk sac, whereas monocytes derive from the bone marrow (Wynn et al., 2013). Kupffer cells are critical players in the innate immune response (Gordon & Taylor, 2005; Taylor et al., 2005) and are located along the hepatic sinusoid where they facilitate their main functions, including phagocytosis as well as antigen processing and presentation (Isibasi et al., 1983) (**Figure 1-9**).

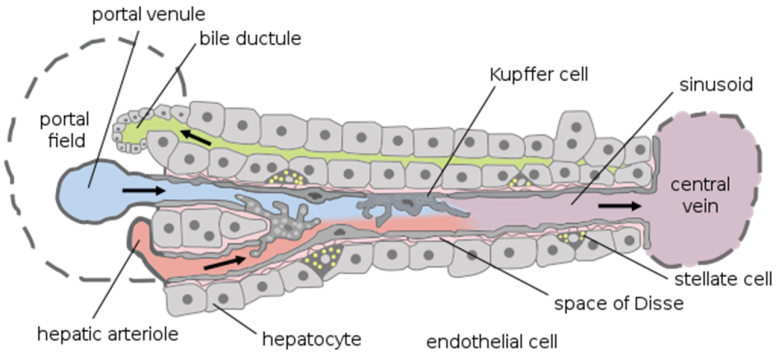

Figure 1-9: **Hepatic microarchitecture**. In the liver, blood flows from portal blood vessels through sinusoids to central veins. In the sinusoids endothelial cells, hepatic stellate cells, and Kupffer cells are located. The highly polarized hepatocytes form cords, and are lined by the sinusoidal capillaries that radiate towards a central vein. Hepatocytes produce bile, which is excreted into canaliculi linked to bile ducts (adapted from (Frevet et al., 2005)).

Kupffer cells produce various inflammatory mediators, such as cytokines, prostaglandins, nitric oxide, and reactive oxygen species, which influence neighboring parenchymal cells (Bilzer et al., 2006). An implication of Kupffer cells has been shown in the pathogenesis of various liver diseases (Diehl, 2002). In fact, studies in obese and diabetic animals have suggested that Kupffer cell dysfunction might be involved in the pathogenesis of NASH (Diehl, 2002; Yang et al., 1997). Furthermore, it has been shown in various animal experiments that the adjacent hepatocytes may be influenced in their lipid metabolism *via* the release of special cytokines from Kupffer cells (Odegaard et al., 2008; Stienstra et al., 2010). It can therefore be concluded that Kupffer cells have an impact in the progression from

steatosis to NASH (Diehl, 2002), and even in the development and modulation of steatosis itself.

An experimental approach was used within this thesis to answer the question, whether Kupffer cells are involved in the modulation of the fatty acid composition. A selective *in vivo* depletion of macrophages was carried out, based on a liposome-mediated intraphagocytic delivery and accumulation of the bisphosphonate clodronate (**Figure 1-10**) (Van Rooijen et al., 1985).

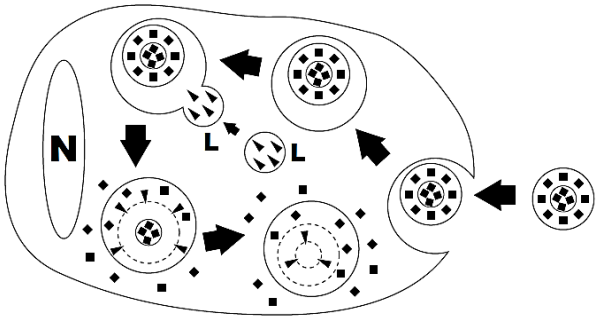

Figure 1-10: Macrophage "suicide". The liposomes with encapsulated clodronate (squares) are ingested by Kupffer cells *via* endocytosis. Fusion with lysosomes (L) leads to disruption of the bilayers of the liposomes through the activation of phospholipases (arrowheads). The more concentric bilayers are disrupted, the greater is the clodronate relase within the cell. Finally, clodronate accumulation leads to cell apoptosis. (N = nucleus of the Kupffer cell). (Courtesy of clodronateliposomes.org)

Liposomes consist of concentric phospholipid bilayers entrapping aqueous compartments, in which hydrophilic molecules dissolved in aqueous solution, such as the non-toxic bisphosphonate clodronate, can be encapsulated (van Rooijen et al., 1996). Clodronate is not toxic and will not pass phospholipid bilayers of cell membranes or liposomes. After injections, the liposomes will be ingested and the phospholipid bilayer of the liposomes disrupts under the influence of lysosomal phospholipases, and releases clodronate intracellularly with the consequence of its accumulation (van Rooijen et al., 1996). At a certain threshold concentration, the cell is irreversibly damaged and dies by apoptosis (**Figure 1-10**). The released free clodronate does not affect other cells because it cannot pass membranes, it has a very short half life, and it is finally removed by the renal system (van Rooijen et al., 1996). An intraperitoneal (*i.p.*) injection of clodronate liposomes leads to a depletion

of macrophages in the abdominal cavity, the liver and the spleen. Here, liposomes arrive in the blood vessels *via* the lymphatic system or directly *via* the portal vein to the liver (**Figure 1-11**).

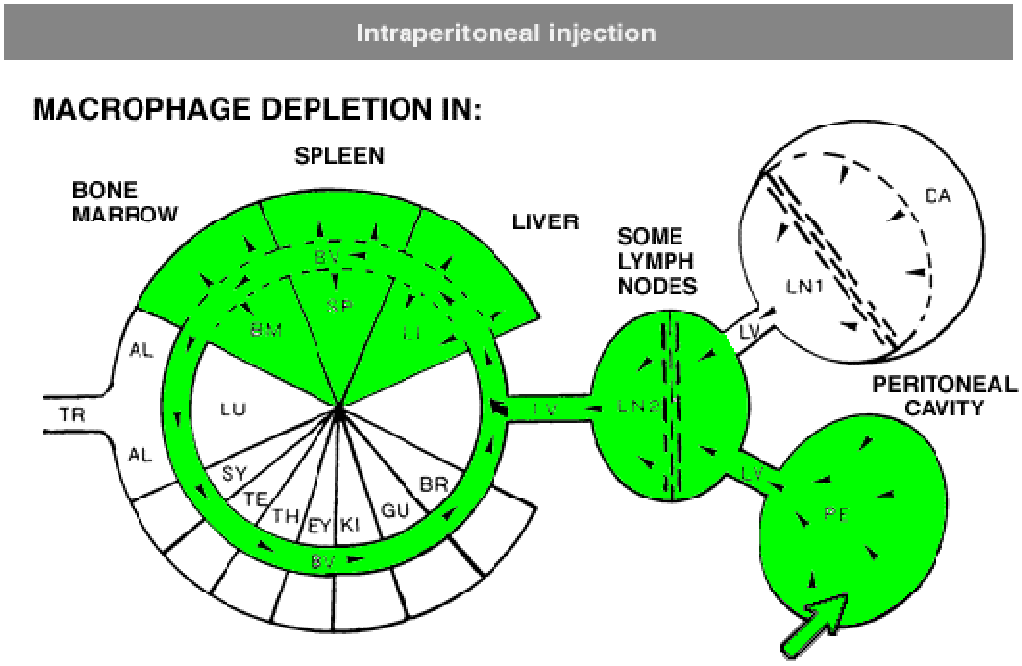

Figure 1-11: Injection scheme of intraperitoneal injections of clodronate liposomes. (Courtesy of clodronateliposomes.org)

In order to answer the question whether Kupffer cells have an implication on lipid composition, we investigated the MCD-induced NASH in the absence of Kupffer cells depleted by administration of liposome-encapsulated clodronate.

1.8 **Aims and Significance**

More than 25% of the population in Western countries are affected by NAFLD. Longstanding NAFLD can ultimately lead to hepatocellular carcinoma (Stickel & Hellerbrand, 2010). Understanding of the underlying pathophysiological mechanisms is therefore of high clinical relevance. The autoantigen p62/IGF2BP2-2, which was found in human HCC, induces steatosis in mice and IGF2BP2 expression was associated with human type 2 diabetes (Christiansen et al., 2009). We therefore hypothesized a putative role of p62 in the development of NASH.

Aim of the present work was to elucidate the pathophysiological role of a liver-specific overexpression of p62 in a murine model of non-alcoholic steatohepatitis. The following questions should be answered:

1. Does p62 affect the pathogenesis of different stages of NAFLD in mice fed the MCD diet? To cover the full spectrum of NAFLD mice were treated for three different time points to evaluate steatosis, NASH, and NASH-induced fibrosis.

2. Does the conditional inhibition of *p62* expression prior to the MCD feeding have an impact on the pathology of NAFLD?

3. Does p62 have an impact on the fatty acid pattern and composition when fed the MCD diet?

4. How do Kupffer cells alter the fatty acid composition in MCD induced steatosis?

2 MATERIALS AND METHODS

2.1 **Materials**

The methionine/choline-deficient (MCD) diet (#960439) and the methionine/choline supplemented control (ctrl) diet (#960441) were purchased from MP Biomedicals (Germany).

Table 2-1: Composition of the methionine/choline-deficient (MCD) diet and the methionine/choline supplemented control (ctrl) diet according to MP Biomedicals.

Ingredients	MCD Amount g/kg diet	ctrl Amount g/kg diet
Sucrose	455.3	455.3
Corn Starch	203.5	203.5
Corn Oil	100.0	100.0
Alphacel Non-Nutritive Bulk	25.0	30.0
AIN 76 Mineral Mix	35.0	35.0
Amino acids and vitamins	176.2	176.2
DL-Methionine	0	3.0
Choline-bitatrat	0	2.0

Clodronate liposomes (5 mg/ml) were obtained from Nico van Rooijen (clodronateliposomes.org; Vrije Universiteit, Netherlands) and prepared as previously described (Van Rooijen & Hendrikx, 2010). Clodronate was a gift from Roche Diagnositics GmbH (Mannheim, Germany). PCR primers and dual-labeled probes were obtained from Eurofins MWG Operon (Ebersberg, Germany). *Taq*-Polymerase (5 U/µl), 10 x *Taq* buffer, and dNTP mix (10 mM each) were from Genscript (Piscataway, NJ, USA), the EvaGreen® qPCR Mix was from Solis BioDyne (Tartu, Estonia). Antibodies for immunhistochemistry and Western blot were purchased as indicated in **table 2-8** and **table 2-6**. All other chemicals were obtained from commercial sources like Roth, Germany and Sigma-Aldrich, Germany, unless indicated otherwise.

2.2 Mice and Treatments

2.2.1 Animal Welfare

All animal procedures were performed under the guidelines of the local animal welfare committee (permission-no.: 34/2010). Mice were maintained under 12-hour dark-light cycles under controlled conditions (temperature 22 ± 2°C and relative humidity of 55 ± 10%) with unrestricted access to food and water until the age of three weeks.

The mice were randomly divided into experimental groups at the age of 3 weeks and fed a MCD diet or a MCD diet supplemented with choline bitartrate (2 g/kg) and DL-methionine (3 g/kg); the latter was designated as a control diet (ctrl). In addition, one group received 25 µg/ml doxycycline in drinking water from mating of the parents until the newborns reached an age of 18 days. Another group received 100 µl / 10 g body weight of a liposome suspension (2 g / 10 ml) clodronate or empty liposomes as control).

2.2.2 Generation of *p62* Transgenic Mice

Male and female *p62* transgenic mice and *LT2* transgenic mice were used as described in (Tybl et al., 2011). *p62*$^+$/*LT2*$^+$ transgenic mice liver-specifically express the human p62 protein (**Figure 1-4)**. *p62* expression is repressed by the TRE-CMV_{min} promoter in the DBA2J *p62* transgenic mice. For experiments animals were crossed with C57BL/6J *LT2* mice, which carry a tetracycline transactivator (Kistner et al., 1996), leading to a derepression of the promoter, thereby allowing *p62* expression in the *p62*$^+$/*LT2*$^+$ offspring (Tybl et al., 2011). DBA2J and C57BL/6J wild-type animals were purchased from Charles River Laboratories, Germany.

2.2.3 Genotyping

An ear biopsy was taken for genotyping and incubated in 89 µl water premixed with 10 µl 10x *Taq* buffer and 1 µl Proteinase K (20 mg/ml) (Roche, Germany) at 55°C for one hour while shaking. After heat-inactivation of Proteinase K at 95°C for 15 min, 1 µl of the supernatant was used in the subsequent PCR reaction.

A single PCR reaction was performed containing 1 µl template, 2.5 U *Taq*-Polymerase, 125 µM dNTPs, 2.0 µl 10 x *Taq* buffer, and 400 nM of forward and reverse primer. The final reaction mixture was made up to 20 µl with sterile water. Primer sequences for *p62* and *tTA* are given in **table 2-2**. The thermal cycling conditions consisted of an initial denaturation step at 95°C for 5 min, followed by 35 cycles consisting of denaturation at 95°C for 30 s, annealing at 57°C for 30 s, and extension at 72°C for 30 s and a final extension at 72°C for 5 min on a C1000 TouchTM Thermal Cycler (Bio-Rad, Germany)

Table 2-2: Primer sequences as used for genotyping PCRs.

Target	Primer sense, 5'→ 3'	Primer antisense, 5'→ 3'	Product size
p62	CATCAAACAGCTGGCG	GTGCCCGATAATTCTGA	450 bp
tTa	GTGCAGAGCCAGCCTT	CCTCGATGGTAGACCCG	150 bp

2.2.4 **Treatment**

All animals were 3 weeks of age at the commencement of the study. The mice were fed one of the two diets: the MCD or the ctrl diet for 2 weeks, 4 weeks, and 12 weeks, respectively. In another setup, one group was fed doxycycline to inhibit *p62* expression prior to MCD diet, another group received clodronate or an empty liposome suspension intraperitoneal by 2 days prior to MCD or ctrl diet, respectively. Liposome injections were repeated every five days to ensure depletion of Kupffer cells throughout the experiment. Mice were given free access to food and water and were weighed daily for the duration of the study. At the end of the treatment period mice were sacrificed by cervical dislocation and blood and liver tissue were collected for analyses.

2.2.5 **Serum Parameters**

Whole blood samples were incubated for one hour at room temperature and subsequently centrifuged for 10 min at 13,500 *x g* at 4°C. The supernatant was

transferred into a fresh tube and diluted 1:3 with 0.9% NaCl, stored at -20°C, or stored at 4°C until measurement.

Serum alanine aminotransferase (ALT), aspartate aminotransferase (AST), glucose, triglycerides (TG), cholesterol, and high density lipoprotein (HDL) levels were determined by a PPE Modular analyzer using Roche® reagents at a constant temperature of 37°C (Roche Diagnostics, Mannheim, Germany). Measurements were performed at the "Zentrallabor des Universitätsklinikums des Saarlandes" (Homburg, Germany).

Interleukin 13 levels were determined by a luminex assay using a BioPlex Pro mouse Plex assay according to the manufacturer´s guidance (Bio-Rad, Germany).

2.2.6 **Preparation of Liver Tissue**

Livers were excised and weighed. Two thirds of the liver tissues were flash-frozen in liquid nitrogen and stored at -80°C and one third was fixed for 24 h in 4% PBS-buffered formalin before paraffin embedding.

2.3 **Bacterial Culture**

The *Escherichia coli* (*E. coli*) strain TOP10 (Invitrogen, Germany) was used as host organism for plasmid amplification. Bacteria were grown under standard conditions in lysogeny broth (LB: 10% tryptone [w/v], 5% yeast extract [w/v], 5% NaCl [w/v] in H_2O, pH 7.5) medium supplemented with ampicillin (100 µg/ml). For selection of single clones, LB_{amp} agar (30% [w/v] agar in LB containing ampicillin) plates were used.

2.3.1 **Generation of Competent *E. coli* by $CaCl_2$ Method**

An overnight culture of 100 ml (OD_{650} = 0.4) was incubated on ice for 30 min, centrifuged (3,000 *x g*, 5 min, 4°C), and resuspended in 2.5 ml ice cold $CaCl_2$ solution containing 75 mM $CaCl_2$ and 15% glycerol. Another 20 ml ice cold $CaCl_2$ were added, and the mixture was incubated on ice for 20 min. Cells were harvested by centrifugation (3,000 *x g*, 5 min, 4°C), resuspended in 2.5 ml $CaCl_2$, aliquoted, and stored at -80°C.

2.3.2 **Real-Time RT-PCR Standard Plasmid Generation**

Standards of the PCR products of the genes of interest were cloned into the pGEM®T Easy vector (Promega, Germany) according to the manufacturer's guidelines or were provided by Prof. Dr. Alexandra K. Kiemer (Saarland University, Pharmaceutical Biology). See **table 2-3** for primer sequences.

2.3.3 **Transformation**

For transformations 50-150 ng plasmid DNA were added to 100 µl competent *E. coli* and were incubated on ice for 20 min. Bacteria were subsequently heat-shocked for 90 s at 42°C and immediately returned on ice for 2 min. 900 µl SOC medium (yeast extract 5 g/l, tryptone 20 g/l, NaCl 0.6 g/l, KCl 0.2 g/l, $MgCl_2$ 10 mM, $MgSO_4$ 10 mM in water) was added to the bacteria, followed by incubation at 37°C at 170 *x g* for 1.5 h. 100 µl of the bacterial suspension was plated on LB_{amp} plates and incubated at 37°C over night.

2.3.4 **Isolation of Plasmid DNA**

Plasmid DNA was isolated from overnight cultures by using the Miniprep plasmid isolation kit (Qiagen, Germany) according to the manufacturer's instructions. The integrity and concentration of the extracted plasmid DNA was determined by UV spectrophotometry at wavelengths of 260 and 280 nm on a BioMate UV Vis spectrophotometer (ThermoElectron, Germany). An extinction of 1 equates a concentration of 50 µg/ml.

2.3.5 **Sequencing of Real-Time RT-PCR Standard Plasmids**

Sequencing reactions were performed by Eurofins MWG (Ebersberg, Germany) with 100 ng plasmid DNA in 16 µl Milli-Q water.

2.4 Agarose Gel Electrophoresis

2.4.1 Detection of DNA

Agarose gels of 0.5-2.5% agarose in 1 x TBE (89.1 mM TrisHCl, 89.1 mM boric acid, 2.21 mM EDTA in distilled water) containing 0.04% [v/v] ethidium bromide for DNA detection were used to analyze the amplified DNA. The samples were mixed with 1/6 volume of gel loading buffer (25 mg bromophenol blue, 25 mg xylenecyanol FF, 1.5 g Ficoll type 400 ad 10 ml distilled water) and loaded onto the gel with 50 bp DNA ladder as reference (Fermentas, Lithuania). Electrophoresis was carried out at 100 V for approximately 45 min in 1 x TBE Buffer. The gels were viewed and analyzed using a UV Transilluminator (Biostep Dark Hood DH-40/50, biostep GmbH, Germany) and the software ArgusX1 (Biostep, Germany).

2.4.2 Detection of RNA

RNA gels containing 1% formaldehyde for RNA stabilization, MOPS buffer (0.02 M 3-(N-morpholino)propanesulfonic acid (MOPS), 5 mM sodium acetate, 0.5 mM EDTA in DEPC-treated distilled water, pH 7) with 1% [w/v] agarose, were used to check RNA integrity. Prior to gel loading, RNA was denatured at 65°C for 5 min in an appropriate volume of loading buffer (10 ml form amide, 3.5 ml formaldehyde, 1.5 ml 10 x MOPS). Samples were separated in 1 x MOPS buffer at 100 V and detected as described in 2.4.1.

2.5 RNA Isolation and Reverse Transcription

2.5.1 RNA Isolation

Total RNA was extracted in 700 µl QIAzol Lysis Reagent (#79306, Qiagen, Germany) using a high-performance dispenser (T25 digital ULTRATURRAX®, IKA®-Werke, Germany) for homogenization of snap-frozen liver tissue samples. After incubation for 5 min at room temperature, 175 µl of chloroform were added. The mixture was vortexed, incubated at room temperature for 2 min, and centrifuged (12,000 *x g*, 15 min, 4°C). Supernatants were transferred into a new reaction tube and RNA was precipitated over night at -20°C by addition of 1 volume of ice-cold isopropanol

(100%). For further processing, samples were centrifuged (12,000 *x g*, 10 min, 4°C) and the resulting pellets were washed with ice-cold ethanol 75% [v/v], dried and dissolved in diethylpyrocarbonate (DEPC) treated water. DNA was digested after RNA isolation using the DNA free kit (Ambion, Germany) according to manufacturer´s instructions. RNA integrity was checked using agarose gel electrophoresis.

2.5.2 **Measurement of RNA Concentration**

Photometric determination of RNA concentrations at 260 nm was carried out using a BioMate UV-Vis spectrophotometer (Thermo Electron, USA). An extinction of 1 equates a concentration of 40 µg/ml.

2.5.3 **Reverse Transcription**

For synthesizing complementary DNA (cDNA) from RNA, reverse transcriptions were performed with the High-Capacity cDNA Reverse Transcription Kit (Applied Biosystems, Germany) according to the manufacturer's instructions. Approximately 200-1,000 ng of RNA were denatured at 65°C for 5 min and placed on ice. The reaction mixture containing 2 µl 10x RT Puffer, 0.8 µl 25x dNTPs (25 mM each), 2 µl Random Primer (10 µM), 1 µl MultiScribe Reverse Transcriptase (4 U/µl), 0.25 µg RNaseOut (10 U/µl) (Invitrogen, Germany) and water to a final volume of 20 µl, was added to the RNA and incubated at 25°C for 10 min followed by 2 h at 37°C and a final inactivation step at 85°C for 5 s. The resulting cDNA was diluted by addition of 80 µl water and used for real-time RT-PCR.

2.6 **Real-time RT-PCR**

A PCR based method for detection and simultaneous quantification of gene expression, real-time quantitative RT-PCR, was used in order to determine the expression of the genes of interest. The method is based on the signal of a fluorescent reporter, which increases in direct proportion to the amount of PCR product in the reaction. The fluorescence emission correlates with the initial amount of target template. Two different detection methods were used: a target specific detection method using fluorescent probes (TaqMan®) labelled with a fluorescent

reporter (FAM) at the 5'-end and a quencher (BHQ1) at the 3'-end, and a detection method with a fluorescent dye (EvaGreen®), which is able to intercalate within the amplified DNA.

2.6.1 **Experimental Procedure**

The real-time PCR reactions were performed on an iCycler iQ5 or a C1000 Touch™ Thermal Cycler with CFX 96™ Realtime System in emulation mode iCycler (Bio-Rad, Germany). Primers and probes used are given in **table 2-3**. Reaction mixtures (25 µl) for the TaqMan® system were assembled on ice, 5 µl template cDNA or standard plasmid solutions were added on a 96 well plate. The reaction mixture contained 2.5 U *Taq*-Polymerase, 2.5 µl 10 x *Taq* buffer, 400 nM of each primer, 100 nM dNTPs, 1.5 or 2.5 pmol dual-labeled probe, and 3-5 mM $MgCl_2$. Probe- and $MgCl_2$-concentrations for each target gene are listed in **table 2-4**. For the EvaGreen® system the reaction mixtures (20 ml) contained 5 µl template cDNA or plasmid standard solutions on a 96 well plate. The reaction mixture contained 1x HOT FIREPol® EvaGreen® qPCR Mix Plus and 80-250 nM of each primer. The primer concentrations for each gene are listed in **table 2-4**. The thermal cycling conditions for the TaqMan® system commenced with an initial denaturation step at 95°C for 8 min, followed by 40 cycles of denaturation at 95°C for 15 s, annealing at 58-64°C for 15 s, elongation at 72°C for 15 s, and a final elongation at 72°C for 25 s. The thermal cycling conditions for the EvaGreen® system had an initial denaturation step at 95°C for 15 min, followed by the 40 cycles as mentioned above. At the end a melting curve from 65°C to 95°C was added to ensure specificity of the primers. The specific annealing temperatures for each gene are given in **table 2-4**. All samples were analyzed in triplicate. The starting amount of cDNA in each sample was calculated using the iCycler iQ5 software package (Bio-Rad, Munich, Germany). Absolute mRNA amounts were normalized to mRNA levels of the murine housekeeping gene *18S* or *Pipa* (*Cyclophilin*), respectively.

Table 2-3: Primer and probe sequences as used for real-time RT-PCR.

mRNA	Accession No.	primer sense, 5'→ 3'	primer antisense, 5'→ 3'	Probe, 5'FAM → 3'BHQ1
Pipa	NM_008907.1	GGCCGATGACGAGCCC	TGTCTTTGGAACTTTGTCTGC	TGGGCCGCGTCTCCTTCGA
hu p62	NM_001007225.1	GTTCCCGCATCATCACTCTTAT	GAATCTCGCCAGCTGTTTGA	TGTGAATCTCTTCATCCCAACCCAGGCT
Tgfb1	NM_011577.1	ACCCTGCCCCTATATTTGGA	CGGGTTGTGTTGGTTGTAGAG	TGGACACACAGTACAGCAAGGTCCT
18S	NR_003278.1	GTAACCCGTTGAACCCCATT	CCATCCAATCGGTAGTAGCG	EvaGreen® qPCR Mix
Ppara	NM_001113418.1	CCTTCCCTGTGAACTGACG	CCACAGAGCGCTAAGCTGT	EvaGreen® qPCR Mix
Col1a1	NM_007742.3	TGTGTGTTCCCTACTCAGCC	TGCTCTCTCCAAACCAGACG	EvaGreen® qPCR Mix
Il1b	NM_008361.3	GAGAGCCTGTGTTTTCCTCC	GAGTGCTGCCTAATGTCCC	EvaGreen® qPCR Mix
Tnf	NM_013693.2	CCATTCCTGAGTTCTGCAAAGG	AGGTAGGAAGGCCTGAGATCTTATC	EvaGreen® qPCR Mix
Hmgcr	NM_008255.2	ATCCAGGAGCGAACCAAGAGAG	CAGAAGCCCCAAGCACAAAC	EvaGreen® qPCR Mix
Srebf1	NM_011480.3	GGCTCTGGAACAGACACTGG	GGCCCGGGAAGTCACTGT	EvaGreen® qPCR Mix
Scd1	NM_009127.4	AGATCTCCAGTTCTTACACGACCAC	CTTTCATTTCAGGACGGATGTCT	EvaGreen® qPCR Mix
Elovl6	NM_130450.2	ACAATGGACCTGTCAGCAAA	GTACCAGTGCAGGAAGATCAGT	EvaGreen® qPCR Mix
Il6	NM_031168	AAGAAATGATGGATGCTACCAAACTG	GTACTCCAGAAGACCAGAGGAAATT	EvaGreen® qPCR Mix
Emr1/F4//80	NM_010130	CTTTGGCTATGGGCTTCCAGTC	GCAAGGAGGACAGAGTTTATCGTG	EvaGreen® qPCR Mix
Ccl2/Mcp1	NM_011333	CCACTCACCTGCTGCTACTCAT	CTGCTGGTGATCCTCTTGT	EvaGreen® qPCR Mix
Mlxipl/ Chrebp	NM_021455.4	CTGGGGACCTAAACAGGAGC	GAAGCCACCCTATAGCTCCC	EvaGreen® qPCR Mix
Cpt1a	NM_013495.2	CTCAGTGGGAGCGACTCTTCA	GGCCTCTGTGGTACACGACAA	EvaGreen® qPCR Mix
G6pc	NM_008061.3	AGGAAGGATGGAGGAAGGAA	TGGAACCAGATGGGAAAGAG	EvaGreen® qPCR Mix
Nos2	NM_010927.3	CTCACTGGGACAGCACAGAA	GATGTGGCCTTGTGGTGAA	EvaGreen® qPCR Mix
Ptgs2/Cox2	XM_192868	TGACCCCCAAGGCTCAAATAT	TGAACCCAGGTCCTCGCTTA	EvaGreen® qPCR Mix
Socs3	NM_007707.3	GCGAGAAGATTCCGCTGGTA	CCGTTGACAGTCTTCCGACA	EvaGreen® qPCR Mix
Ctgf	NM_010217.2	CTCCACCCGAGTTACCAATGACAA	CCAGAAAGCTCAAACTTGACAGGC	EvaGreen® qPCR Mix
Fasn	NM_007988.3	GGCTGCTACAAACAGACCAT	CACGGTAGAAAAGGCTCAGT	EvaGreen® qPCR Mix
Nlrp3	NM_145827.3	AGCCTTCCAGGATCCTCTTC	CTTGGGCAGCAGTTTCTTTC	EvaGreen® qPCR Mix
Pycard/Asc	NM_023258.4	CCAGGGTCACAGAAGTGGAC	CACGAACTGCCTGGTACTGT	EvaGreen® qPCR Mix
Srebf2	NM_033218.1	ACCTAGACCTCGCCAAAGGT	CGGATCACATTCCAGGAGA	EvaGreen® qPCR Mix
Tnfsf12/ Tweak	NM_011614.3	CTCATCTTAAGGCTGCCCCC	AAGGCCCCTCAGTGAACTTG	EvaGreen® qPCR Mix
Tfrc	Nm_011638.4	TTCCTACATCATCTCGCTTAT	CATAGTGTTCATCTCGCCAGA	EvaGreen® qPCR Mix
Hamp	NM_032541.1	TTGCGATACCAATGCAGAAGA	GATGTGGCTCTAGGCTATGTT	EvaGreen® qPCR Mix

Table 2-4: dNTP, dual-labelled probe-, $MgCl_2$ concentration, primer concentrations, and annealing temperatures as used for real-time RT-PCR.

mRNA	dNTPs	probe	$MgCl_2$	primer	annealing
Pipa	125 µM	1.5 pmole	3 mM	400 nM	60°C
hu p62	125 µM	1.5 pmole	5 mM	400 nM	60°C
Tgfb1	125 µM	1.5 pmole	4 mM	400 nM	60°C
18S	EvaGreen® qPCR Mix			200 nM	58°C
Ppara	EvaGreen® qPCR Mix			250 nM	60°C
Col1a1	EvaGreen® qPCR Mix			250 nM	60°C
Il1b	EvaGreen® qPCR Mix			250 nM	60°C
Tnf	EvaGreen® qPCR Mix			250 nM	60°C
Hmgcr	EvaGreen® qPCR Mix			250 nM	60°C
Srebf1	EvaGreen® qPCR Mix			100 nM	60°C
Scd1	EvaGreen® qPCR Mix			200 nM	60°C
Elovl6	EvaGreen® qPCR Mix			100 nM	60°C
Il6	EvaGreen® qPCR Mix			200 nM	60°C
Emr1F4//80	EvaGreen® qPCR Mix			150 nM	60°C
Ccl2/Mcp1	EvaGreen® qPCR Mix			250 nM	60°C
Mlxipl/Chrebp	EvaGreen® qPCR Mix			250 nM	60°C
Cpt1a	EvaGreen® qPCR Mix			250 nM	60°C
G6pc	EvaGreen® qPCR Mix			250 nM	60°C
Nos2	EvaGreen® qPCR Mix			200 nM	61°C
PtgsCox2	EvaGreen® qPCR Mix			250 nM	60°C
Socs3	EvaGreen® qPCR Mix			150 nM	57°C
Ctgf	EvaGreen® qPCR Mix			200 nM	60°C
Fasn	EvaGreen® qPCR Mix			150 nM	60°C
Nlrp3	EvaGreen® qPCR Mix			100 nM	59°C
Pycard/Asc	EvaGreen® qPCR Mix			200 nM	60°C
Srebf2	EvaGreen® qPCR Mix			250 nM	61°C
Tnfsf12/Tweak	EvaGreen® qPCR Mix			250 nM	61°C
Tfrc	EvaGreen® qPCR Mix			250 nM	60°C
Hamp	EvaGreen® qPCR Mix			250 nM	60°C

2.6.2 **Standard Dilution Series**

Real-time RT-PCR efficiency and quantification of target mRNAs in cDNA samples were determined using standards from 10 to 0.0001 attomoles of the real-time RT-PCR standard plasmid per well (2.3.2). The plasmids were diluted in TE buffer (AppliChem, Germany) and run alongside the samples to generate a standard curve. The necessary amount of plasmid DNA was calculated by the following formula:

c (target-DNA) [µmol/ml] = c (plasmid) [µg/ml] / MW * l

with MW = molecular weight of the DNA (approx. 660 g/mol) and l = length of plasmid and insert in bp.

2.6.3 **Quantification**

Quantification was done by comparing the calculated square mean values of transgenic samples with wild-type samples. The calculation was performed by the CFX Manager Software (Bio-Rad, Germany) in consideration of PCR efficiency (90-110%) and the R^2 value (>0.990) to ensure reproducibility. Square mean values of both, transgenic and wild-type animals, were normalized to an appropriate endogenous housekeeping gene.

2.7 **Western Blot Analysis**

2.7.1 **Preparation of Protein Samples**

Protein samples were either isolated from (A) QIAzol Lysates (2.5.1) or in (B) Laemmeli buffer. (A) Total protein was extracted in 700 µl QIAzol Lysis Reagent from the intermediate and lower phase of 2.5.1 after transferring it into a new reaction tube. 100% ethanol was added and subsequently vortexed. 1-bromo-3-chloropropane and distilled water were added, samples were vortexed and centrifuged (12,000 *x g*, 5 min, 4°C). 100% ethanol was added to the intermediate and lower phase, vortexed, and centrifuged (12,000 *x g*, 5 min, 4°C). After washing with 100% ethanol, the pellets were dissolved in 1% SDS. Protein concentrations were determined by the BCA Protein Assay kit (Thermo Fischer, USA) according to manufacturer´s guidelines. (B) Total protein was extracted in 500 µl lysis buffer (50 mM TrisHCL, pH 7.4, 1 mM EDTA, 150 mM NaCl, 1% Triton-X 100, 5 mM NaF, 0.25% Na-deoxycholate, 2 mM $NaVO_3$ and 1 x protease inhibitor (Complete from Roche, Germany) in distilled water) using a homogenizer (Kontes Pellet Pestle, ThermoFisher, Germany). Samples were centrifuged (14,000 *x g*, 15 min, 4°C), 250 µl of the supernated mixed with 750 µl 3x SDS-Sample buffer (188 mM TrisHCl, pH 6.8, 6% [w/v] SDS, 30% [w/v] glycerol, 0.015% [w/v] bromophenol blue and 15% [w/v] β-mercaptoethanol in distilled water), denatured at 95°C for 5 min, and stored at

-20°C. Protein concentrations were determined by the BCA Protein Assay kit (Thermo Fischer, USA) according to manufacturer´s guidelines using the protein lysates without 3x SDS-Sample buffer.

2.7.2 **SDS-Polyacrylamide Gel Electrophoresis (SDS-PAGE)**

Table 2-5: Composition of a 12% gel

	resolving gel	**stacking gel**
distilled water	6.6 ml	2.1 ml
30% acrylamide / 0.8% bisacrylamide solution	8 ml	0.5 ml
TrisHCl (1.5 M, pH 8.0)	5 ml	
TrisHCl (1 M, pH 6.8)		0.38 ml
SDS (10% [w/v])	200 µl	30 µl
APS (10% [w/v])	200 µl	30 µl
TEMED	20 µl	3 µl

(A) Samples were thawed on ice and diluted with 1% SDS in order to obtain the same protein amount. The samples were mixed with Roti®-Load 2 loading buffer and denatured for 10 min at 95°C. (B) Appropriate sample volumes were loaded onto the gel. A prestained protein marker (#671 Fermentas, Germany) was used to estimate molecular masses. Marker and samples were loaded onto the gel and separated in electrophoresis buffer (24.8 mM TrisHCl, 1.92 mM glycine, 0.1% [w/v] SDS) for 60 min at 80 V, followed by 2.5 h at 120 V. Gel preparation and electrophoresis were carried out using the BioRad Mini PROTEAN system (BioRad, Germany).

2.7.3 **Blotting**

Using the Mini-Transblot cell (Bio-Rad, Germany) the separated protein samples were transferred to a polyvinylidene fluoride (PVDF) membrane (Immobilon-FL, Millipore, Germany). Prior to blotting, the membrane was incubated in methanol for 30 s. Sponges, blotting papers, gel and membrane were equilibrated in transfer buffer (24.8 mM TrisHCl, 1.92 mM glycin, 0.05% [w/v] SDS, 20% methanol), followed

by gel sandwich preparation. Blotting was carried out overnight at 80 mA. In order to block unspecific binding sites the membranes were incubated with Rockland Blocking Buffer (RBB) for near-infrared Western blotting (Rockland, USA) for 1 h at room temperature prior to immunodetection.

2.7.4 **Immunodetection**

Antibodies were either diluted in PBS-T (0.1% [v/v] Tween 20 in PBS ($NaHPO_4$ 8.0 mmol/l, KH_2PO_4 1.5 mmol/l, NaCl 160 mmol/l in water)) containing 5% [m/v] dried milk powder (MP) or BSA or in RBB according to **table 2-6**. Membranes were incubated with primary antibodies with an incubation time and temperature as indicated in **table 2-6**. Subsequently, the membranes were washed twice with the primary antibody diluent, followed by two washing steps with PBST. Then, membranes were incubated with the labeled secondary antibody for 2 h at room temperature. After two washing steps with PBST followed by two washing steps with PBS for 5 min, blots were scanned with an Odyssey Infrared Imaging System (LI-COR Bioscience, Germany), and relative signal intensities were determined using the Odyssey software.

Table 2-6: Antibody dilutions, incubation time and temperature and secondary antibodies for immunodetection

Antibody (Source)	**Dilution**	**incubation**	**secondary antibody**
hu p62 (self made)	1:2,000 in PBST + 5% BSA	1 h at RT	anti rabbit 680 1:5,000 in RBB 1 h RT
Tubulin (Sigma-Aldrich, Germany)	1:1,000 in PBST + 5% MP	2 h at RT	anti mouse 800 1:10,000 in RBB 2 h RT
FASN (Cell Signaling , USA)	1:1,000 in RBB	2 h at RT	anti rabbit 680 1:5,000 in RBB 2 h RT
SREBF1 (Abcam, USA)	1:200 in PBST + 5% MP	2 h at RT	anti mouse 800 1:10,000 in RBB 1.5 h RT

Antibody (Source)	**Dilution**	**incubation**	**secondary antibody**
PPARA (Abcam, USA)	1:1,000 in PBST + 5% MP	18 h at 4°C	anti rabbit 680 1:5,000 in RBB 1.5 h RT
ELOVL6 (Sigma-Aldrich, Germany)	1:1,000 in PBST + 5% BSA	18 h at 4°C	anti rabbit 680 1:5,000 in RBB 2 h RT
Caspase 1 (Abcam, USA)	1:750 in RBB	18 h at 4°C	anti rabbit 680 1:5,000 in RBB 2 h RT
Interleukin-1 beta (R&D Systems, USA)	1:750 in RBB	3 h at RT	anti goat 800 1:10,000 in RBB 2h RT

2.8 Quantitative Determination of Thiobarbituric Acid Reactive Substances (TBARS)

Products of lipid peroxidation (conjugated dienes, lipid hydroperoxides, and thiobarbituric acid reactive substances) were measured by a fluorometric assay according to (Ohkawa et al., 1979). 10-20 mg liver tissues were homogenized in 1 x PBS ($NaHPO_4$ 8.0 mmol/l, KH_2PO_4 1.5 mmol/l, NaCl 160 mmol/l in water) containing 1% phosphatase inhibitor cocktail II (Sigma, Germany) and centrifuged. For protein precipitation 100 µl lysate were mixed with 200 µl ice cold 10% trichloroacetic acid and after incubation on ice, centrifuged for 10 min at 14,000 *x g*. The clear supernatant was mixed with equal volume of TBA (0.67% [w/v] in water) and heated for 15 min at 100°C. After cooling down to room temperature the fluorescence intensity of the samples was measured in duplicate on a 96 well plate at $\lambda_{ex/em}$ = 530 nm / 572 nm on the Wallac Victor^{TM}. TBARS are expressed as malondialdehyde (MDA) equivalents as µmol per mg liver tissue. A MDA standard is used to create a standard curve against which unknown samples were plotted.

2.9 **Fatty Acid Profile Analysis**

Approximately 10 mg dry weight of flash-frozen liver tissue sample were lyophilized to dryness, dissolved in a mixture of 500 µl methanol/toluene/sulfuric acid (50:50:2 [v/v/v]), and incubated at 55°C overnight. Subsequently, 400 µl of a 0.5 M NH_4CO_3, 2 M KCl solution were added to the sample, which was then centrifuged at room temperature. 100 µl of the upper phase were transferred to a gas chromatographic (GC) vial and measured. Fatty acid analysis was performed on an Agilent 6890N gas chromatograph coupled to an Agilent 5973N mass selective detector (both Agilent Technologies, Germany) and equipped with a non-polar J&WDB-5HT capillary column. Fatty acid measurements were performed by Katja Gemperlein (Saarland University, Pharmaceutical Biotechnology).

2.10 **Liver Histology and Quantitative Scoring System**

For histological examination, paraffin-embedded liver tissue specimens were cut in 0.5 µm sections, and stained with hematoxylin-eosin (HE) for histological features of steatohepatitis, with Sirius Red to evaluate hepatic collagen deposition and fibrosis, and Prussian Blue for iron deposition. Immunhistochemistry (IHC) was performed for a comprehensive characterization of the murine NASH model. Two investigators (Assoz. Prof. Dr. Johannes Haybäck, Medical University of Graz and Dr. Sonja M. Kessler, Pharmaceutical Biology, Saarland University), blinded to experimental conditions, examined sections for steatosis, apoptosis, fibrosis, portal and lobular inflammation, lobular infiltration, ductular reaction, hepatocellular iron, and p65 nuclear translocation as shown in **table 2-7**.

Table 2-7: Scoring system for steatosis, apoptosis, fibrosis, portal and lobular inflammation, lobular infiltration, ductular reaction, hepatocellular iron, and p65 nuclear translocation

scoring system			assessed by
steatosis	score 0	none	HE
	score 1	<5% of parenchyma involved	
	score 2	>5-20% of parenchyma involved	
	score 3	>20% of parenchyma involved	
	score 4	>50% of parenchyma involved	

scoring system	assessed by	scoring system	assessed by
apoptosis	score 0	none	HE and cleaved
	score 1	<2/20x	caspase 3 IHC
	score 2	2-4/20x	
	score 3	>4/20x	
fibrosis	score 0	none	Sirius Red
	score 0.2-0.8	mild perisinusoidal	
	score 1	perisinusoidal	
	score 2	portal/periportal and/or septal	
	score 3	portal/periportal and septal	
	score 4	cirrhosis	
portal inflammation	score 0	none to minimal	HE
	score 1	greater than minimal	
lobular inflammation	score 0	none	HE
	score 1	<2/20x	
	score 2	2-4/20x	
	score 3	>4/20x	
lobular infiltration with neutrophils	score 0	none	HE
	score 1	few	
	score 2	many	
ductular reaction	score 0	none	HE and K19 IHC
	score 1	rare-few (1-6)	
	score 2	many (>6)	
	score 3	cirrhosis with few	
	score 4	cirrhosis with many	
hepatocellular iron	score 0	no granules	Prussian Blue
	score 1	zone 1, granules seen at 40x	
	score 2	granules seen at 20x	
	score 3	granules seen at 10x	
	score 4	granules seen at 10x in zone 1 and 2	
Mallory Denk bodies	score 0	none	p62/sequestosome IHC and Ubiquitin IHC
	score 1	present	
nuclear translocation of p65	score 0	none	NFKB IF
	score 1	1-5 positive nucleoli/20x	
	score 2	6-12 positive nucleoli/20x	
	score 3	>13 positive nucleoli/20x	

2.10.1 **Fixation and Embedding of Liver Tissue and Preparation of Slides**

After roughly 24 h formalin-fixed liver tissues were embedded in an automated Tissue-Tek VIP (Sakura Finetek, Japan), and dehydrated with 7 x 100% ethanol followed by 3x xylol and embedded in paraffin. With a microtome 0.5 µm slices were cut from paraffin-embedded liver tissues.

2.10.2 **Staining and Embedding**

Due to the water solubility of the staining reagents, paraffin slides were hydrated with a series of xylol, followed by a series of alcohol (3 x 100% ethanol) prior to the actual staining. For HE stain slides were incubated for 10 min in hematoxylin, followed by blueing with running water for 5 min, and incubation in eosin for 2 min. The cell nucleus is stained magenta-blue, whereas the cytoplasm appears red-pink.

For Sirius Red stain slides were incubated with hematoxylin for 10 min followed by blueing for 10 min. Then, slides were incubated in Sirius Red solution (1/1,000 Direct Red 80 (Sigma-Aldrich, Germany) in picric acid solution 1.8% (saturated) (Sigma-Aldrich, Germany) for 1 h. The slides were subsequently washed twice in water with 0.5% acetic acid. Cells were stained yellow and collagen fibers red in bright field, collagen V appeared green and collagen I yellow-red under polarized light due to their birefringence. For polarization microscopy slides were put between two linear polarizing filters on Leica Stereomikroskop M 165 C microscope and through rotating one filter into a crossed position the birefringence appeared.

The Prussian blue stain began with incubation in a solution of saturated potassium hexacyanoferrate in water with 10% hydrogen chloride for 10 min, followed by a washing step with water and 10 min staining in a nuclear fast red solution (Sigma-Aldrich, Germany, #N069). Cells were stained pink and iron granules were stained blue.

Slides were dehydrated in a series of alcohol (3 x 100% ethanol) and 4 times xylol, prior to embedding with Entellan® (Merck, Germany, #107961) and then covered with a coverslip for long-term storage.

2.10.3 **Immunohistochemistry**

Paraffin sections were used for immunohistochemistry of cleaved caspase-3, a marker for apoptotic cells; alpha actin (smooth muscle), a marker for activated stellate cells; F4/80, a surface marker of mouse macrophages; cytokeratin 19, a marker for oval/progenitor cells, and cholangiocytes; ubiquitin and p62/sequestosome, both markers for Mallory Denk bodies, human p62/IGF2BP2-2 and the NFKB subunit p65. Immunohistochemical staining was performed after demasking of the sections with the appropriate method listed in **table 2-8**. The sections were immunostained with the appropriate antibody: concentration, incubation time, and temperature are listed in **table 2-8**. Subsequently, immunodetection was performed using distinct detection kits as listed in **table 2-8** according to the instructions of the manufacturer´s manual. After that, counterstaining with hematoxylin or DAPI for immunofluorescence (IF) was performed and sections were dehydrated and embedded with Entellan® (Merck, Germany, #107961). As negative controls sections were incubated without primary antibody.

Table 2-8: Antibody dilutions, demasking, incubation time, temperature, and immunodetection

Antibody (source)	demasking of antigens	dilution	incubation	detection system
cleaved caspase-3 (Cell Signaling , USA)	citrate buffer pH 6.0, 95°C, 10 min, water bath	1:1,000	18 h at 4°C	Dako CSA II with CSA Rabbit link / DAB
alpha SMA (Epitomics, USA)	citrate buffer pH 6.0, 95°C, 10 min, water bath	1:2,000	18 h at 4°C	Dako CSA II with CSA Rabbit link / DAB
F4/80 (AbD Serotec, UK)	citrate buffer pH 6.0, 95°C, 10 min, water bath	1:1,000	18 h at 4°C	Vectastain Peroxidase Elite ABC kit / DAB
K 19 (Epitomics, USA)	Epitop retrieval solution (Dako), 40 s, water bath	1:500	60 min at RT	Dako Envision / AEC
Ubiquitin (Dako, Denmark)	protease block 10 min	1:300	30 min at RT	Dako Real™ detection system / AEC
p62/sequestosome (Progen, Germany)	citrate buffer pH 6.0, 40 s, microwave	1:100	60 min at RT	Dako Envision / AEC
NFKB-p65 (Neomarkers, USA)	citrate buffer pH 6.0, 95°C, 10 min, water bath	1:1,000	18 h at 4°C	IF with Alexa Fluor 546 (Invitrogen, Germany) as secondary antibody
hu p62 (IGF2BP2-2) (selfmade)	citrate buffer pH 6.0, 40 s, microwave	1:1,000	60 min at RT	Dako Envision / AEC

2.10.4 Lipid Staining and Staining for Unesterified "Free" Cholesterol on Cryo Sections

Lipid accumulation and unesterified cholesterol was measured on frozen liver tissue sections (5 µm), and cut on a cryostat Frigocut 2800 (Reichert Jung, Germany). Sections were mounted on superfrost slides (ThermoScientific, Germany) and air dried. For lipid staining slides were treated as follows: after 2 min fixation with 4% neutral buffered formalin at RT, slides were incubated for 3 min in 50% ethanol followed by 3 min in Scharlach Red solution (0.3% [m/v] Scharlach Red (Roth, Germany, #0327.1) in 1:1 acetone with 70% ethanol), rinsed in 70% ethanol and counterstained with hematoxylin. Slides were embedded in a glycerin-gelatin gel. For staining of unesterified cholesterol, liver sections were fixed for 15 min in 4% neutral buffered formalin, and washed with PBS, and then treated with 10% fetal calf serum (FCS) in PBS for 30 min. Filipin (Sigma Chemicals, Germany) was dissolved in a small volume of dimethylsulfoxide, then diluted to 0.25 mg/ml in 10% FCS/PBS and added to the tissue for 1 h at room temperature. Slides were washed with 10% FCS/PBS once and PBS twice. Slides were coverslipped using FluorSave™ Reagent (Calbiochem, Germany), and after 24 h at 4°C slides were examined using Zeiss Cell Observer (Zeiss, Germany).

2.11 Statistics

Data analysis and statistics were performed using Microsoft Office 2010 software and OriginPro 8.6G. Effect of genotype, MCD diet, and their interactions were displayed as mean and median values ± SEM with 9-12 animals per group. Statistical differences were estimated by Kruskal-Wallis-ANOVA for nonparametric samples followed by post-hoc-analysis with Mann-Whitney-U-test. Differences were considered statistically significant when p values were less than 0.05.

3 RESULTS

3.1 *p62* Expression

The expression of the transgene p62/IGF2BP2-2 was quantified by real-time RT-PCR on transcript levels and Western blot analyses for protein expression throughout the experiment. Immunhistochemistry was used to determine the localization of the protein. We detected a consistent mRNA expression in MCD and ctrl diet fed animals for 2 and 4 weeks (**Figure 3-1A**). After 12 weeks the transcript levels dropped (**Figure 3-1A**). Still, protein expression was shown for all transgenic animals even after 12 weeks (**Figure 3-1B**). Immunohistochemical analyses of p62 confirmed the absence of p62/IGF2BP2-2 in wild-type animals and its expression in transgenic animals in a heterogenic cytosolic distribution (**Figure 3-1C**).

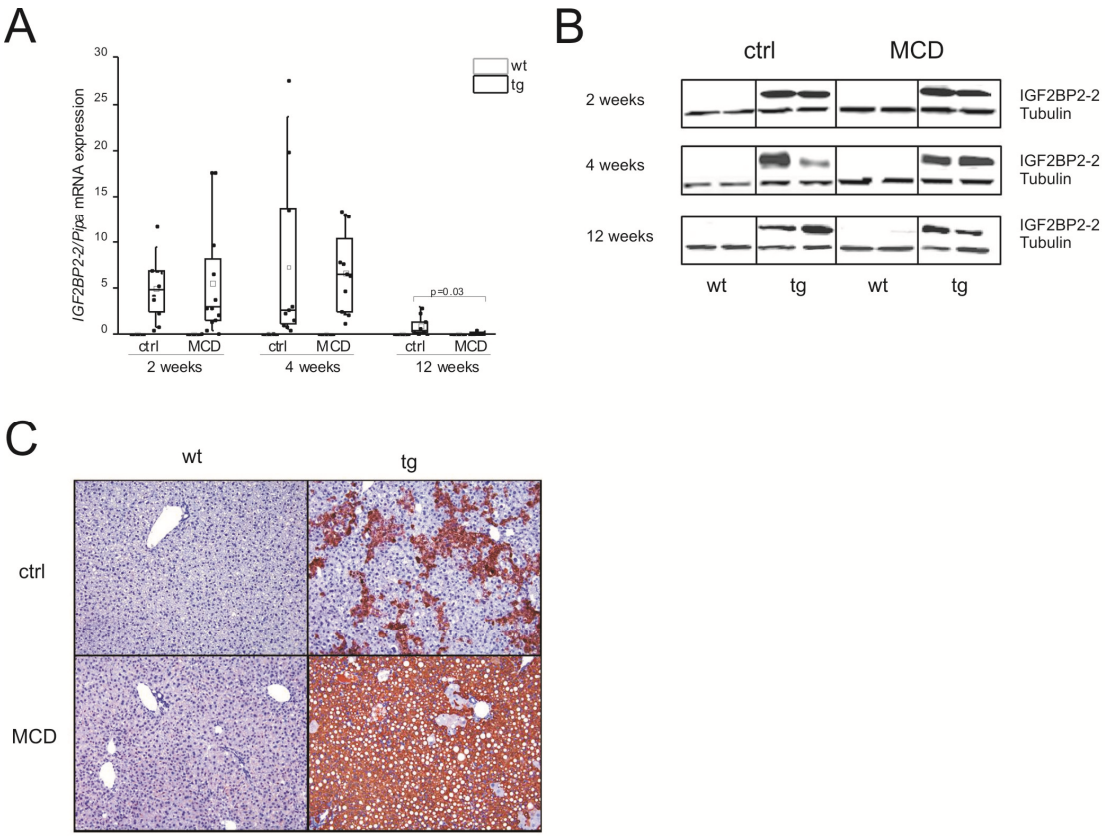

Figure 3-1: p62/IGF2BP2-2 expression in mice. (**A**) mRNA expression was determined by real-time RT-PCR of *p62/IGF2BP2-2* and is shown as ratio against the housekeeping gene *Pipa* (*cyclophilin*). Data are represented as individual values and box plots with median (—) and mean (□) in a five-number summary (n=9-12). (**B**) p62/IGF2BP2-2 protein expression verified by Western blot analysis. Representative blots from animals fed the MCD diet for 2, 4, and 12 weeks are shown. (**C**) Representative paraffin-embedded liver sections of mice fed the MCD diet for 2 weeks showed immunohistochemical stain for p62/IGF2BP2-2 expression (original magnification 200x).

3.2 p62 Amplifies Murine NASH and NASH-Induced Fibrosis

3.2.1 General Effects of the Dietary Manipulation

Mice of both genotypes exhibited different characteristics typical for the MCD diet. These comprised a loss of body and relative liver weight through feeding the MCD diet (**Figure 3-2**). All animals had a starting weight of around 10 ± 2 g and subsequently lost around 20-40% of body weight on the MCD diet, whereas animals on the ctrl diet gained weight (**Table 3-1**). MCD fed animals were cachectic, as seen in figure 3-2 compared to animals on ctrl diet after 12 weeks. Due to reduced VLDL from the liver (Anstee & Goldin, 2006), serum triglycerides and cholesterol were reduced in MCD animals, as were serum glucose levels. Elevated AST and ALT levels indicated liver damage induced by the MCD diet (**Table 3-1**).

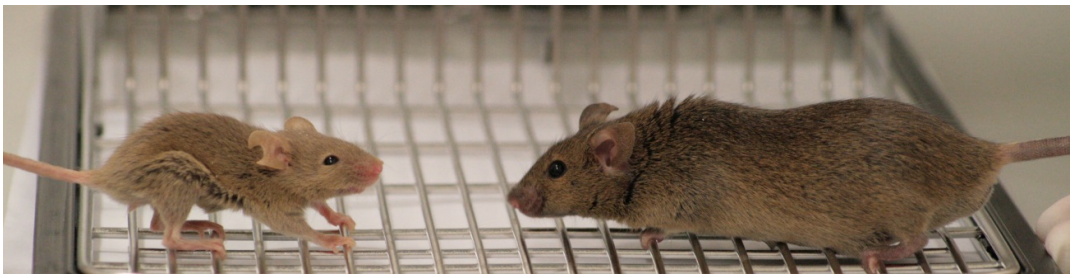

Figure 3-2: **Photograph of mice fed the MCD** (left) and ctrl (right) diet for 12 weeks.

Table 3-1: Weight parameters, serum parameters, and lipids of *p62* transgenic and wild-type mice fed the MCD diet for 2, 4, or 12 weeks. Values are expressed as mean ± SEM

	2 weeks				4 weeks				12 weeks			
	Ctrl		MCD		ctrl		MCD		ctrl		MCD	
	wt	tg	wt	tg	wt	tg	wt	tg	wt	tg	wt	tg
number animals [n]	10	10	12	12	10	10	12	12	10	9	9	11
body weight change [%]	91.3 ± 5.7	88 ± 6.2	-19.3 ± 0.9†	**-18.4 ± 0.9†‡**	103.9 ± 7.0	121.2 ± 11.3	-31.3 ± 1.3†	**-28.5 ± 1.3†‡**	188.2 ± 11.6	205 ± 16.1	-35.3 ± 1.4†	**-36.7 ± 0.7†‡**
relative liver weight [% of body weight]	4.8 ± 0.1	4.6 ± 0.1	3.4 ± 0.1†	**4.0 ± 0.2*†‡**	4.2 ± 01	4.1 ± 0.1	3.4 ± 0.1†	**3.5 ± 0.2†‡**	4.1 ± 0.3	4.1 ± 0.2	4.1 ±0.3	4.0 ± 0.3
serum ALT [U/L]	288.9 ± 83	233 ± 20	418 ± 36†	**469 ± 73†‡**	189 ± 38	222 ± 25	235 ± 40	209 ± 46	210 ± 25	**114 ± 14***	131 ± 16†	149 ± 24
serum AST [U/L]	1,568 ± 224	1,535 ± 162	2,404 ± 125†	**2,544 ± 207†‡**	1,845 ± 204	1,712 ± 253	2,813 ± 286†	3,057 ± 346†	2,322 ± 385	**1,171 ± 188***	2,088 ± 217	2,341 ± 202†
serum triglycerides [mg/dl]	244 ± 19	219 ± 17	107 ± 5†	**128 ± 11†‡**	211 ± 18	203 ± 21	95 ± 7†	**106 ± 5†‡**	234 ± 32	204 ± 23	71 ± 6†	**72 ± 5†‡**
serum HDL [mg/dl]	93.6 ± 6	97.5 ± 4	24.4 ± 2†	**20.9 ± 4†‡**	112 ± 8	119 ± 8	15 ± 2†	**18 ± 2†‡**	128 ± 11	140 ± 9	10 ± 0.5†	**12 ± 2†‡**
serum glucose [mg/dl]	234 ± 27	179 ± 15	67 ± 10†	**59 ± 7†‡**	193 ± 13	253 ± 36	59 ± 7†	**40 ± 5*†‡**	211 ± 25	200 ± 15	58 ± 8†	**64 ± 6†‡**
serum cholesterol [mg/dl]	122 ± 6	125 ± 5	47 ± 3†	**65 ± 8†‡**	135 ± 10	144 ± 5	33 ± 2†	**46 ± 5*†‡**	164 ± 15	164 ± 11	22 ± 2†	**26 ± 3†‡**
liver cholesterol [µg/mg liver dry weight]	11.5 ± 0.7	10.5 ± 0.8	14.9 ± 1.5†	**19.2 ± 1.5†‡**	12.3 ± 2.1	13.5 ± 2.1	13.9 ± 2.1	**20.3± 2.1*†‡**	14.6 ± 1.3	14.0 ± 2.6	14.0 ± 2.6	17.1 ± 2.4
Liver fatty acids [µg/mg liver dry weight]	106 ± 5	91 ± 8	140 ± 9†	**206 ± 16*†‡**	106 ± 21	116 ± 17	158 ± 24	**205 ± 24†‡**	126 ± 11	143 ± 21	233 ± 39	**261 ± 41‡**

* $p<0.05$ in comparison to wild-type

† $p<0.05$ in comparison to control diet

‡ $p<0.05$ in comparison to wild-type on control diet

3.2.2 **Steatosis**

Macroscopic examination of the livers from MCD and control diet animals showed distinct alterations in *p62* transgenic animals: Wild-type animals in the control diet showed no macroscopic abnormalities, whereas *p62* transgenic livers appeared more yellowish and showed bright areas (**Figure 3-3**). Livers from animals on MCD were conspicuously smallish compared to livers from ctrl diet. MCD livers appeared pale with a visible change of the microarchitecture of the liver, which was more pronounced in *p62* transgenic animals (**Figure 3-3**).

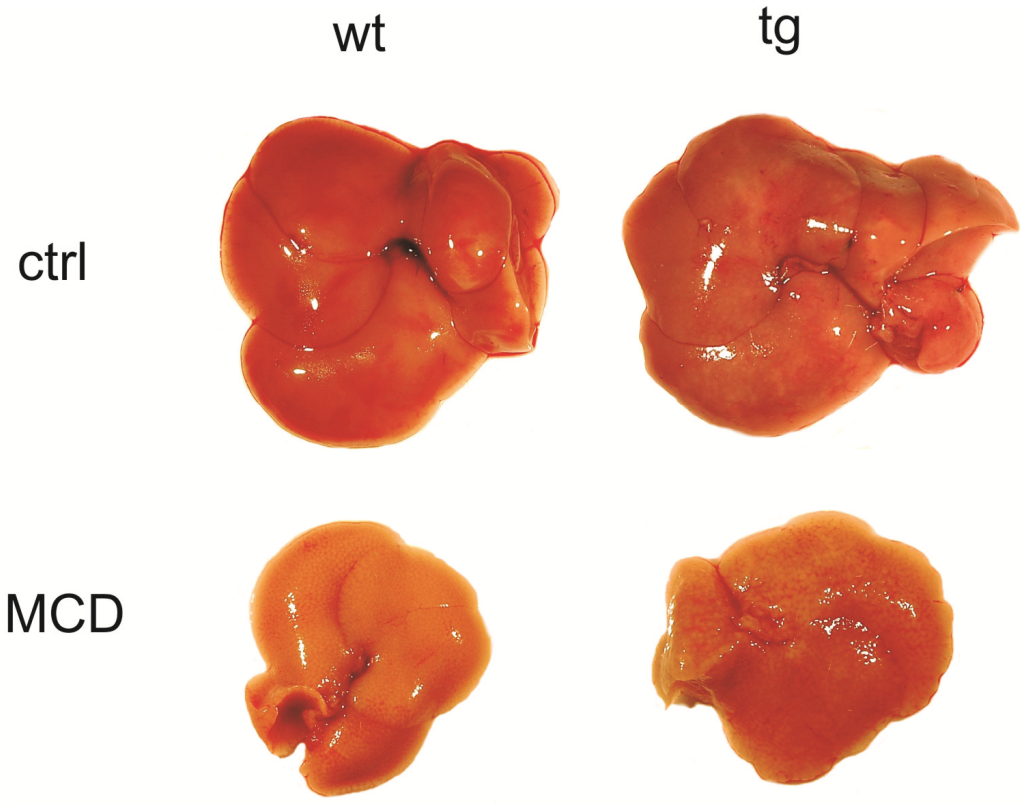

Figure 3-3: **Representative macroscopic pictures** of the livers from animals fed with the respective diet for 12 weeks. All pictures were taken in the same manner regarding objective and distance.

Animals of both genotypes developed steatosis on the MCD diet. However, histological analyses showed an amplification of mediovesicular steatosis in *p62* transgenic animals compared to their wild-type littermates as early as 2 weeks (p=0.04) (**Figure 3-4A, B**). The relative liver weight was significantly increased in

transgenics (p=0.02) (**Table 3-1**) and therefore consistent with the histological changes.

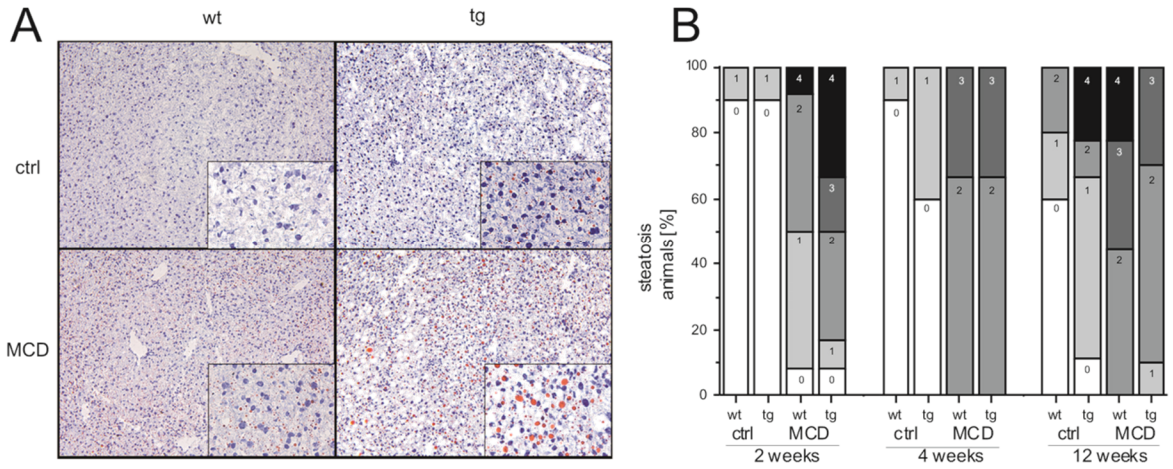

Figure 3-4: p62 amplifies steatosis. (**A**) Liver sections stained to demonstrate lipid accumulation by Scharlach red staining on cryo sections from animals fed with the respective diet for 2 weeks (original magnification 200x and 500x for inserts). (**B**) Steatosis score shows percentage of animals classified into appropriate scores (see table 2-7).

In order to determine whether the p62-mediated amplification of NASH is based on the steatosis already present in the beginning of MCD feeding due to early *p62* expression, a temporal inhibition of *p62* expression prior to feeding the MCD diet was performed by feeding doxycycline. Thus, *p62* expression started at the same time as feeding the diet. Prior to the experiment a preliminary test was performed to determine the correct doxycycline concentration as well as the onset of *p62* expression after withdrawal of doxycycline. Doxycycline was fed either in a concentration of 25 µg/ml or 50 µg/ml in drinking water. Animals were subsequently sacrificed 2, 3, 4, or 5 days after doxycycline withdrawal. After 2 days of doxycycline withdrawal no *p62* expression was detectable with both concentrations, whereas after 3 days *p62* expression was restored (**Figure 3-5A**). For the actual experiment a concentration of 25 µg/ml doxycycline was used up until 2 days prior to feeding the MCD diet for 3 weeks.

In the actual experiment *p62* expression was confirmed by measuring the mRNA expression rate (**Figure 3-5B**). Histological evaluation revealed a significantly

increased steatosis in transgenics compared to wild-type animals without doxycycline (**Figure 3-5C**). In addition, a tendency of increased steatosis through doxycycline feeding was seen in wild-type animals (**Figure 3-5C**). Hence, *p62* expression leads to increased steatosis irrespective of an early or simultaneous expression.

To determine the underlying mechanistic origin of steatosis formation in *p62* transgenic animals, animals without doxycycline feeding were used.

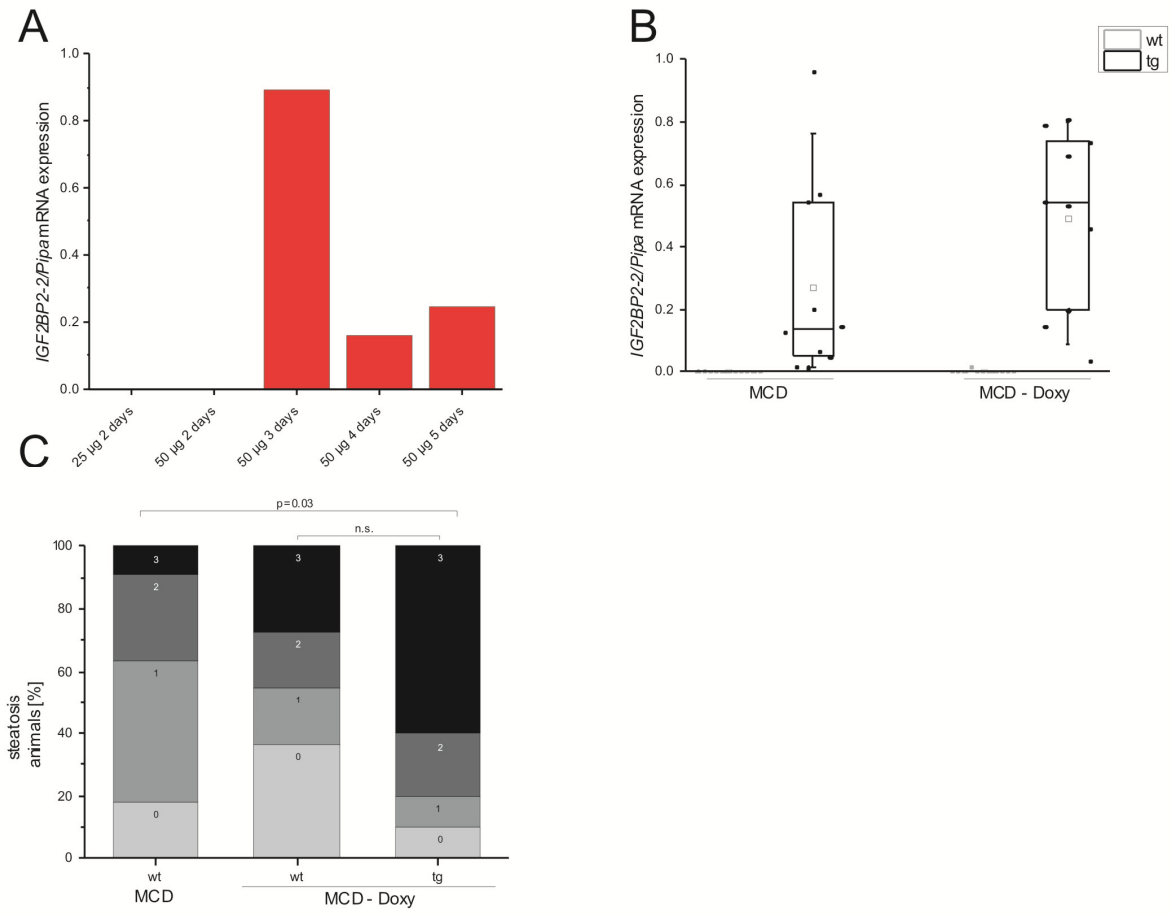

Figure 3-5: Doxycycline-dependent temporal suppression of *p62* expression. (**A**) Preliminary test with single animals fed with 25 µg/ml doxycycline until 2 days or 50 µg/ml doxycycline in drinking water until 2, 3, 4, or 5 days prior to sacrificing the animals. *p62* is shown as ratio against the housekeeping gene *Pipa (cyclophilin)*. (**B**) Actual experiment with animals fed with 25 µg/ml doxycycline up until 2 days prior to feeding of the MCD diet for 3 weeks. Relative mRNA expression of *p62* is shown as ratio against the housekeeping gene *Pipa*. Data are represented as individual values and box plots with median (—) and mean (□) in a five-number summary (n=10). (**C**) Steatosis score with percentage of animals classified into appropriate scores (see table 2-7).

GC-MS analyses of hydrolyzed lipids revealed significantly higher levels of hepatic fatty acids in *p62* transgenic mice (**Figure 3-6A**), whereas serum triglycerides were not found to be different from wild-type animals (**Table 3-1**). The hepatic fatty acid pattern further indicated strong alterations in *p62* transgenic animals compared to their wild-type littermates after 2 weeks on the MCD diet (**Table 3-2**). In particular, a more pronounced accumulation of monounsaturated fatty acids compared to saturated and polyunsaturated fatty acids was seen in transgenic animals (**Figure 3-6B-D**). Both the elevated ratio of palmitoleic acid (C16:1) to palmitic acid (C16:0) (**Figure 3-6E**) and a very pronounced induction of oleic acid (C18:1) indicated an increased desaturase activity (**Figure 3-6F**). In fact, the desaturase stearoyl-CoA desaturase (*Scd*) 1, being responsible for the formation of C16:1 and C18:1 fatty acids, tended to be increased in *p62* transgenic animals, despite a strong downregulation upon the MCD diet (**Figure 3-7A**). After 4 and 12 weeks the increased steatosis formation due to p62 expression disappeared as seen histologically (**Figure 3-4**) and confirmed by GC-MS analyses (**Table 3-3, 3-4**).

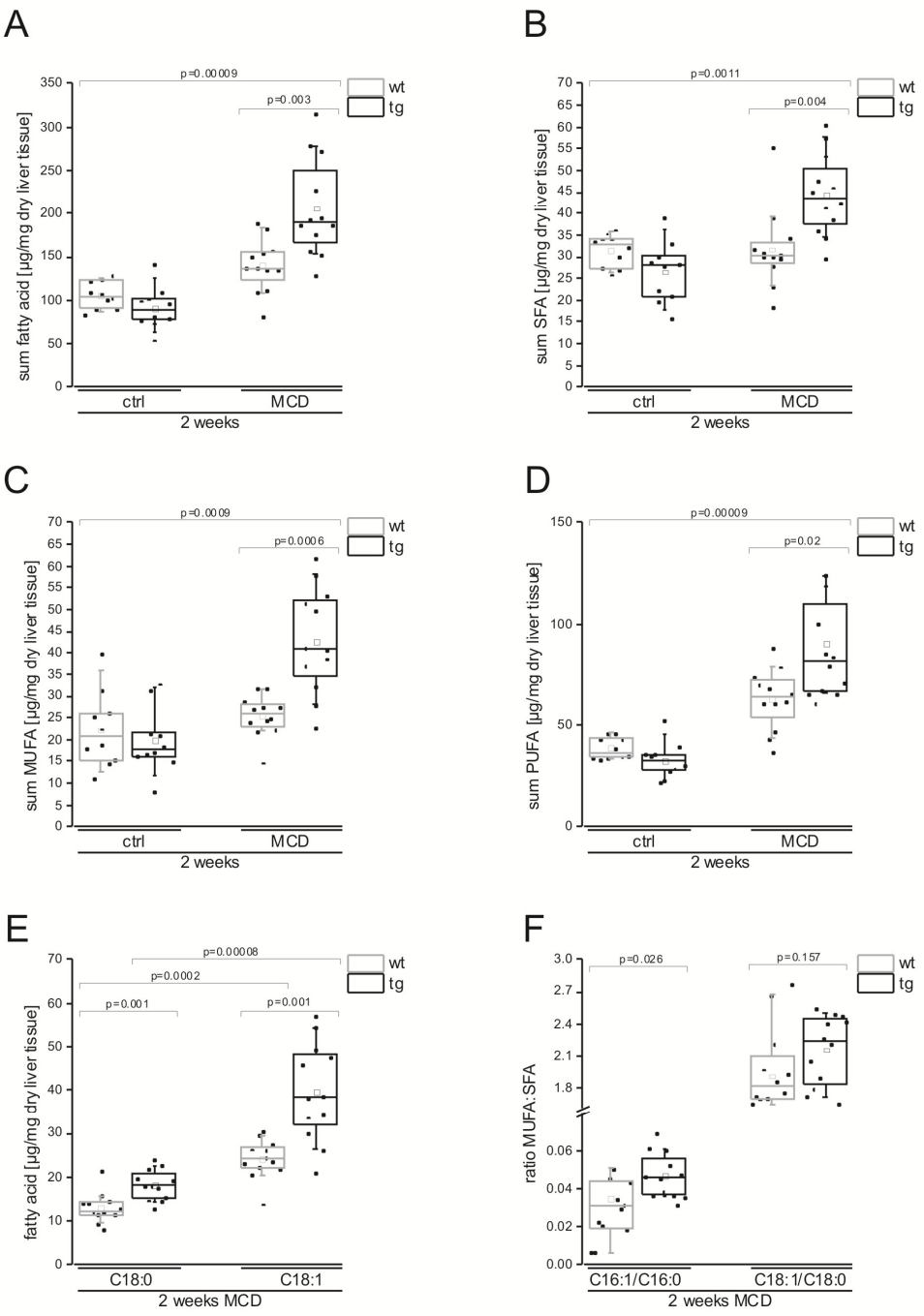

Figure 3-6: p62 alters fatty acid pattern. (**A-F**) GC-MS fatty acid analyses of mice fed the MCD or ctrl diet for 2 weeks. Liver tissues were lyophilized and analyzed by GC-MS. Sum of all fatty acids (**A**), sum of saturated fatty acids (SFA) (**B**), sum of monounsaturated fatty acids (MUFA) (**C**), sum of polyunsaturated fatty acids (PUFA) (**D**), and stearic acid (C18:0), as well as oleic acid (C18:1) (**E**) are represented as individual values and box plots with median (—) and mean (□) in a five-number summary (n=9-12). (**F**) Ratios of C16:1/C16:0 and C18:1/C18:0 from animals fed the MCD diet for 2 weeks are likewise displayed.

Table 3-2: GC-MS fatty acid analyses of mice fed the MCD or ctrl diet for 2 weeks. Values [µg/mg dry liver tissue] are expressed as mean ± SEM (n=9-12). Liver tissues were lyophilized and analyzed by GC-MS.

Fatty acid	ctrl wt	ctrl tg	*a*	MCD wt	*b*	MCD tg	***c***	*d*	*e*
12:0	0.004 ± 0.001	0.001 ± 0.001	0.027	n.d.	0.0009	0.003 ± 0.002	**0.166**	0.619	0.07
14:0	0.25 ± 0.04	0.25 ± 0.05	0.970	0.24 ± 0.04	0.817	0.43 ± 0.04**	**0.003**	0.023	0.005
15:0	0.01 ± 0.003	0.01 ± 0.003	0.113	0.02 ± 0.01	0.105	0.05 ± 0.01*	**0.035**	0.0007	0.002
16:0	17.23 ± 0.79	16.08 ± 1.43	0.623	17.16 ± 1.63	0.531	23.85 ± 1.65**	**0.006**	0.005	0.0033
16:1	1.69 ± 0.29	1.51 ± 0.30	0.570	0.57 ± 0.10	0.00009	1.13 ± 0.12**	**0.005**	0.817	0.138
17:0	0.11 ± 0.01	0.06 ± 0.01**	0.021	0.23 ± 0.03	0.00002	0.34 ± 0.03*	**0.01**	0.0009	0.0001
17:1	0.02 ± 0.01	0.01 ± 0.01	0.046	0.003 ± 0.003	0.023	0.01 ± 0.01	**0.514**	0.619	0.117
18:0	12.64 ± 0.57	9.41 ± 0.81**	0.006	13.08 ± 0.97	0.817	18.15 ± 1.00**	**0.0014**	0.0003	0.0009
18:1	20.13 ± 2.51	17.98 ± 2.07	0.678	24.11 ± 1.28	0.106	39.66 ± 3.27***	**0.001**	0.0003	0.0009
18:2	17.88 ± 0.87	16.42 ± 1.60	0.241	23.90 ± 2.15	0.060	36.28 ± 6.34*	**0.040**	0.0027	0.004
18:3	0.23 ± 0.05	0.27 ± 0.10	0.571	1.50 ± 0.28	0.00009	2.99 ± 0.46**	**0.003**	0.00009	0.00009
20:0	0.22 ± 0.05	0.10 ± 0.03	0.045	0.14 ± 0.03	0.373	0.33 ± 0.05***	**0.0007**	0.00009	0.138
20:1	0.40 ± 0.03	0.30 ± 0.04*	0.045	0.81 ± 0.14	0.023	1.99 ± 0.27**	**0.002**	0.00009	0.00009
20:2	0.45 ± 0.04	0.53 ± 0.06	0.385	1.67 ± 0.17	0.00009	2.94 ± 0.25***	**0.0006**	0.00009	0.00009
20:3	1.09 ± 0.09	0.89 ± 0.14	0.186	2.87 ± 0.37	0.00009	5.15 ± 0.44***	**0.0006**	0.00009	0.00009
20:4	13.69 ± 0.58	10.37 ± 0.80**	0.011	16.49 ± 1.15	0.044	23.20 ± 1.81**	**0.006**	0.00009	0.00015
22:0	0.59 ± 0.11	0.29 ± 0.07*	0.031	0.31 ± 0.03	0.093	0.50 ± 0.03***	**0.0007**	0.038	0.921
22:1	0.01 ± 0.003	0.003 ± 0.003	0.387	0.01 ± 0.01	0.933	0.04 ± 0.01	**0.091**	0.035	0.129
22:4	0.57 ± 0.05	0.51 ± 0.08	0.273	4.24 ± 0.48	0.00009	6.25 ± 0.56*	**0.0036**	0.00009	0.00009
22:6	4.72 ± 0.28	3.82 ± 0.29*	0.054	12.08 ± 0.90	0.00009	14.06 ± 1.05	**0.214**	0.00009	0.00009
23:0	0.08 ± 0.01	0.04 ± 0.004***	0.0003	0.08 ± 0.01	0.921	0.10 ± 0.01	**0.194**	0.0002	0.223
24:0	0.42 ± 0.02	0.31 ± 0.02**	0.003	0.45 ± 0.02	0.249	0.63 ± 0.05**	**0.0013**	0.0001	0.0009

a = p-value of comparison of ctrl wt and ctrl tg

b = p-value of comparison of wt ctrl and wt MCD

c = p-value of comparison of MCD wt and MCD tg

d = p-value of comparison of tg ctrl and tg MCD

e = p-value of comparison of wt ctrl and tg MCD

Table 3-3: GC-MS fatty acid analyses of mice fed the MCD or ctrl diet for 4 weeks. Values [µg/mg dry liver tissue] are expressed as mean ± SEM (n=9-12). Liver tissues were lyophilized and analyzed by GC-MS.

Fatty acid	ctrl wt	ctrl tg	*a*	MCD wt	*b*	MCD tg	***c***	*d*	*e*
12:0	0.003 ± 00.2	0.005 ± 0.003	0.871	0.004 ± 0.004	0.543	0.003 ± 0.003	**1**	0.543	0.543
14:0	0.45 ± 0.12	0.50 ± 0.14	0.734	0.44 ± 0.08	0.817	0.62 ± 0.10	**0.260**	0.307	0.156
15:0	0.03 ± 0.01	0.05 ± 0.01*	0.087	0.07 ± 0.02	0.211	0.03 ± 0.02	**0.095**	0.053	0.318
16:0	19.65 ± 3.98	22.88 ± 4.16	0.623	21.78 ± 3.58	0.717	29.32 ± 3.99	**0.260**	0.176	0.223
16:1	2.89 ± 0.92	2.65 ± 0.91	0.970	0.74 ± 0.21	0.023	1.09 ± 0.22	**0.340**	0.081	0.081
17:0	0.12 ± 0.02	0.17 ± 0.03	0.140	0.33 ± 0.06	0.019	0.34 ± 0.07	**0.977**	0.044	0.008
17:1	0.05 ± 0.02	0.05 ± 0.03	0.609	n.d	0.008	n.d	**1**	0.053	0.008
18:0	12.20 ± 2.07	14.08 ± 1.93	0.571	21.62 ± 2.97	0.027	28.99 ± 3.42	**0.175**	0.0022	0.0009
18:1	19.47 ± 4.68	19.77 ± 3.93	0.970	25.50 ± 4.72	0.448	32.80 ± 4.92	**0.403**	0.060	0.044
18:2	14.12 ± 2.63	17.35 ± 2.75	0.385	32.26 ± 4.74	0.008	43.56 ± 4.82	**0.141**	0.0007	0.0003
18:3	0.18 ± 0.05	0.31 ± 0.07	0.112	2.19 ± 0.46	0.0003	2.73 ± 0.54	**0.665**	0.00009	0.00009
20:0	0.33 ± 0.11	0.33 ± 0.09	0.427	0.20 ± 0.05	0.234	0.31 ± 0.08	**0.619**	0.869	0.765
20:1	0.49 ± 0.10	0.63 ± 0.11	0.427	1.13 ± 0.25	0.060	1.13 ± 0.29	**0.885**	0.336	0.234
20:2	0.40 ± 0.09	0.60 ± 0.08	0.064	1.83 ± 0.34	0.0027	2.30 ± 0.41	**0.507**	0.0005	0.0003
20:3	1.00 ± 0.27	1.27 ± 0.25	0.273	2.82 ± 0.52	0.011	3.41 ± 0.54	**0.371**	0.005	0.0022
20:4	11.65 ± 2.09	12.39 ± 1.46	0.734	20.20 ± 3.11	0.052	22.91 ± 2.91	**0.707**	0.005	0.009
22:0	0.56 ± 0.15	0.54 ± 0.10	0.791	0.12 ± 0.07	0.002	0.43 ± 0.10*	**0.019**	0.621	0.448
22:1	0.04 ± 0.03	0.03 ± 0.02	0.545	n.d	0.129	n.d	**1**	0.021	0.129
22:4	0.37 ± 0.08	0.56 ± 0.08	0.140	3.95 ± 0.83	0.0011	3.54 ± 0.71	**0.862**	0.0011	0.0011
22:5	0.04 ± 0.02	0.07 ± 0.02	0.322	0.77 ± 0.20	0.0007	0.51 ± 0.13	**0.339**	0.088	0.029
22:6	2.28 ± 0.35	2.55 ± 0.32	0.791	7.47 ± 1.06	0.005	8.21 ± 1.16	**0.977**	0.0001	0.00009
23:0	0.07 ± 0.01	0.09 ± 0.01	0.473	0.06 ± 0.02	0.505	0.04 ± 0.03	**0.119**	0.006	0.015
24:0	0.34 ± 0.07	0.40 ± 0.05	0.571	0.50 ± 0.07	0.093	0.66 ± 0.10	**0.285**	0.027	0.016
24:1	0.14 ± 0.05	0.06 ± 0.04	0.231	n.d	0.008	0.17 ± 0.06**	**0.007**	0.157	0.751
sum FA	106.0 ± 20.85	115.88 ± 16.55	0.678	157.87 ± 24.11	0.156	204.74 ± 23.71	**0.285**	0.009	0.008
sum SFA	33.75 ± 6.34	39.06 ± 6.09	0.521	45.12 ± 6.78	0.277	60.74 ± 7.71	**0.194**	0.044	0.019
Sum MUFA	23.08 ± 5.59	23.19 ± 4.87	0.910	27.36 ± 5.15	0.621	35.19 ± 5.25	**0.341**	0.121	0.060
sum PUFA	36.93 ± 7.94	40.09 ± 4.16	0.678	71.49 ± 10.48	0.023	88.47 ± 10.03	**0.285**	0.0009	0.0017

a = p-value of comparison of ctrl wt and ctrl tg

b = p-value of comparison of wt ctrl and wt MCD

c = p-value of comparison of MCD wt and MCD tg

d = p-value of comparison of tg ctrl and tg MCD

e = p-value of comparison of wt ctrl and tg MCD

Table 3-4: GC-MS fatty acid analyses of mice fed the MCD or ctrl diet for 12 weeks. Values [µg/mg dry liver tissue] are expressed as mean ± SEM (n=9-12). Liver tissues were lyophilized and analyzed by GC-MS.

Fatty acid	ctrl wt	ctrl tg	*a*	MCD wt	*b*	MCD tg	***c***	*d*	*e*
12:0	0.04 ± 0.02	0.07 ± 0.02	0.037	0.05 ± 0.01	0.128	0.07 ± 0.04	**0.433**	0.281	1
14:0	0.53 ± 0.11	0.70 ± 0.09	0.153	0.84 ± 0.19	0.131	0.75 ± 0.15	**0.761**	0.879	0.342
15:0	0.04 ± 0.01	0.09 ± 0.01**	0.005	0.22 ± 0.08	0.004	0.19 ± 0.06	**0.790**	0.323	0.077
16:0	25.57 ± 2.96	29.00 ± 3.73	0.391	30.26 ± 4.91	0.391	33.56 ± 5.04	**0.761**	0.543	0.245
16:1	2.85 ± 0.66	3.83 ± 0.58	0.131	2.13 ± 0.47	0.596	1.98 ± 0.42	**0.820**	0.019	0.342
17:0	0.16 ± 0.02	0.21 ± 0.02*	0.079	0.37 ± 0.07	0.025	0.35 ± 0.05	**0.649**	0.095	0.01
17:1	0.07 ± 0.03	0.11 ± 0.03	0.373	0.01 ± 0.01	0.155	n.d	**0.315**	0.0007	0.027
18:0	16.12 ± 1.45	16.39 ± 2.66	0.488	26.04 ± 4.17	0.131	31.76 ± 4.80	**0.494**	0.028	0.018
18:1	25.00 ± 4.01	29.00 ± 3.97	0.540	39.56 ± 7.06	0.094	45.56 ± 8.48	**0.820**	0.197	0.098
18:2	17.68 ± 1.40	20.93 ± 4.50	0.653	53.26 ± 11.59	0.005	64.14 ± 11.90	**0.649**	0.005	0.002
18:3	0.31 ± 0.07	0.60 ± 0.10*	0.025	4.01 ± 0.92	0.004	3.18 ± 0.71	**0.543**	0.0006	0.0002
20:0	0.21 ± 0.05	0.37 ± 0.12	0.540	0.54 ± 0.13	0.037	0.40 ± 0.08	**0.323**	0.543	0.113
20:1	0.65 ± 0.11	0.80 ± 0.15	0.488	1.60 ± 0.40	0.153	1.70 ± 0.38	**0.879**	0.081	0.038
20:2	0.39 ± 0.04	0.72 ± 0.16*	0.155	2.69 ± 0.49	0.0038	2.48 ± 0.38	**0.649**	0.0011	0.0001
20:3	1.07 ± 0.13	1.52 ± 0.28	0.307	5.22 ± 0.97	0.005	4.52 ± 0.71	**0.595**	0.0024	0.0002
20:4	14.71 ± 1.49	13.33 ± 1.86	0.236	27.08 ± 4.53	0.055	24.06 ± 4.27	**0.649**	0.081	0.130
22:0	0.40 ± 0.08	0.47 ± 0.11	0.967	0.39 ± 0.07	0.903	0.42 ± 0.06	**1**	0.939	0.504
22:1	0.01 ± 0.01	0.05 ± 0.02*	0.092	0.13 ± 0.05	0.014	0.03 ± 0.02*	**0.044**	0.242	0.643
22:4	0.52 ± 0.07	1.05 ± 0.37	0.206	7.76 ± 2.25	0.055	7.65 ± 1.35	**0.939**	0.0004	0.0001
22:5	0.07 ± 0.02	0.15 ± 0.03*	0.055	1.73 ± 0.42	0.0009	1.04 ± 0.18	**0.129**	0.0003	0.0001
22:6	2.73 ± 0.29	2.79 ± 0.25	0.903	8.59 ± 1.66	0.008	6.12 ± 0.80	**0.171**	0.004	0.003
23:0	0.07 ± 0.01	0.06 ± 0.01	0.270	0.03 ± 0.01	0.016	0.01 ± 0.01	**0.242**	0.0008	0.0014
24:0	0.23 ± 0.03	0.27 ± 0.03	0.236	0.42 ± 0.10	0.094	0.25 ± 0.05	**0.128**	1	0.379
24:1	0.14 ± 0.04	0.10 ± 0.05	0.270	0.20 ± 0.09	0.967	0.28 ± 0.05	**0.538**	0.044	0.060
sum FA	125.84 ± 11.47	143.28 ± 20.85	0.967	232.99 ± 39.38	0.0662	260.69 ± 41.39	**0.879**	0.040	0.032
sum SFA	43.37 ± 4.24	47.93 ± 6.21	0.653	59.49 ± 9.51	0.206	67.82 ± 10.00	**0.595**	0.149	0.053
sum MUFA	28.74 ± 4.76	33.89 ± 4.21	0.596	43.62 ± 7.82	0.111	49.55 ± 9.19	**0.761**	0.323	0.113
sum PUFA	39.11 ± 2.90	47.47 ± 9.46	0.967	115.94 ± 21.07	0.006	126.23 ± 21.58	**0.879**	0.006	0.001

a = p-value of comparison of ctrl wt and ctrl tg

b = p-value of comparison of wt ctrl and wt MCD

c = p-value of comparison of MCD wt and MCD tg

d = p-value of comparison of tg ctrl and tg MCD

e = p-value of comparison of wt ctrl and tg MCD

Due to the p62-induced amplification of hepatic lipid content the hepatic expression of genes involved in lipogenesis, fatty acid catabolism, as well as cholesterol and glucose metabolism were analyzed. An array of lipogenic genes was investigated with the most distinct effect of p62 on the expression of the lipogenic transcription factor sterol regulatory binding transcription factor (*Srebf*) 1, which was increased after 2 and 4 weeks (**Figure 3-7B**). The lipogenic gene fatty acid synthase (*Fasn*) (**Figure 3-7C**), was significantly downregulated upon MCD feeding in both genotypes without significant alterations between the genotypes. Protein analyses of FASN confirmed the observed transcriptional downregulation (**Figure 3-7D**).

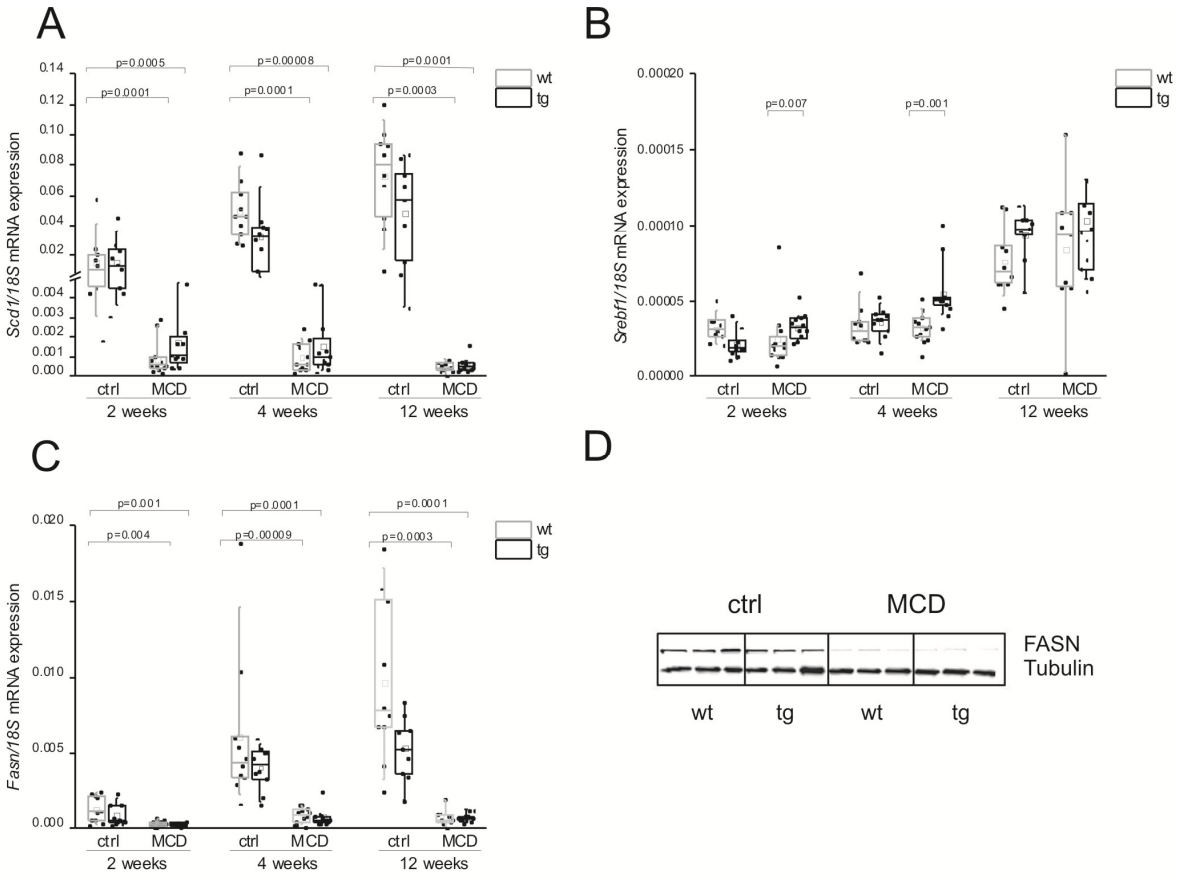

Figure 3-7: Expression of lipogenic genes. The ratio of (**A**) *Scd1*, (**B**) *Srebf1*, and (**C**) *Fasn* against the housekeeping gene *18S* is shown. Data are represented as individual values and box plots with median (—) and mean (□) in a five-number summary (n=9-12). (**D**) FASN protein expression as verified by Western blot analysis. Representative Western blot from animals fed the MCD and ctrl diet for 12 weeks is shown.

The expression of p62 had no consistent effect on neither the mRNA expression nor protein levels of the lipolysis regulator peroxisome proliferator-activated receptor (*Ppar*) a (**Figure 3-8A, B**), and of the promotor of β-oxidation, carnitine palmitoyl-transferase (*Cpt*) 1a (**Figure 3-8C**).

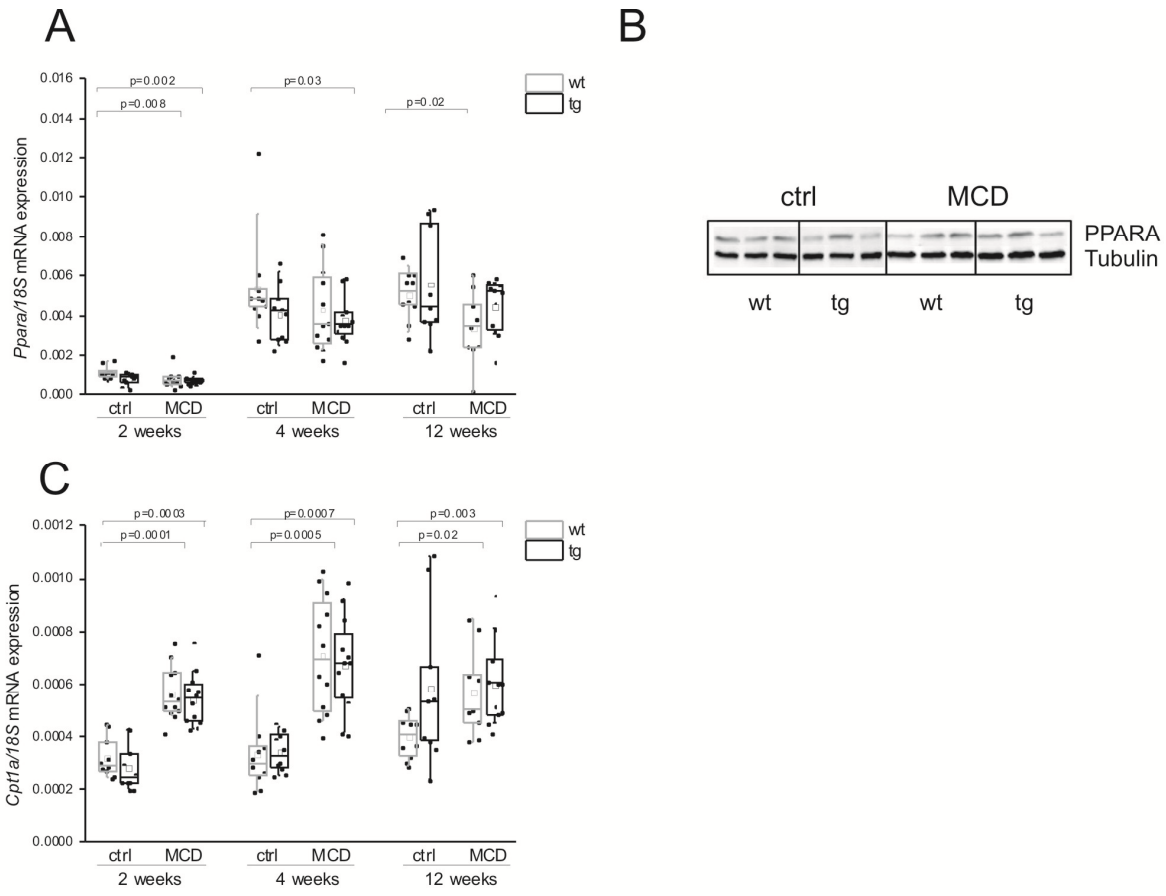

Figure 3-8: Lipolytic gene and protein expression. Gene expression of (**A**) *Ppara* and (**C**) *Cpt1a*. The ratio against the housekeeping gene *18S* is shown. Data are represented as individual values and box plots with median (—) and mean (□) in a five-number summary (n=9-12). (**B**) PPARA protein expression verified by Western blot analysis. Representative Western blot from animals fed the MCD and ctrl diet for 2 weeks is shown.

The expression of the transcription factor MLX interacting protein-like (*Mlxipl*), also known as carbohydrate response element binding protein (*Chrebp*), as a regulator of glycolysis and lipogenesis was downregulated due to the MCD diet itself. This effect

was further amplified in *p62* transgenic mice (**Figure 3-9A**). Concordantly, we observed a downregulation of serum glucose levels in the MCD fed animals with an even more pronounced decrease after 4 weeks in *p62* transgenics (p=0.04) (**Table 3-1**). The gene expression analysis of the rate-limiting enzyme for gluconeogenesis, glucose-6-phosphatase (*G6pc*), revealed a downregulation by the MCD diet with no effect of p62 (**Figure 3-9B**).

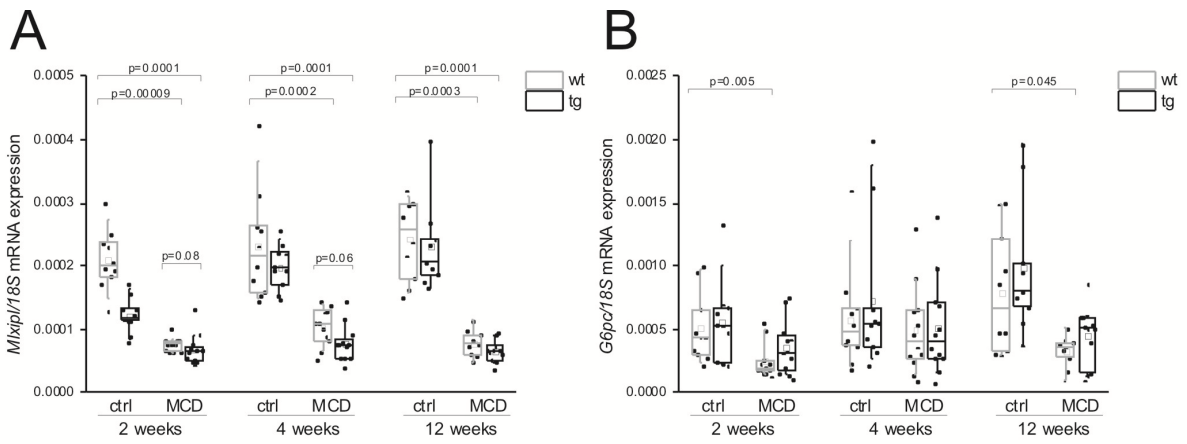

Figure 3-9: Altered glucose metabolism on the MCD diet and during p62 expression. Gene expression of (**A**) *Mlxip/Chrebp* and (**B**) *G6pc* is displayed as ratio against the housekeeping gene *18S*. Data are represented as individual values and box plots with median (—) and mean (□) in a five-number summary (n=9-12).

Both liver cholesterol and serum cholesterol were distinctly elevated in *p62* transgenic mice (**Figure 3-10A, B**). Filipin staining for free cholesterol revealed a significant increase of free cholesterol in *p62* transgenic animals on the MCD diet (**Figure 3-10C, D**). Accordingly, the mRNA levels of the rate-limiting enzyme for cholesterol synthesis, Hmg-CoA reductase (*Hmgcr*), were upregulated after 2 weeks (**Figure 3-10E**). Still, expression of the cholesterol metabolism-related transcription factor sterol regulatory element binding transcription factor (*Srebf*) 2 was significantly increased only after 4 weeks (**Figure 3-10F**).

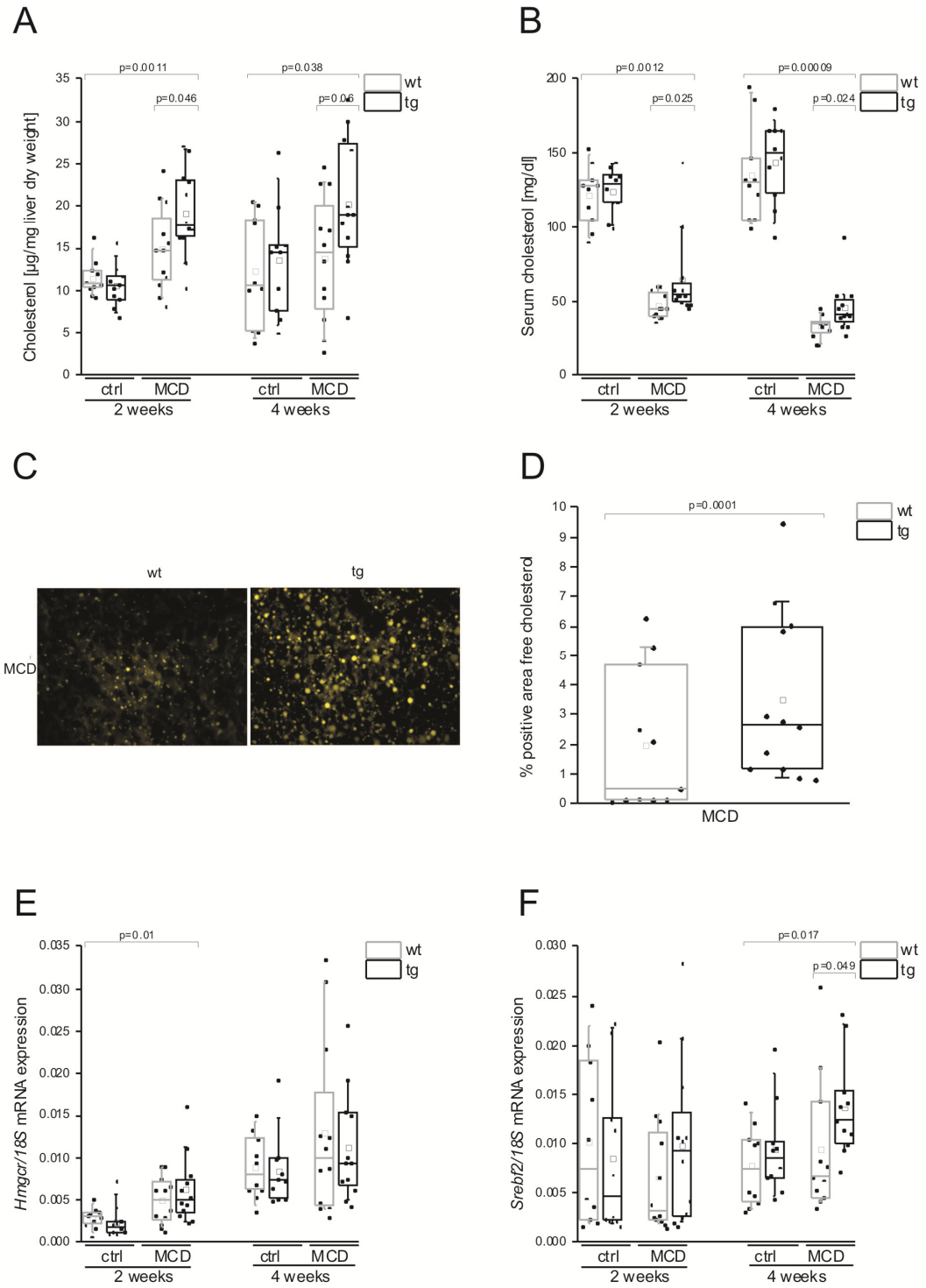

Figure 3-10: p62 expression elevates serum and liver cholesterol. (**A**) Hepatic and (**B**) serum cholesterol concentrations in mice fed the respective diet for 2 or 4 weeks. (**C**) Representative cryo sections stained with Filipin for hepatic free cholesterol in mice fed the MCD diet for 4 weeks (original magnification 400x) with (**D**) corresponding quantification (mean out of 5 randomly picked sections on the slide). (**E-F**) Relative hepatic mRNA expression of *Hmgcr* (**E**) and *Srebf2* (**F**) are shown as ratio against *18S*. Data are represented as individual values and box plots with median (—) and mean (□) in a five-number summary (n=9-12).

3.2.3 **Inflammation**

Regarding NASH as an inflammatory liver disease we investigated the effect of p62 on inflammation in more detail. After 2 weeks on the MCD diet histological analyses of HE stained liver sections revealed first changes towards a steatohepatitic phenotype with increased inflammatory infiltrations (**Figure 3-11A**). *p62* transgenic mice revealed a trend towards a higher inflammatory response throughout the experiment on MCD and control diet, with significant changes after 2 and 4 weeks for lymphocytic infiltrations (p=0.02 and p=0.01, respectively) (**Figure 3-11B, C**).

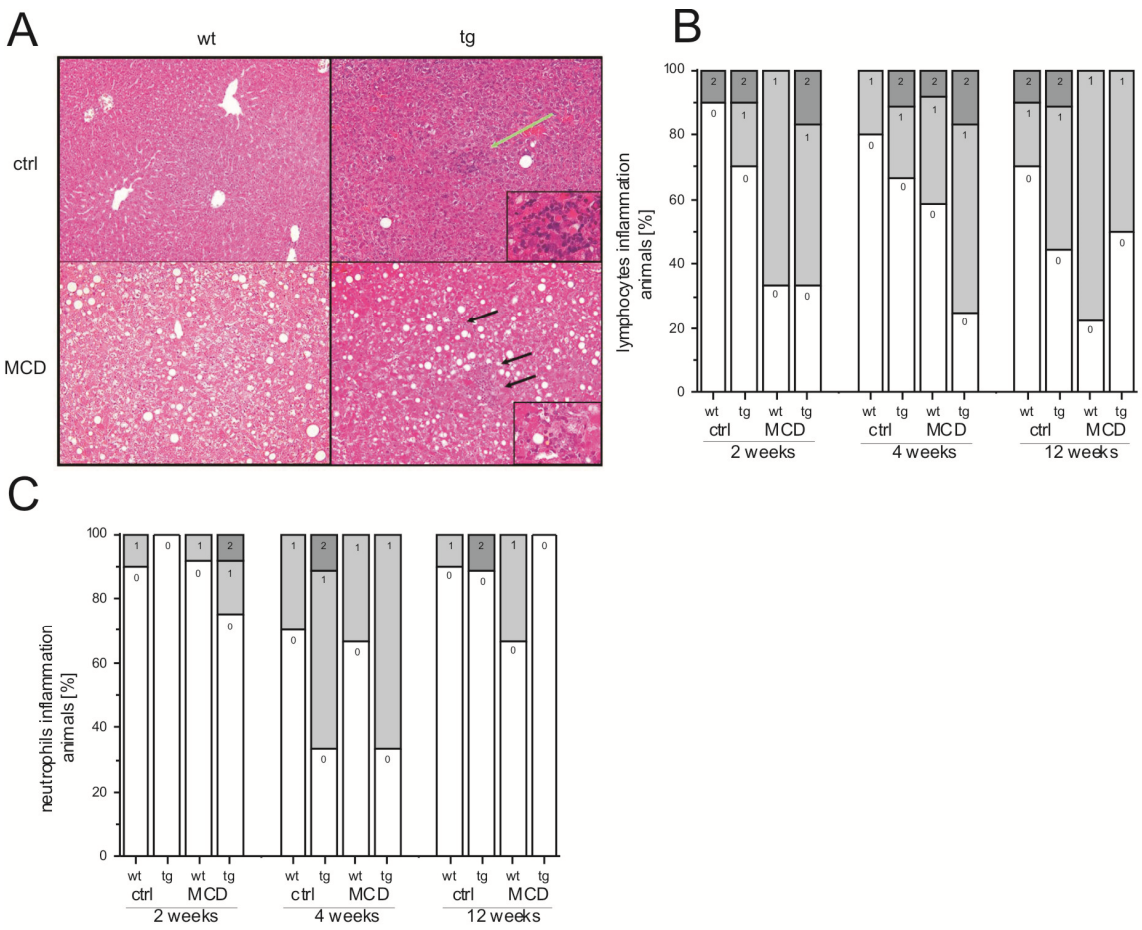

Figure 3-11: p62 expression increases inflammation. (**A**) Representative HE stains of paraffin-embedded liver sections from mice treated for 4 weeks with MCD or ctrl diet (original magnification 200x and 500x for inserts). The green arrow indicates neutrophilic infiltration, whereas the black arrows show the lobular lymphocyte inflammation. Inflammation scores show percentage of animals classified into appropriate scores with (**B**) for lobular lymphocyte inflammation and (**C**) for lobular neutrophil infiltrations (table 2-7).

After 4 weeks steatohepatitis became manifest by the formation of Mallory Denk bodies detected by immunohistochemical staining of sequestosome and ubiquitin (**Figure 3-12**).

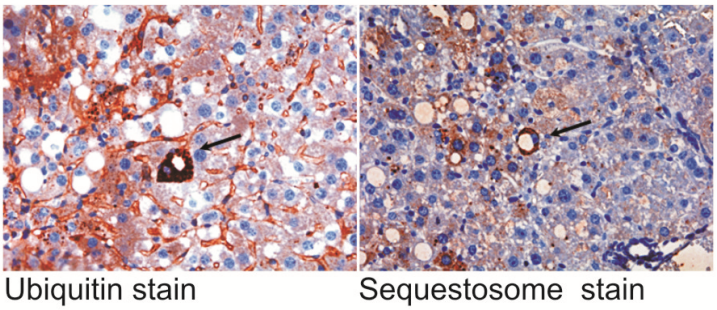

Figure 3-12: NASH manifestation due to MCD diet. Immunohistochemical stain against ubiquitin (left panel) and sequestosome (right panel) for appearance of Mallory-Denk bodies in *p62* transgenic animals after 4 weeks on the MCD diet (original magnification 500x).

As oxidative stress is regarded as a hallmark and amplifier of hepatic inflammation (Yesilova et al., 2005), we assessed hepatic iron deposition and lipid peroxidation, both indicators of oxidative stress (Fujita et al., 2009). Both genotypes on the MCD diet had elevated hepatic iron deposition at all time points with a significantly higher iron accumulation in *p62* transgenic mice (p=0.002, p=0.03, and p=0.02 for 2, 4, and 12 weeks) (**Figure 3-13A, B**). An increased transcript level of the catalytic iron carrier transporter transferrin receptor (*Tfrc*) (**Figure 3-13C**) as well as an upregulation of the hormone hepcidin, also known as hepcidin antimicrobial polypeptide (*Hamp*), as a regulator of iron homeostasis was associated with this observation (**Figure 3-13D**).

Since hepatocellular iron is known as a promoter of oxidative stress, we assessed lipid peroxidation. Here, p62 expression significantly increased lipid peroxidation as analyzed by TBARS assay. At 2 weeks, even control diet fed transgenics exhibited increased TBARS levels compared to wild-types (p=0.038) (**Figure 3-13E**).

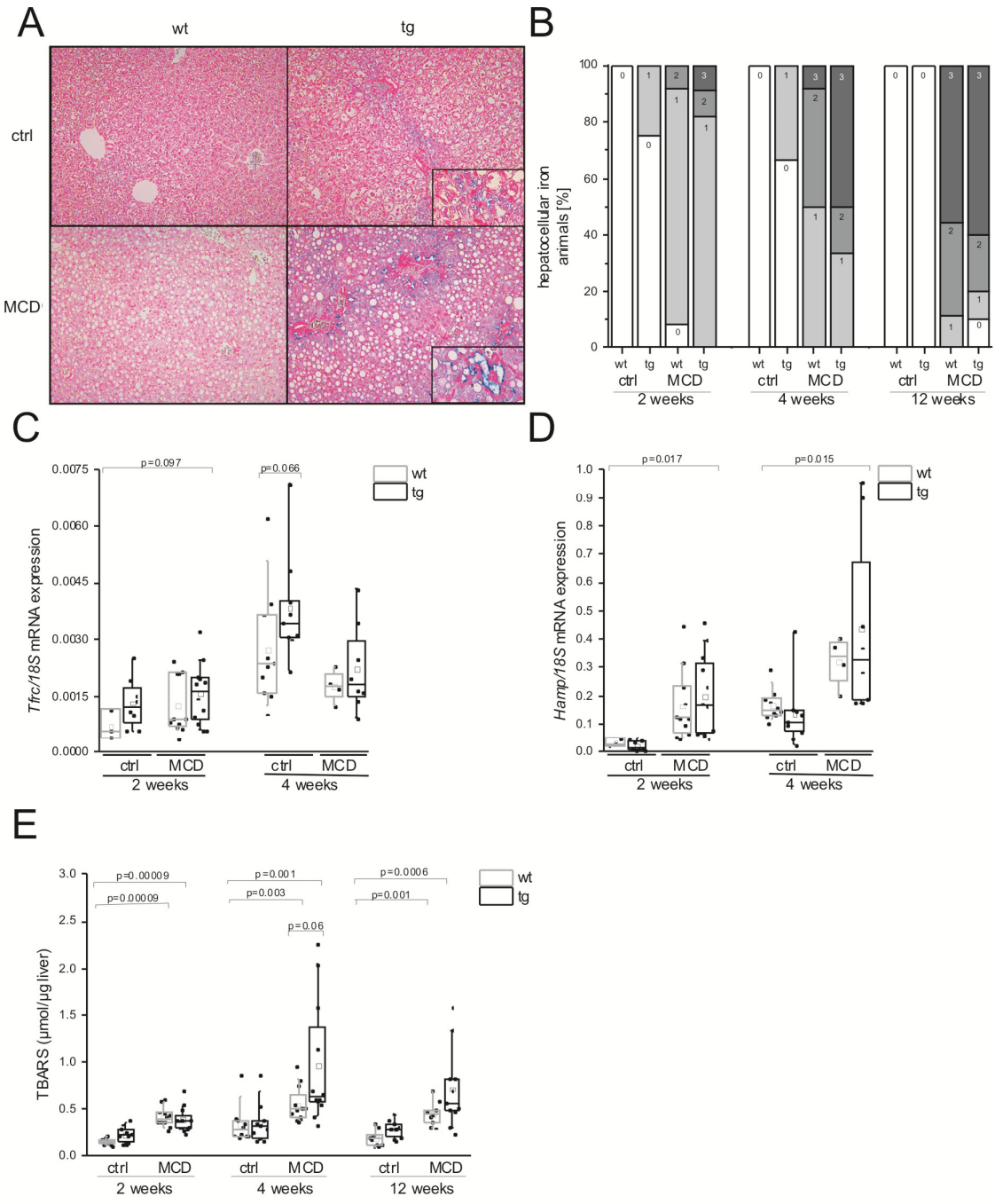

Figure 3-13: **p62 expression leads to increased iron accumulation and ROS production.** (**A**) Representative paraffin-embedded liver sections stained with Prussian blue for iron accumulation from animals fed the respective diet for 4 weeks (original magnification 200x and 500x for inserts) with the corresponding hepatocellular iron score (**B**) for all time points (table 2-7). Relative hepatic mRNA expression of the iron homeostatis regulation genes (**C**) catalytic transferrin receptor (*Tfrc*) and (**D**) hepcidin antimicrobial polypeptide (*Hamp*) are shown as ratio against the housekeeping gene *18S*. Data are represented as individual values and box plots with median (—) and mean (□) in a five-number summary (n=2-12). (**E**) Hepatic thiobarbituric acid reactive substances (TBARS) were measured to indicate lipid peroxidation and represented as individual values and box plots with median (—) and mean (□) in a five-number summary (n=9-12).

The inflammatory response is mediated by transcription factors, NFKB being the most important one of them (He & Karin, 2011). The activation of NFKB was assessed by immunofluorescence and the detection of nuclear translocation of its subunit p65 (**Figure 3-14A**). The *p62* transgenic animals showed a strong tendency for increased nuclear translocation with a significant increase even in the control diet after 12 weeks (**Figure 3-14B**).

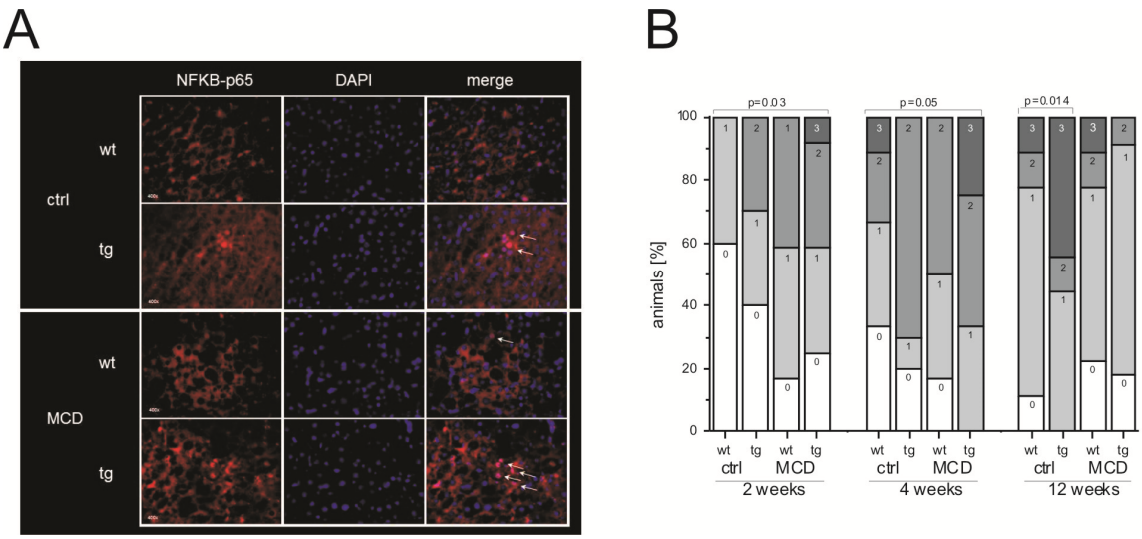

Figure 3-14: **p62 expression amplifies the activation of NFKB.** (**A**) Immunofluorescent staining with anti-NFKB-p65 (red, left panel), DAPI for nuclei (blue, middle panel), and merge (right panel) shows activation of NFKB through translocation to the nucleus (white arrows) with the corresponding scoring (**B**). The scoring displays percentage of animals classified into appropriate scores (see table 2-7).

The relative mRNA expression of some key inflammatory cytokines and chemokines regulated by NFKB was measured. Consistent with the histological results an elevated inflammatory response manifested as an inflammatory gene transcript profile with elevated levels of tumor necrosis factor (*Tnf*) and inducible nitric synthase 2 (*Nos2*) at 2 and 4 weeks in *p62* transgenic mice (**Figure 3-15A, B**). The MCD diet further led to an upregulation of prostaglandin-endoperoxide synthase (*Ptgs/Cox*) 2, and of the chemokine (C-C motif) ligand 2 (*Ccl2/Mcp1*) with a further amplification in *p62* transgenic animals (**Figure 3-15C, D**). The hepatic expression of interleukin 6 was in

general very low, but the livers from *p62* transgenic mice appeared to have somewhat higher *Il6* expression levels (**Figure 3-15E**). In addition, the expression of the suppressor of cytokine signaling (*Socs*) 3, which is strongly induced by a variety of cytokines and plays an important role in NASH (Tilg, 2010; Yoshimura et al., 2007), is upregulated after 2 weeks in *p62* transgenic animals and tends to be further increased also at later time points (**Figure 3-15F**).

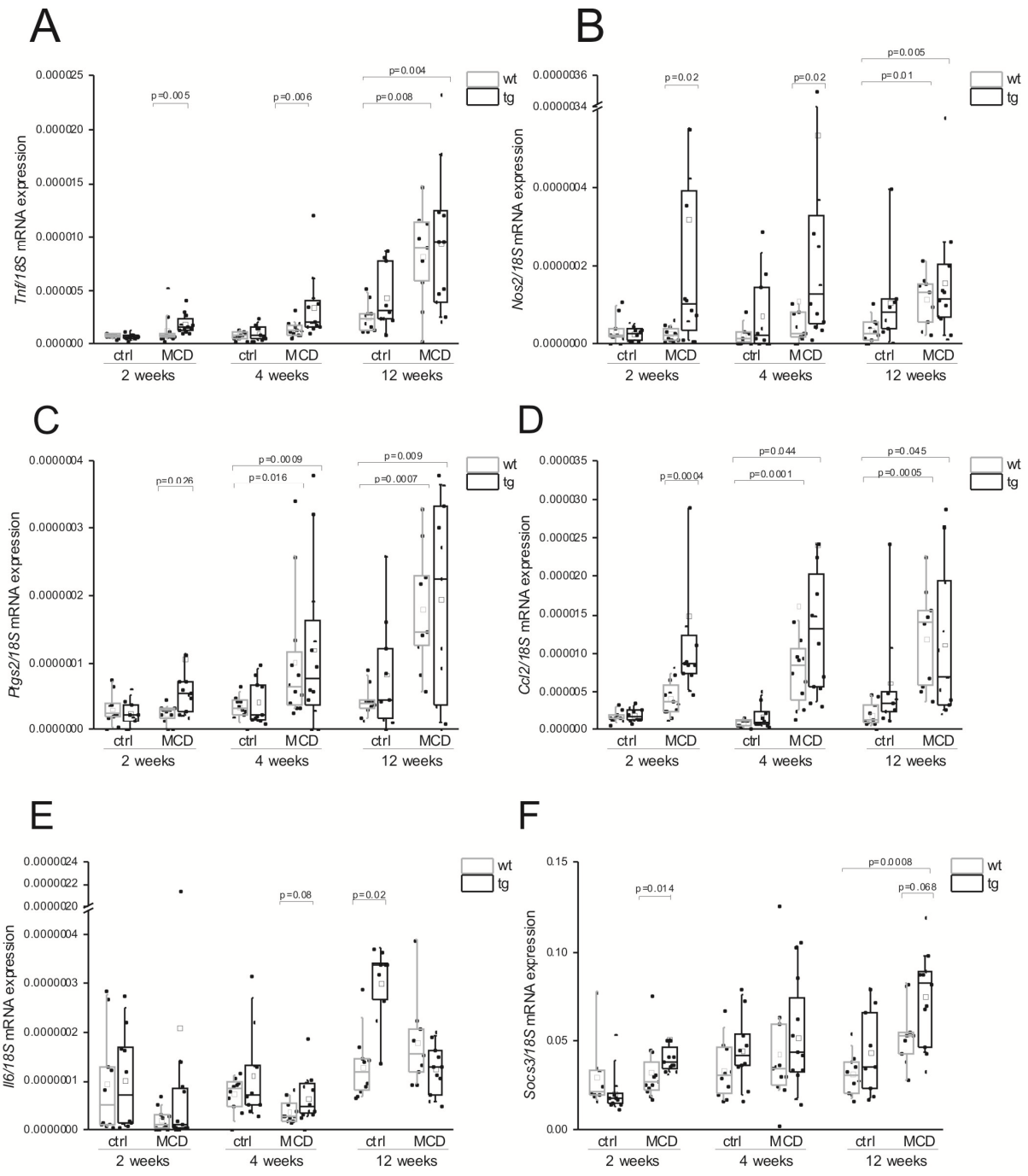

Figure 3-15: p62 amplifies the inflammatory response in NASH. Gene expression analysis of an array of cytokines and chemokines with (**A**) tumor necrosis factor (*Tnf*), (**B**) inducible nitric oxide synthase (*Nos*) 2, (**C**) prostaglandin-endoperoxid synthase (*Ptgs/Cox*) 2, (**D**) chemokine (C-C motif) ligand 2 (*Ccl2/Mcp1*), (**E**) interleukin (*Il*) 6 and, (**F**) suppressor of cytokine signaling (*Socs*) 3 from whole liver by quantitative real-time RT-PCR are expressed as ratio against the *18S* housekeeping gene. Data are represented as individual values and box plots with median (—) and mean (□) in a five-number summary (n=9-12).

A statistically significant upregulation of Interleukin (*Il*) 1b mRNA as a downstream target of NFKB activation was measured as early as 2 weeks in *p62* transgenic mice (**Figure 3-16A**). Since protein levels of hepatic IL-1beta (2.4-fold increase with p=0.014) as well as the inflammasome components *Nlrp3* and *Asc* tended to be increased in *p62* transgenics, an elevated inflammasome activation can be assumed (**Figure 3-16B-D**).

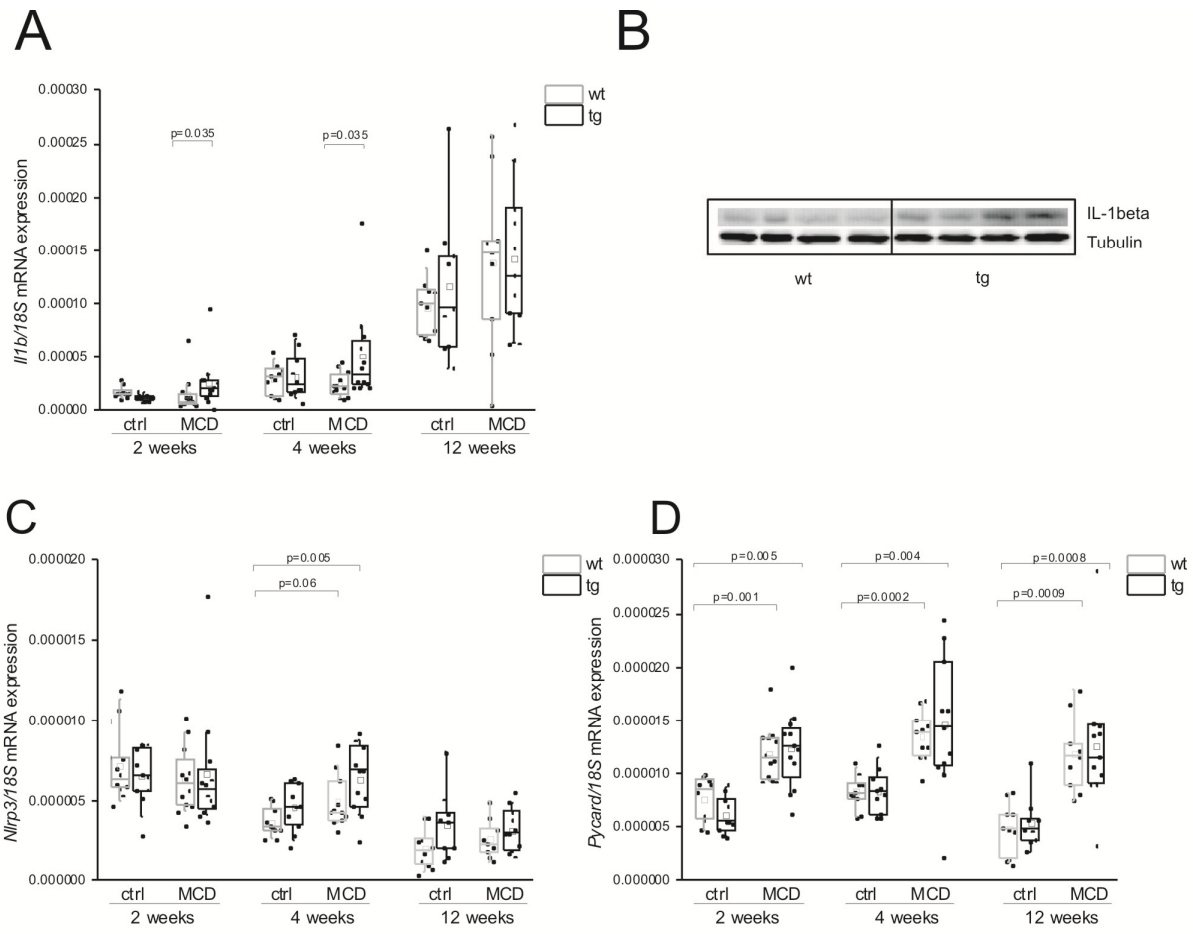

Figure 3-16: **p62 leads to inflammasome activation**. Gene expression analyses of (**A**) interleukin (*Il*)1b from whole liver by quantitative real-time RT-PCR is expressed as ratio against *18S* as housekeeping gene. Data are represented as individual values and box plots with median (—) and mean (□) in a five-number summary (n=9-12). (**B**) IL-1beta protein expression verified by Western blot analysis. Representative blot from animals fed the MCD diet for 4 weeks is shown. (**C, D**) Gene expression analysis of the inflammasome components (**C**) NLR family, pyrin domain containing 3 *Nlrp3* and (**D**) PYD and CARD domain containing (*Pycard/Asc*) are likewise displayed.

3.2.4 **Fibrosis**

Liver fibrosis represents a classical outcome of chronic liver diseases as one third of NASH patients progresses to fibrosis (Farrell & Larter, 2006). We therefore examined the effects of p62 in fibrosis development. In the portal tracts of livers from MCD-fed animals increased bile ductule formation was observed, some of them invaded into parenchyma (**Figure 3-17A** lower panel). Interestingly, *p62* transgenic animals showed a significantly higher proportion of these ductular reactions (DR) when fed the MCD diet (p=0.025) (**Figure 3-17B**). The proliferating ductular cells were confirmed by keratin 19 staining (**Figure 3-17A** upper panel). Recently, the cytokine tumor necrosis factor (ligand) superfamily, member 12 or also known as TNF-like weak inducer of apoptosis (*Tnfsf12/Tweak*) was shown to induce a DR (Bird et al., 2013): a slight induction was detectable in *p62* transgenic animals (**Figure 3-17C**).

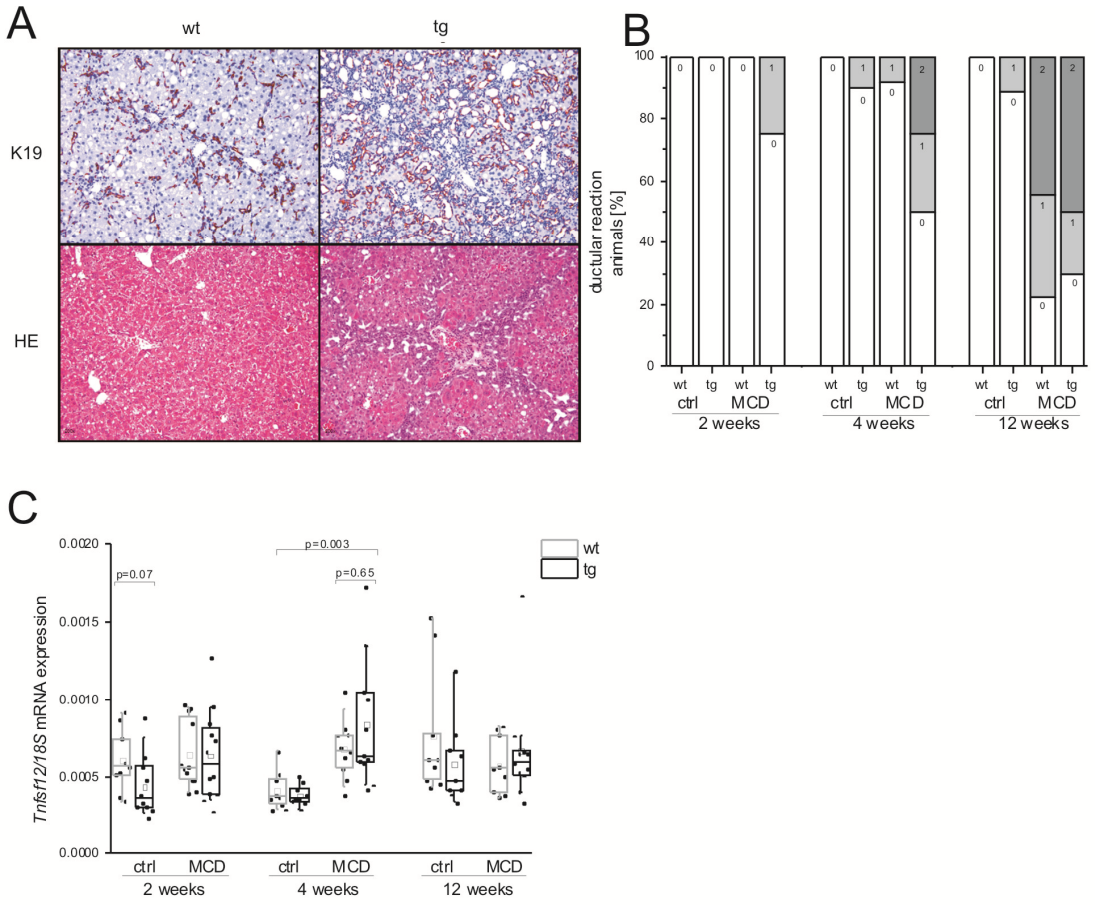

Figure 3-17: Ductular reaction upon p62 expression and MCD diet. (**A**) Representative paraffin-embedded liver sections of mice fed the MCD diet for 4 weeks showed a prominent ductular reaction on HE stained slides (lower panel, original magnification 200x). Immunohistochemical stain for keratin (K) 19 on paraffin-embedded liver sections are displayed (upper panel, original magnification 200x). (**B**) Scoring for ductular reactions demonstrated as percentage of animals classified into appropriate scores (table 2-7). (**C**) Relative hepatic mRNA expression of tumor necrosis factor (ligand) superfamily, member 12 (*Tnfsf12/Tweak*) are shown as ratio against the housekeeping gene *18S*. Data are represented as individual values and box plots with median (—) and mean (□) in a five-number summary (n=9-12).

Sirius Red staining revealed increased collagen deposition in *p62* transgenic animals (p=0.02) (**Figure 3-18A, B**) in the portal tract, around the central vein, and in the lobule in a perisinusoidal distribution. Under polarized light the birefringence of yellow-red collagen I and green collagen IV could be clearly distinguished and confirmed the observations made by light microscopy (**Figure 3-18C**).

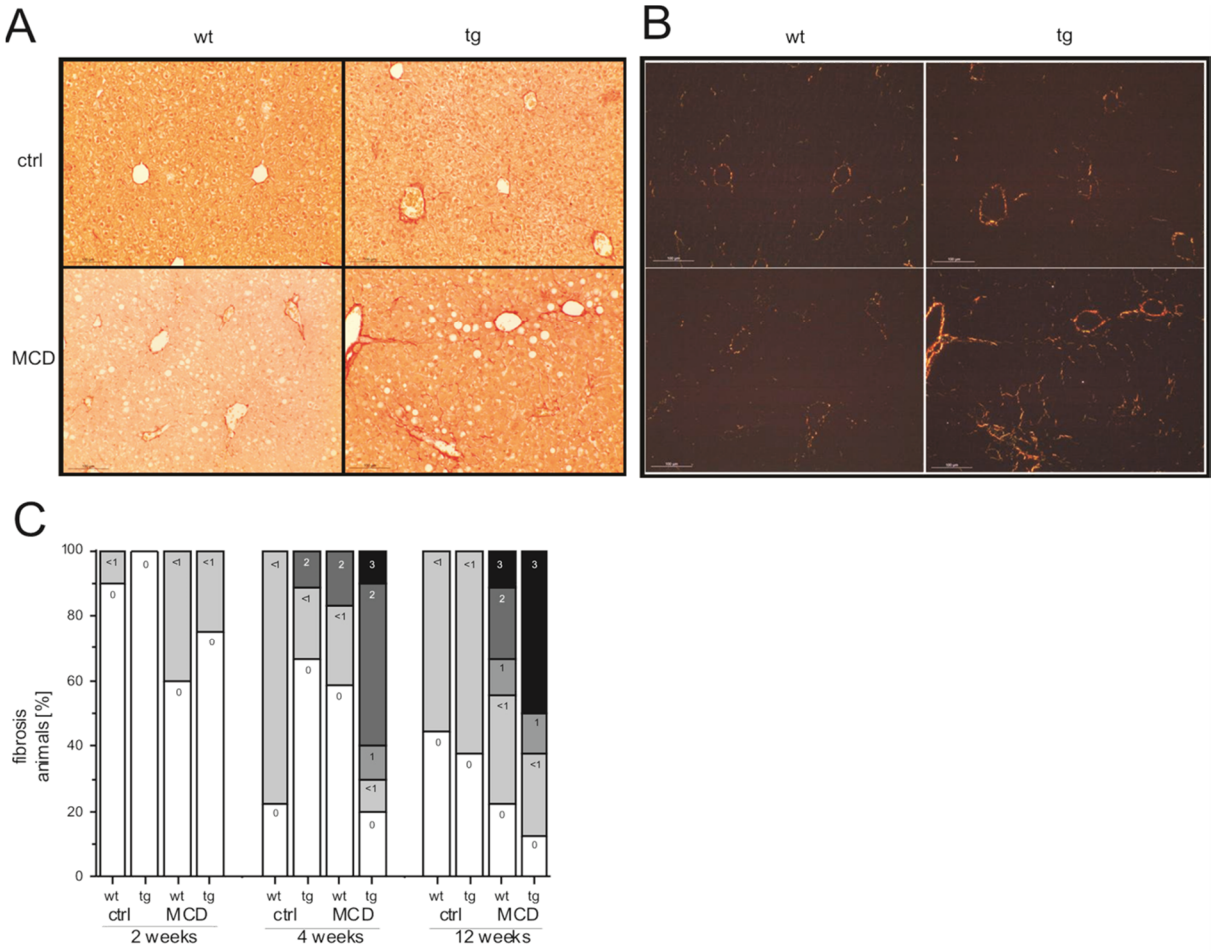

Figure 3-18: Fibrotic action of p62. (**A, B**) Collagen deposition in the liver was visualized by Sirius red staining on paraffin-embedded liver sections with brightfield microscopy (**A**) and with polarization microscopy (**B**) (original magnification 200x) and the corresponding fibrosis score (**C**) with percentage of animals classified into appropriate scores (see table 2-7).

Real-time RT-PCR showed an increased procollagen (*Col1a*) 1 mRNA expression already after 2 weeks in *p62* transgenic animals, with a further amplification at later time points (**Figure 3-19A**). In order to determine the upstream mechanisms for

collagen deposition the mRNA expression of tissue growth factor (*Tgf*) b and connective tissue growth factor (*Ctgf*) were determined. Interestingly, *Tgfb* showed a downregulation throughout the observation period, whereas *Ctgf* was elevated in MCD-fed animals with a significant increase in *p62* transgenic animals already after 2 weeks (**Figure 3-19B, C**). At the same time an upregulation of serum interleukin 13 was detectable in these animals (**Figure 3-19D**). Most interestingly, also transgenic animals on the ctrl diet revealed a pronounced upregulation of serum IL-13 (**Figure 3-19D**).

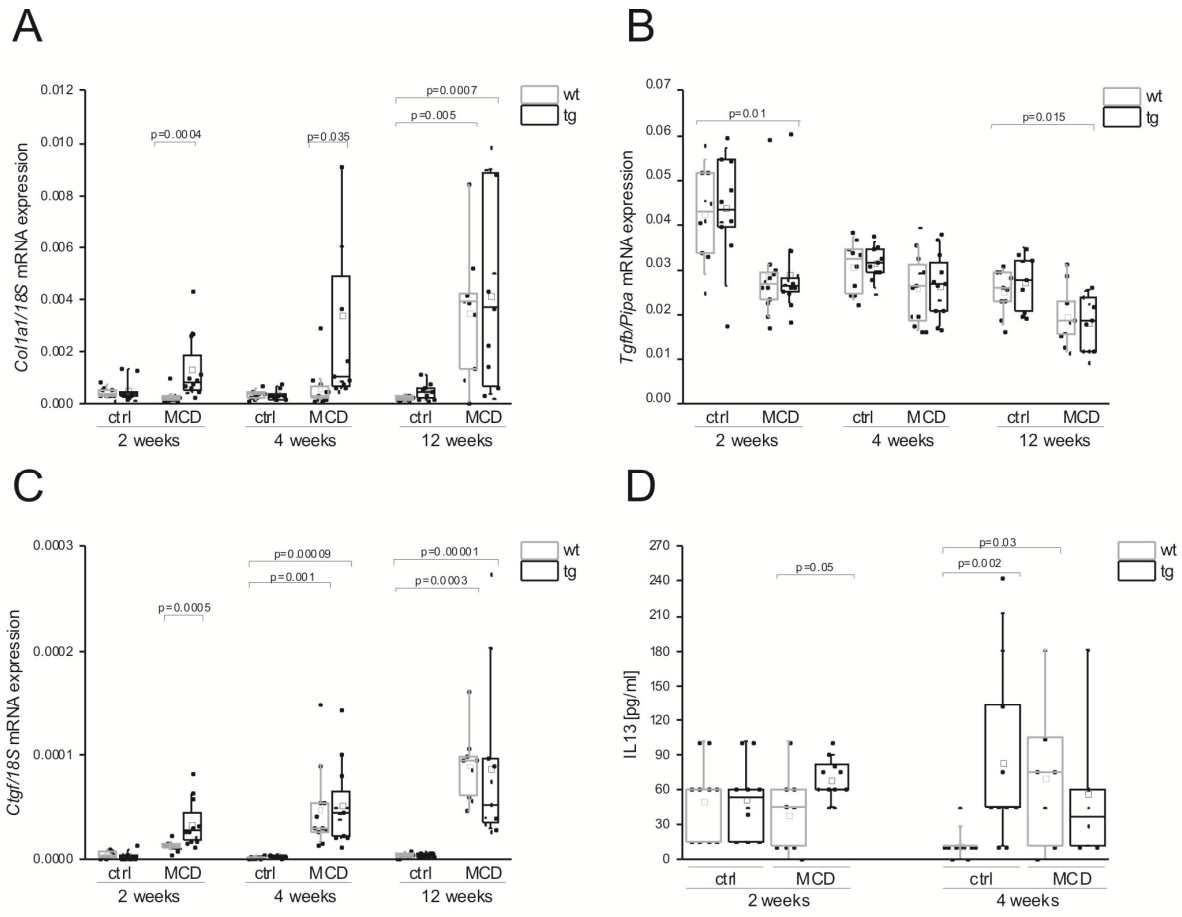

Figure 3-19: TGF-beta-independent collagen expression through p62. Relative mRNA expression of procollagen (*Col1a*) 1 (**A**), tissue growth factor (*Tgf*) b (**B**), and connective tissue growth factor (*ctgf*) (**C**) are shown as ratio against the housekeeping gene *18S* or *Pipa*. Data are represented as individual values and box plots with median (—) and mean (□) in a five-number summary (n=9). (**D**) Serum levels of interleukin (IL) 13 measured by Luminex assay are represented as individual values and box plots with median (—) and mean (□) in a five-number summary (n=9-12).

3.3 **Kupffer Cells as Lipid Modulators in NAFLD**

Liver specific macrophages, Kupffer cells (KC), play an important role in liver homeostasis and inflammatory response, as well as in NASH development (Leroux et al., 2012; Rivera et al., 2007). Little is known about the impact of Kupffer cells on lipid composition. To assess this issue a selective KC depletion was performed. Depletion of KCs was confirmed by its downregulation on mRNA level by 80% (p=0.00006) (**Figure 3-20A**). An immunohistochemical staining against the KC specific marker egf-like module containing, mucin-like, hormone receptor-like (*Emr/F4/80*) 1 further confirmed the successful KC depletion (**Figure 3-20B**).

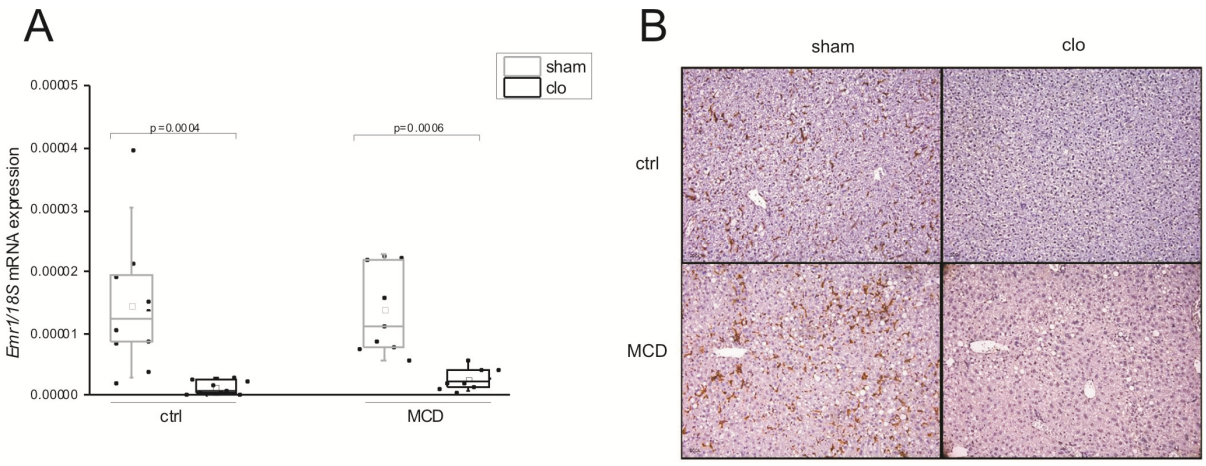

Figure 3-20: Successful Kupffer cell depletion by clodronate liposomes. Relative mRNA expression of (**A**) egf-like module containing, mucin-like, hormone receptor-like (*Emr/F4/80*) 1 is shown as ratio against the housekeeping gene *18S*. Data are represented as individual values and box plots with median (—) and mean (□) in a five-number summary (n=9-10). (**B**) Immunohistochemical stain against F4/80 as KC marker in animals after 3 weeks on the MCD diet with simultaneous administration of clodronate (Clo) or empty (sham) liposomes (original magnification 200x).

Histological evaluation of KC-depleted slides revealed a strong variability regarding steatosis, with low and high steatosis scores. However, the mean of the clodronate-treated group was not significantly different compared to the sham group (**Figure 3-21A** and data not shown). Still, GC-MS analyses demonstrated downregulation of cholesterol and fatty acid deposition (**Figure 3-21B**). Serum analyses of triglycerides

showed a downregulation in the ctrl and an upregulation in the MCD diet upon KC depletion (**Table 3-5, Table 3-6**).

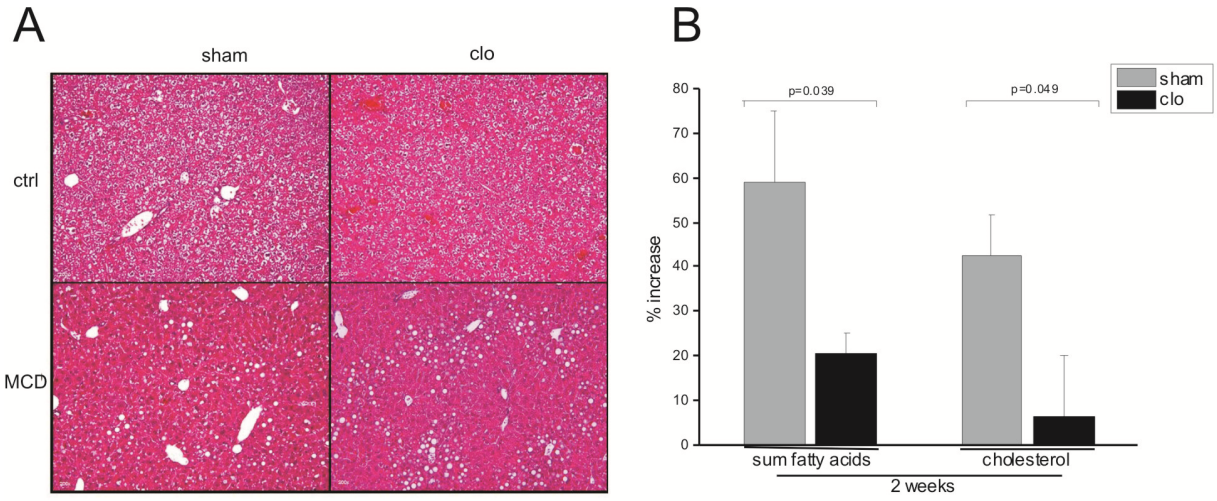

Figure 3-21: Steatosis formation in NAFLD without Kupffer cells. (**A**) Representative liver sections stained with HE from animals fed with the respective diet for 3 weeks with simultaneous administration of clodronate (Clo) or empty (sham) liposomes (original magnification 200x). (**B**) Liver tissues were lyophilized and analyzed by GC-MS.% increase of MCD fed animals compared to ctrl are displayed for the sum of all fatty acids as well as hepatic cholesterol (n=9-10).

Table 3-5: Weight and serum parameters of mice fed the MCD or ctrl diet for 3 weeks with simultaneous administration of clodronate (Clo) or empty (sham) liposomes. Values are expressed as mean ± SEM (n=9-10). * p<0.05 to sham, † p<0.05 to ctrl diet, ‡ p<0.05 to sham on ctrl

	3 weeks			
	Ctrl		**MCD**	
	sham	**clo**	**sham**	**clo**
number animals [n]	10	10	9	9
body weight change [%]	122.6 ± 6.2	90.1 ± 6.3*	-17.8 ± 0.5†	-19.3 ± 0.9†‡
relative liver weight [% of body weight]	4.6 ± 0.1	4.2 ± 0.1	3.4 ± 0.1†	3.8 ± 0.1
serum ALT [U/L]	89 ± 11	79 ± 9	108 ± 12	127 ± 12 †‡
serum AST [U/L]	2,208 ± 310	2,071 ± 293	2,508 ± 211	2,572 ± 509
serum triglycerides [mg/dl]	232 ± 21	153 ± 13*	72 ± 4†	94 ± 6*†‡
serum HDL [mg/dl]	89 ± 6	92 ± 8	35 ± 2†	20 ± 2*†‡
serum glucose [mg/dl]	192 ± 15	185 ± 11	91 ± 9†	77 ± 8†‡
serum cholesterol [mg/dl]	120 ± 7	127 ± 8	47 ± 3†	46 ± 3†‡

Table 3-6: GC-MS fatty acid analyses of mice fed the MCD or ctrl diet for 3 weeks with simultaneous administration of clodronate (Clo) or empty (sham) liposomes. Values [µg/mg dry liver tissue] are expressed as mean ± SEM (n=9-10). Liver tissues were lyophilized and analyzed by GC-MS.

Fatty acid	ctrl sham	ctrl Clo	*a*	MCD sham	*b*	MCD Clo	*c*	*d*	*e*
12:0	0.01 ± 0.002	0.02 ± 0.003	0.273	0.02 ± 0.001	0.005	0.02 ± 0.003	0.665	0.066	0.0017
14:0	0.37 ± 0.07	0.39 ± 0.08	0.970	0.41 ± 0.03	0.267	0.49 ± 0.06	0.736	0.307	0.111
15:0	0.05 ± 0.01	0.06 ± 0.01	0.678	0.11 ± 0.01	0.0009	0.11 ± 0.01	0.885	0.013	0.0009
16:0	20.54 ± 2.19	22.33 ± 3.88	0.970	25.59 ± 2.63	0.168	24.25 ± 0.66	0.962	0.02	0.206
16:1	2.02 ± 0.46	2.07 ± 0.44	0.970	1.22 ± 0.15	0.143	1.63 ± 0.17	0.092	0.903	0.903
16:2	0.01 ± 0.001	0.03 ± 0.01	0.045	0.10 ± 0.01	0.0004	0.13 ± 0.02	0.597	0.001	0.0003
17:0	0.18 ± 0.02	0.21 ± 0.03	0.212	0.47 ± 0.03	0.0004	0.40 ± 0.03	0.136	0.0038	0.0005
17:1	0.08 ± 0.02	0.08 ± 0.02	0.970	0.04 ± 0.02	0.258	0.08 ± 0.01	0.188	0.902	0.437
18:0	14.25 ± 1.33	16.19 ± 2.46	0.521	20.90 ± 1.61	0.007	18.29 ± 0.48	0.229	0.016	0.006
18:1	19.67 ± 2.14	21.85 ± 3.49	0.91	31.51 ± 3.72	0.046	25.72 ± 1.48	0.268	0.03	0.066
18:2	19.98 ± 2.94	18.71 ± 4.07	0.427	28.85 ± 3.89	0.168	16.71 ± 3.14	0.03	0.775	0.307
18:3	0.33 ± 0.05	0.45 ± 0.11	0.970	1.83 ± 0.29	0.0004	2.12 ± 0.21	0.47	0.0003	0.0003
20:0	0.35 ± 0.09	0.23 ± 0.04	0.85	0.31 ± 0.11	0.689	0.32 ± 0.03	0.962	0.131	0.596
20:1	0.56 ± 0.10	0.68 ± 0.10	0.427	1.63 ± 0.17	0.0004	1.63 ± 0.15	0.81	0.0005	0.0007
20:2	0.67 ± 0.09	0.84 ± 0.11	0.241	2.76 ± 0.28	0.0004	2.42 ± 0.19	0.470	0.0003	0.0003
20:3	1.41 ± 0.19	1.30 ± 0.18	0.623	4.05 ± 1.99	0.0006	4.16 ± 0.37	0.885	0.0003	0.0005
20:4	16.19 ± 1.54	18.01 ± 2.78	0.623	22.63 ± 1.99	0.011	19.18 ± 0.71	0.163	0.02	0.016
22:0	0.90 ± 0.21	0.78 ± 0.11	0.85	0.69 ± 0.05	0.894	0.61 ± 0.03	0.163	0.488	0.775
22:1	0.04 ± 0.01	0.03 ± 0.01	0.85	0.07 ± 0.01	0.015	0.09 ± 0.01	0.268	0.0017	0.01
22:2	0.01 ± 0.003	0.01 ± 0.002	0.91	0.01 ± 0.005	0.011	0.04 ± 0.01	0.361	0.0007	0.002
22:4	0.74 ± 0.11	0.84 ± 0.12	0.571	5.75 ± 0.65	0.0004	5.15 ± 0.62	0.413	0.0003	0.0003
22:5	0.15 ± 0.02	0.17 ± 0.02	0.521	0.88 ± 0.10	0.0004	0.95 ± 0.11	0.962	0.0003	0.0003
22:6	7.72 ± 0.84	8.90 ± 1.20	0.521	20.70 ± 2.38	0.0011	14.88 ± 0.72	0.112	0.003	0.0009
23:0	0.15 ± 0.02	0.22 ± 0.03	0.09	0.25 ± 0.02	0.007	0.22 ± 0.01	0.312	0.596	0.025
24:0	0.58 ± 0.08	0.66 ± 0.08	0.678	0.84 ± 0.06	0.015	0.74 ± 0.04	0.136	0.153	0.008
ratio 16:1/16:0	0.09 ± 0.01	0.09 ± 0.01	0.791	0.01 ± 0.01	0.009	0.07 ± 0.01	0.092	0.206	0.153
ratio 18:1/18:0	1.40 ± 0.14	1.36 ± 0.10	0.970	1.50 ± 0.14	0.625	1.41 ± 0.09	0.665	0.596	0.433

p-value of comparison of a = ctrl sham and ctrl Clo,

b = ctrl sham and sham MCD,

c = MCD sham and MCD Clo,

d = ctrl Clo and MCD Clo,

e = sham ctrl and MCD Clo

Interestingly, the C18:C16 fatty acid ratio was increased upon the MCD diet and abolished due to KC depletion (**Figure 3-22**), indicating a KC-facilitated alteration in the fatty acid metabolism. Since *Elovl6* is responsible for the conversion of C16 to C18, its mRNA expression as well as protein levels were investigated. The transcript level of *Elovl6* was unchanged in the MCD diet, but in the crtl diet a downregulation due to KC depletion was observed (**Figure 3-23A**). Its protein levels tended to be downregulated (50% downregulation without statistical difference) upon clodronate administration (**Figure 3-23B**). *Fasn* mRNA expression was downregulated in the absence of KC, whereas its protein expression was not altered due to KC depletion (**Figure 3-23C, D**). No change at transcript level was detected for *Scd1* upon KC depletion in the MCD diet, which was in conjunction with an unmodified C16:1/C16:0 and C18:1/C18:0 ratio (**Figure 3-23E, Table 3-6**), whereas MCD diet alone led to a *Scd1* downregulation as seen before. Furthermore, a significant downregulation in the absence of KC in mice fed the ctrl diet was detected (**Figure 3-23E**).

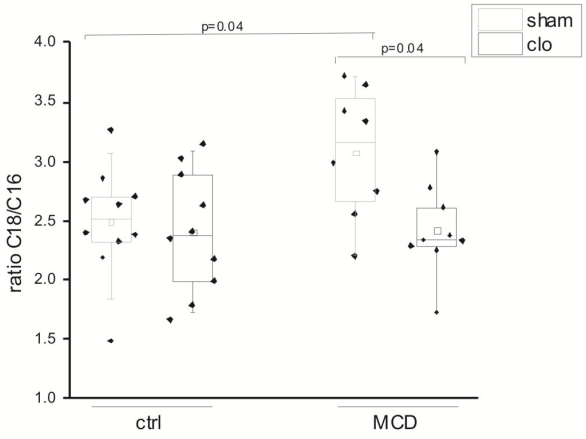

Figure 3-22: Altered fatty acid pattern upon KC depletion. GC-MS fatty acid analyses of mice fed the MCD or ctrl diet for 3 weeks with simultaneous administration of clodronate (Clo) or empty (sham) liposomes. Liver tissues were lyophilized and analyzed by GC-MS. Ratio of C16/C18 fatty acids are displayed as individual values and box plots with median (—) and mean (□) in a five-number summary (n=9-10).

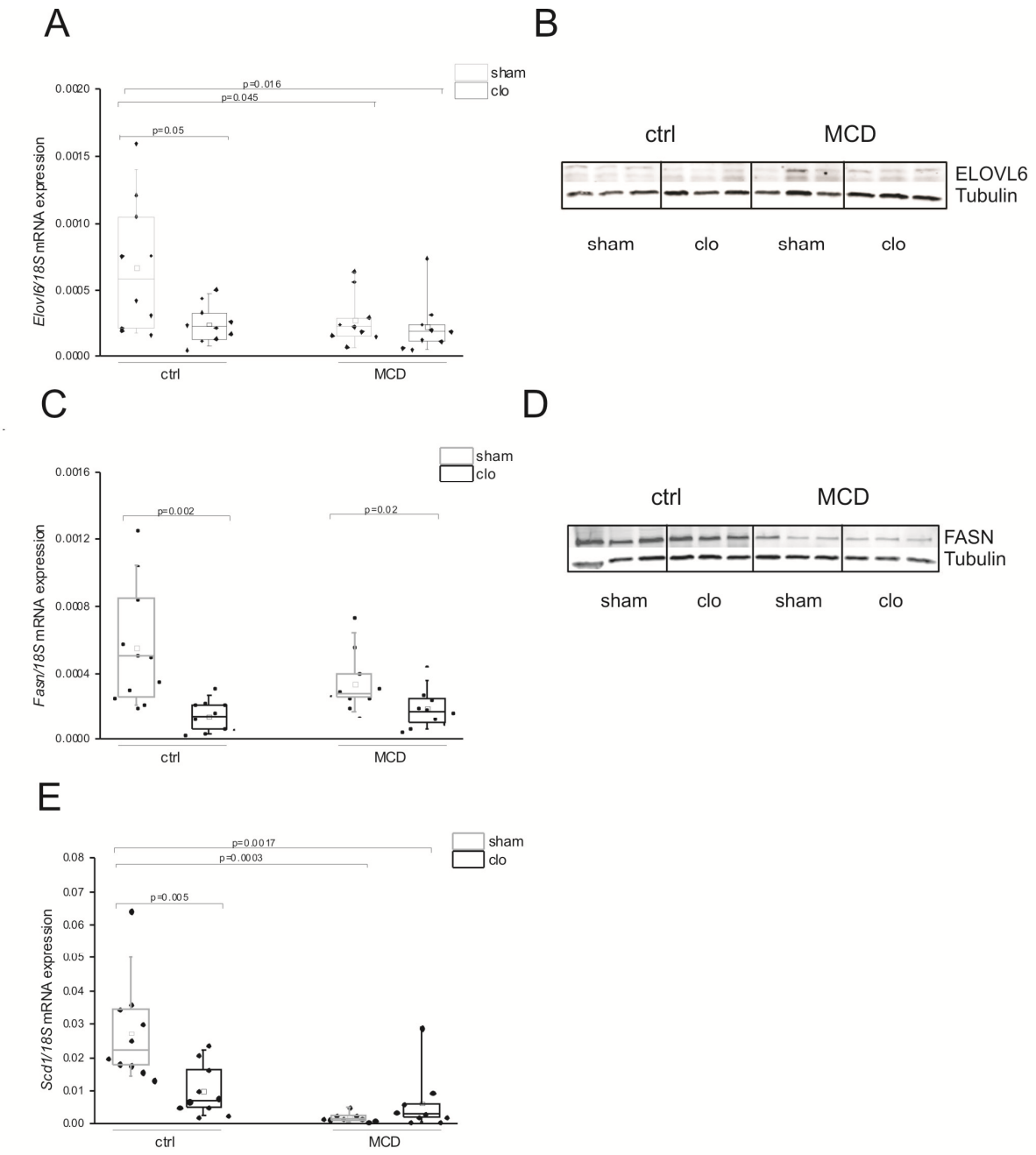

Figure 3-23: **Kupffer cell depletion alters gene expression of fatty acid metabolism**. (**A**) Gene expression analyses of *Elovl6* from whole liver by quantitative real-time RT-PCR is expressed as ratio against the housekeeping gene *18S*. (**B**) ELOVL6 protein expression verified by Western blot analysis. Representative Western blot from animals fed the MCD diet for 3 weeks with simultaneous administration of clodronate (Clo) or empty (sham) liposomes is shown. Gene expression analyses of (**C**) *Fasn* and (**D**) FASN protein expression verified by Western blot analysis are shown. Gene expression analyses of (**E**) *Scd1* expressed as ratio against the housekeeping gene *18S* is shown. Data are represented as individual values and box plots with median (—) and mean (□) in a five-number summary (n=9-10).

Lipid peroxidation was not altered by KC depletion, despite an upregulation due to the MCD diet (**Figure 3-24A**). Upon KC depletion only a slight decrease was found for the expression of proinflammatory cytokines and chemokines, possibly due to the heterogeneity of the clodronate treated samples (**Figure 3-24B**)

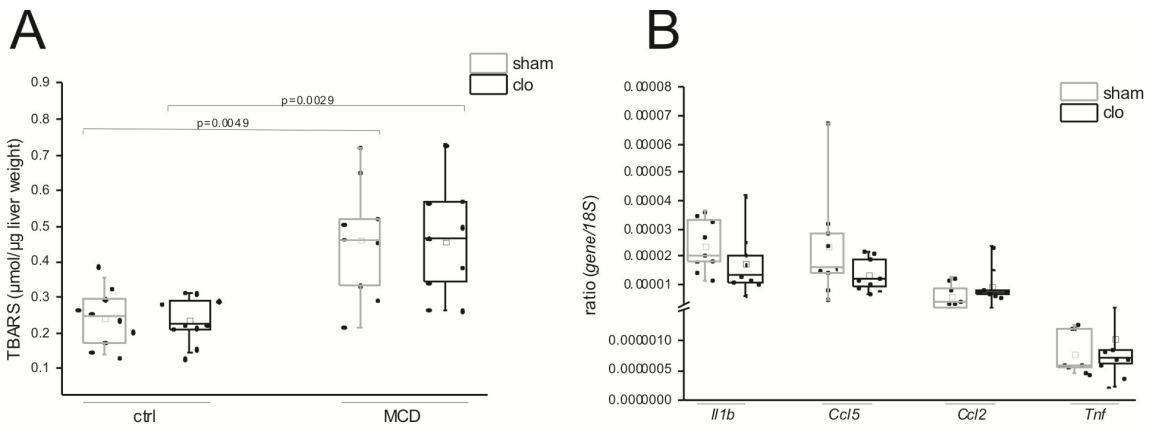

Figure 3-24: ROS production and cytokine profile unaltered upon Kupffer cell depletion. (**A**) Hepatic thiobarbituric acid reactive substances (TBARS) were measured to indicate lipid peroxidation and are represented as individual values and box plots with median (—) and mean (□) in a five-number summary (n=9-10). (**B**) Gene expression profile of cytokines and chemokines expressed as ratio against *18S* as housekeeping gene is shown. Data are represented as individual values and box plots with median (—) and mean (□) in a five-number summary (n=9-10).

4 DISCUSSION

Longstanding NASH with progression to fibrosis and cirrhosis is considered as a risk factor for the development of HCC. p62/IGF2BP2-2 was recognized as tumor-associated antigen (TAA) and serum autoantibodies against p62 were suggested as biomarkers in cancer immunodiagnostics (Liu et al., 2011a). p62 is expressed in cirrhotic nodules (Lu et al., 2001) and in human HCC (Zhang et al., 1999; Liu et al., 2013), and most recent data report that p62 expression correlates with poor prognosis in patients with HCC (Kessler et al., 2013). Since p62 induces steatosis (Tybl et al., 2011) and genome-wide association (GWA) studies of type 2 diabetes samples revealed an association with IGF2BP2 (Christiansen et al., 2009), we hypothesized an impact of p62 on metabolic diseases. The purpose of this study was to examine the role of p62 in the pathogenesis of NASH. The liver-specific overexpression of p62 amplified and/or accelerated all stages in disease development of NAFLD.

4.1 **p62 Expression and Its Heterocellular Distribution**

The mRNA and protein expression of the human transgene p62 in all double positive *p62*$^{+}$*/LT2*$^{+}$ transgenic animals used for this study was confirmed by real-time RT-PCR and Western blot, respectively. Here, some disparities among the transgenic animals were detected. This phenomenon might in part be explained by the occurrence of a heterocellular expression pattern of the transgene as seen by immunohistochemistry.

Heterocellular or mosaic expression has been reported in a variety of transgenic mouse models (Kramer et al., 2006; Serova et al., 2009; Sharif et al., 2004), but still the nature of this mosaicism remains unclear. Explanations for this variegated transgene expression have been published. A possible reason might be due to a transgene position effect (Festenstein et al., 1996; Henikoff, 1992). Here, a distinction has been made between a stable position, in particular near suppressing heterochromatin, where the expression is influenced by the integration site and the variegating position with the result of two cell populations, one expressing and one silenced (Martin & Whitelaw, 1996). Another approach assumes that the variegated silencing is due to repeated copy numbers of the integrated transgene (Garrick et al., 1998). However, heterocellular expression was also seen in animals with a single

copy of the transgene and with a location of the transgene far from heterochromatin regions (Ramírez et al., 2001). Furthermore, gene silencing might be a result of DNA methylation, but is not necessarily the cause of it (Razin & Cedar, 1991). Notwithstanding, as in *p62* transgenic animals neither the integration site nor the copy number is known, one can only speculate about the occurrence of this heterocellular expression.

4.2 General Effects of the MCD Diet

The mechanism of steatosis formation in the MCD dietary model of NASH is based on the restricted availability of methionine and choline as essential precursors for phosphatidylcholine synthesis (Vance & Vance, 1985). Phosphatidylcholine represents an essential component of very low density lipoproteins (VLDL), which in turn facilitate the major export pathway of tryglycerides in hepatocytes (Yao & Vance, 1988). Therefore, impaired VLDL production leads to an accumulation of triglycerides within hepatocytes and subsequent steatosis (Vance & Vance, 1985; Yao & Vance, 1988). In accordance, all animals fed the MCD diet showed low serum triglycerides and cholesterol values as well as a distinct degree of steatosis. With these observations a loss of body weight in animals fed the MCD diet was associated as seen in other studies with this dietary model (Rinella et al., 2008; Rinella & Green, 2004; Yamazaki et al., 2008). This weight loss might in part be a result of hypermetabolism (Rizki et al., 2006) during normal food intake (Rinella et al., 2008).

Animals fed the MCD diet had elevated AST and ALT levels indicating liver damage as previously reported in other studies (Kirsch et al., 2003; Yamazaki et al., 2008).

4.3 p62 Amplifies Steatosis

As already shown for *p62* transgenic animals on normal chow (Tybl et al., 2011), p62 livers on MCD showed increased hepatic lipid levels and a histologically elevated steatosis only at early time points. To determine whether the p62-mediated amplification of steatosis is due to p62-induced steatosis prior to MCD feeding, a

temporal inhibition of *p62* expression prior to MCD feeding was performed. Here, *p62* expression led to increased steatosis irrespective of an early or simultaneous start of *p62* expression suggesting that a temporal inhibition of p62 has no effect on steatosis development. Therefore, all further studies were performed without doxycycline treatment, as tetracycline as well as doxycycline are known to modulate lipid metabolism (Böcker et al., 1981).

Thin-layer chromatographic analyses of extracts from lyophilized liver tissue of mice treated with the MCD diet from this study revealed a 3-fold increased accumulation of triglycerides (Laggai et al., 2013). The same analyses revealed that the amount of phosphatidylethanolamin (PE) was increased and phosphatidylcholine (PC) was decreased (Laggai et al., 2013) as seen previously reported for the MCD model (Larter et al., 2008).

The GC-MS analyses of free fatty acids provided a detailed picture of the fatty acid alterations in *p62* transgenic animals. Here, the rate of MUFA was increased to a higher extent than the SFA and PUFA indicating alterations in the fatty acid metabolism as seen in both NASH and NASH-related HCC (Muir et al., 2013). Interestingly, increased MUFA are correlated with hypertriglyceridemia and obesity (Okada et al., 2005; Paillard et al., 2008), even when they are not exogenously ingested, but rather synthesized within the liver. Desaturases represent the rate-limiting enzymes for the production of palmitoleic (C16:1) and oleic acid (C18:1) with SCD1 being the predominant form in the liver (Miyazaki et al., 2006; Ntambi & Miyazaki, 2004). In this study, an increase of *Scd1* in *p62* transgenic animals, despite a strong downregulation through the MCD diet, was found. This reflects the observations seen in the lipidomic analyses with an increased ratio of oleic to stearic acid and palmitoleic to palmitic acid. In human NASH-related HCC tissues an upregulation of SCD was found likewise (Muir et al., 2013), and its activity was related to hypertriglyceridemia (Attie et al., 2002). The expression of *Fasn* was found to be downregulated upon the MCD diet without differences among the genotypes, similar to other murine models of steatohepatitis (Glosli et al., 2005; Jones et al., 2013; Matsuzaka et al., 2012) and human NASH (Caballero et al., 2009).

Despite the downregulation of its target genes the most prominent upregulation of the lipogenic transcription factor *Srebf1* seems to contribute to the development of steatosis in *p62* transgenic animals. It is known that two key transcription factors are responsible for the regulation of lipogenesis, glycolysis, and gluconeogenesis: SREBF1 and CHREBP (Mlxipl). Both transcription factors share the regulation of lipogenic genes in a symbiotic manner (Dentin et al., 2005; Iizuka & Horikawa, 2008). However, it has recently been shown that *Srebf1* overexpression leads to downregulation of *Chrebp* (Dubuquoy et al., 2011). We therefore suggest that p62-induced *Srebf1* is responsible for the p62-facilitated *Chrebp* downregulation. Our observation of reduced *Chrebp* expression is consistent with low serum glucose levels as seen in *Chrebp* k/o mice (Iizuka et al., 2004). In accordance, the MCD diet led to a slight downregulation of the catalytic glucose-6-phosphatase (*G6pc*), the key enzyme in hepatic glucose metabolism, which was also found in human subjects with a fatty liver (Konopelska et al., 2011). These results emphasize the strong interaction between hepatic carbohydrate and fatty acid metabolism.

In addition to lipogenesis, steatosis might be a result of diminished lipolysis or reduced lipid export. Since serum lipids were not different between wild-type and *p62* transgenic animals, the latter can be excluded. *Ppara*, a regulator for mitochondrial and peroxisomal β-oxidation, and microsomal ω-oxidation, was slightly downregulated in *p62* transgenic mice similar to findings in human NAFLD patients (Nakamuta et al., 2007). It is also known that a lack of *Ppara* renders the liver more susceptible to MCD diet-induced steatohepatitis (Ip et al., 2003).

Taken together, both increased lipogenesis and slightly reduced lipolysis contributed to the steatosis formation in *p62* transgenic animals.

4.4 p62 Aggravates ROS Production by Increased Free Cholesterol and Iron

p62 transgenic mice fed the MCD diet showed hyperlipidemia with increased serum cholesterol levels. These findings are particularly interesting when bearing in mind that the MCD diet is known for lowered serum TG levels and in this particular respect

differs from human NASH (Anstee & Goldin, 2006). Thus, *p62* transgenic animals display a more human-like lipid protein profile as also serum HDL tends to be downregulated as it was found in human NASH (Koruk et al., 2003). To our knowledge the increase in hepatic total and free cholesterol is the first time that a hepatic cholesterol accumulation is documented in a nutritional mouse model without additional cholesterol substitution. Increased dietary cholesterol intake is associated with risk and severity of NAFLD and is paralleled by hepatic free cholesterol accumulation in humans as well as in experimental settings (Musso et al., 2013). Besides dietary cholesterol intake cellular cholesterol accumulation might be a result of disturbed cholesterol homeostasis (Musso et al., 2013). Here, we report enhanced endogenic cholesterol biosynthesis as the transcription factor *Srebf2* as well as its target gene, the rate-limiting enzyme *Hmgcr*, were upregulated in *p62* transgenic mice. These findings are in agreement with observations made in human samples, where inhibition of HMGCR by statins leads to NASH resolution (Athyros et al., 2013) and the severity of NASH is positively correlated with the expression of these genes (Min et al., 2012).

Apart from that, others reported no correlation of *Srebf2* with hepatic cholesterol despite elevated *Hmgcr* (Graham et al., 2010). In the same study, cholesterol biosynthesis was found to be positively correlated with iron accumulation: additional iron intake led to deposition of free cholesterol and its upregulated biosynthesis (Graham et al., 2010). Furthermore, hepatocellular iron deposition was reported to be elevated in human NASH patients (Fujita et al., 2009) and NASH-related HCC patients (Sorrentino et al., 2009). In our model, iron deposition was distinctly elevated in *p62* transgenic animals. Recently, the interactions between hepatic iron and lipid metabolism have been reviewed (Ahmed et al., 2012), which underlined the interactions of both. In fact, variations in hepatic iron levels can directly lead to a modulation of lipogenesis, lipid storage and secretion, as iron is an integral part of several lipid metabolism related enzymes (Ahmed et al., 2012). In *p62* transgenic mice, the iron accumulation might induce *Scd1* expression. Moreover, Scd1 activity has been shown to be iron-dependent, as the protein contains iron as a cofactor (Pigeon, 2001).

p62 transgenic animals revealed a pronounced increase in hepcidin (*Hamp*) mRNA expression, which represents an indicator of elevated iron deposition. Hepcidin is a master iron-regulatory protein, which is secreted by hepatocytes in response to elevated body iron stores (Wang et al., 2005b) and inflammation *via* IL-6 and IL-1 (Lee et al., 2005). It therefore has been suggested as a biomarker for inflammation. In human NAFLD patients with iron accumulation a significantly higher hepatic *Hamp* expression was found compared to NAFLD patients without iron accumulation (Aigner et al., 2008). Interestingly, the study also demonstrated a positive correlation with TNF expression (Aigner et al., 2008). The regulatory function of hepcidin on iron homeostasis is based on its binding to the protein ferroportin and its subsequent degradation leading to a diminished cellular iron export of enterocytes (Ganz & Nemeth, 2006; Nemeth et al., 2004). Thus, increased hepcidin leads to decreased iron uptake from the intestine as feedback loop in response to iron accumulation.

Cellular uptake of iron also occurs as iron bound to transferrin *via* transferrin receptors (Tfr) and as ferrous iron *via* the transmembrane protein divalent metal transporter-1 (DMT-1) (Crichton & Charloteaux-Wauters, 1987; Mims & Prchal, 2005). The expression of the transferrin receptor 1 (*Tfrc*) was not altered or even downregulated upon the MCD diet as it was seen in human NAFLD patients with iron accumulation (Aigner et al., 2008). Noteworthy, *p62* transgenic animals revealed a slightly increased *Tfrc* expression. In this context, a notable sequence similarity between the promotor sequence of Tfrc and the IGF2 promotor was demonstrated (Wang et al., 2005a), indicating a possible interaction of p62. In this context, it is important to know, that p62 expression correlates with Igf2 expression in *p62* transgenic animals as well as in human HCC tissues (Kessler et al., 2013; Tybl et al., 2011).

Enhanced iron accumulation is also related to enhanced lipid peroxidation (Fujita et al., 2009) in *p62* transgenics, as iron deposits positively correlate with lipid peroxidation. Iron is known to catalyze the production of reactive oxygen species, which can then initiate cellular damage and lipid peroxidation (Philippe et al., 2007). Reactive oxygen species have been suggested as critical contributors to the second hit (Seki et al., 2002). The marked lipid peroxidation and iron deposition in *p62*

transgenic mice fed the MCD diet is likely to play a role in the accelerated transition from steatosis to steatohepatitis.

4.5 **p62 Aggravates Inflammation in the Pathogenesis of NASH**

Progression from steatosis to steatohepatitis in NAFLD occurs *via* a number of additional steps upon the steatotic liver (Day & James, 1998). Previous work has demonstrated a distinct increase of cytosolic NFKB-p65 in *p62* transgenic animals, which we hypothesized to enhance an inflammatory response upon respective stimuli (Tybl et al., 2011). In fact, we here observed an elevated activation of NFKB in *p62* transgenic mice accompanied by increased lymphocyte and neutrophil infiltrations. Hence, *p62* transgenic animals are more prone to the inflammatory response in this model of NASH. Concordantly, gene expression of inflammatory cytokines and chemokines was elevated in these animals. Among these genes *Mcp1/Ccl2* as downstream target gene of NFKB activation (Leclercq et al., 2004) was induced in MCD fed *p62* transgenic mice. Pharmacological inhibition of MCP1 has been shown to ameliorate steatohepatitis in the MCD diet suggesting a detrimental role for this chemokine in NASH (Baeck et al., 2011).

The cytokine *Tnf* mRNA was likewise increased in *p62* transgenic animals fed the MCD diet. Interestingly, TNF is strongly related to the fatty acid metabolism as it negatively regulates the expression of *Ppara*, leading to decreased catabolism (Glosli et al., 2005). It was also seen in TNF receptor deficient mice on the MCD diet that steatosis was blunted (Tomita et al., 2006), whereas administration of TNF into mice and rats induced steatosis (Endo et al., 2007; Feingold et al., 1989). In human NAFLD patients enhanced serum levels of TNF are a strong indicator for the progression from steatosis to NASH (Abiru et al., 2006). Surprisingly, we detected a lower apoptosis rate in *p62* transgenic mice by IHC of cleaved caspase-3 (supplementary data), contrasting the apoptosis-inducing effect of TNF (Feldstein et al., 2003). Additionally, *p62* transgenic animals showed less liver damage as indicated by low transaminase levels, which is in contrast to elevated AST and ALT levels in human NASH (Albano et

al., 2005). Both, less apoptosis and liver damage confirm the cytoprotective properties of p62 (Kessler et al., 2013; Tybl et al., 2011).

Recently, inflammasome activation has been demonstrated as a hallmark of steatohepatitis and free cholesterol (Csak et al., 2011; Ioannou et al., 2013). Furthermore, the product of inflammasome activation, IL-1beta, was reported to promote hepatic steatosis *via* suppression of Ppara (Stienstra et al., 2010). The inflammasome is a multiprotein complex, which cleaves pro-IL-1beta into secreted IL-1beta (Szabo & Csak, 2012). Here, we show its activation as confirmed by upregulation of *Nlrp3*, *Pycard/Asc*, and *pro-IL1b* mRNA levels as well as increased IL-1beta protein levels in *p62* transgenic animals.

Summarizing the effect of hepatocellular p62 expression on the progression towards NASH, we conclude an amplification of the inflammatory response due to the enhanced activation of NFKB, activation of the inflammasome, and a distinct cytokine profile in *p62* transgenic animals on MCD.

4.6 p62 Promotes Fibrogenesis *via* TGF-beta-independent Collagen Production

In NASH inflammation activates collagen producing stellate cells leading to fibrosis (Rombouts & Marra, 2010). In this model increased *procollagen 1* expression and sinusoidal fibrosis, predominantly found in a central distribution pattern similar to human NASH-related fibrosis (Kleiner et al., 2005), was already found at early time points in these animals. These findings are in concordance with reports on p62 expression in human HCC and cirrhotic nodules (Lu et al., 2001). In conjunction with the accelerated fibrosis formation, a pronounced ductular reaction was observed. Recently, several studies indicated ductular reactions secondary to the activation of hepatic progenitor cells (HPC) as an additional mechanism for fibrogenesis (De Lima et al., 2008), which is correlated to progressive fibrosis in human NASH (Richardson et al., 2007).

Besides other stimuli, an activation of HPC to differentiate into biliary epithelial cells and to form ductules was demonstrated to be dependent on the Tweak/Fn14 pathway (Jakubowski et al., 2005). Tweak (*Tnfsf12*) is a growth regulator with a broad target spectrum, including cell survival, proliferation, or induction of cytokines and Fn14 is its possible TNF-like receptor (Campbell et al., 2004). In this study, *Tweak* expression was slightly induced in *p62* transgenics after 4 weeks on MCD correlating with the most distinct appearance of DRs. However, the underlying cause of DRs formation needs further investigations.

Elucidating the molecular mechanism of fibrogenesis in *p62* transgenic mice on the MCD diet, the expression levels of *Tgfb* and its downstream target gene *Ctgf* were measured. Surprisingly, *Tgfb* levels were unchanged or rather downregulated in animals fed the MCD diet, whereas *Ctgf* expression was highly induced in animals fed the MCD diet, suggesting a TGF-beta independent production of collagen. In fact, Liu et al. demonstrated that the cytokine interleukin 13 induces *Ctgf* irrespective of TGF-beta (Liu et al., 2011b). Indeed, serum IL-13 levels were increased in *p62* transgenic mice, suggesting an IL-13 dependent *Ctgf* expression resulting in liver fibrosis. Similarly, it was reported that in human NASH patients serum IL-13 levels were increased and the inhibition of the IL-13 receptor in a rat model of NASH led to reduction in fibrosis (Shimamura et al., 2008).

In summary, p62 expression cause a ductular reaction and increased collagen deposition probably *via* a *Ctgf* induced, TGF-beta independent pathway.

4.7 **Kupffer Cells Modulate Fatty Acid Metabolism in NAFLD**

In NAFLD a better understanding of the contribution of inflammatory cells on the development and diseases progression is critical. The liver resident macrophages, Kupffer cells (KC), have been reported to contribute to NASH development and are known to modulate the lipid metabolism of the adjacent hepatocytes (Stienstra et al., 2010; Tomita et al., 2006). GC-MS analyses of hepatic free fatty acids and cholesterol levels confirmed a less pronounced lipid accumulation in livers of KC depleted animals. Histological analyses and gene expression analyses of inflammatory

mediators, however, did not reveal statistical differences, most likely due to a large inter-sample variability.

Interestingly, a pronounced downregulation of serum triglycerides along with a downregulation of the lipogenic genes *Elovl6*, *Fasn*, and *Scd1* was observed in KC depleted animals on the ctrl diet. These findings support the notion of KC being fat-producing cells and modulators of fatty acid metabolism of adjacent hepatocytes (Leroux et al., 2012; Rivera et al., 2007). Furthermore, a downregulation of the C18:C16 ratio in the absence of KC indicated a downregulation of the elongase activity as confirmed by the downregulation of *Elovl6* mRNA and protein expression level. In human NASH *Elovl6* expression was likewise found to be positively correlated with severity of steatosis and NASH, and its knockout in mice leads to amelioration of NASH pathogenesis (Matsuzaka et al., 2012; Muir et al., 2013). Similar findings were seen in an animal study of arteriosclerosis, in which macrophage-specific *Elovl6* deficient animals ameliorated foam cell formation and progression to arteriosclerosis (Saito et al., 2011).

Taken together, the presented data indicate that KCs have an implication on lipid metabolism due to the modulation of lipogenic genes.

5 SUMMARY

The incidence of NAFLD has been rising in the last decades. Understanding the underlying mechanisms responsible for the pathogenesis of the progression from simple steatosis to NASH and the subsequent transition to fibrosis and HCC is therefore of highest clinical interest.

In this study, we investigated the effect of the liver-specific overexpression of p62/IGF2BP2-2 in mice on the progression of NASH and NASH-induced fibrosis.

p62 was originally isolated as autoantigen from a HCC patient and is overexpressed in HCC patients and in pre-malignant cirrhotic nodules. p62 overexpression in mice induces a fatty liver phenotype and increases cytosolic NFKB-p65 suggesting a susceptibility towards an inflammatory stimulus.

Within this study liver-specific overexpression of p62 was shown to amplify steatosis in MCD diet-induced NAFLD. p62 modulates lipid metabolism by increasing lipogenesis and decreasing lipolysis. Despite attenuated cell damage in *p62* transgenic animals, the mice exhibited an amplified inflammation with consecutive fibrosis.

The aggravated transition from steatosis to NASH was mediated by increased iron accumulation within the parenchyma and a subsequent rise in cholesterol synthesis. The p62-mediated increase of free cholesterol in turn led to increased ROS and lipid peroxidation. These events led to an elevated inflammatory response. Here, a pronounced NFKB activation with corresponding inflammatory cytokine profile was seen in *p62* transgenic animals. Accordingly, inflammasome activation was demonstrated in *p62* livers.

Most interestingly, p62 induced a ductular reaction as well as an early onset of fibrosis. The molecular mechanism of fibrogenesis in *p62* transgenic animals revealed an IL-13-dependent activation of CTGF irrespective of TGF-beta leading to collagen synthesis.

Taken together, this study provides evidence for a pathophysiological role of p62 in the progression from NAFLD towards NASH and fibrosis.

6 OUTLOOK

Since the MCD diet alone did not lead to tumorgenesis in *p62* transgenic animals in the used treatment period further studies are needed to investigate a potential pathophysiological role of p62 in the transition from NASH to HCC.

A model to assess this question would be to characterize the impact of p62 expression in animals fed the MCD diet with simultaneous administration of a carcinogen, such as diethylnitrosamine (DEN).

Another approach would be to feed a high-fat diet to the *p62* transgenic animals, as this diet would model the NAFLD induced by obesity. Moreover, this diet might reveal the effect of p62 expression on fatty acid metabolism more clearly.

At last, irrespective of the diet leading to NAFLD, liver cell isolation with subsequent cell type classification might provide further information on the complex interplay of p62 expressing hepatocytes with the other liver resident cells in the pathophysiology of NAFLD and HCC.

SUPPLEMENT

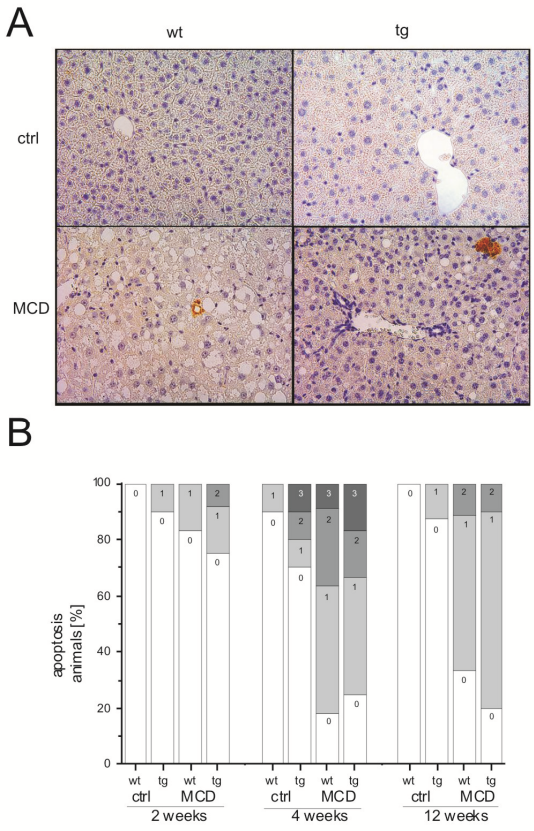

Suppl.: Immunohistochemistry of cleaved caspase-3.
(**A**) Representative pictures of mice fed the ctrl or MCD diet for 4 weeks and
(**B**) scoring of apoptosis with n=9-10

REFERENCES

Abiru, S., Migita, K., Maeda, Y., Daikoku, M., Ito, M., Ohata, K., Nagaoka, S., Matsumoto, T., Takii, Y., Kusumoto, K., Nakamura, M., Komori, A., Yano, K., Yatsuhashi, H., Eguchi, K., & Ishibashi, H. 2006. Serum cytokine and soluble cytokine receptor levels in patients with non-alcoholic steatohepatitis. *Liver Int*, 26(1): 39-45.

Ahmed, U., Latham, P. S., & Oates, P. S. 2012. Interactions between hepatic iron and lipid metabolism with possible relevance to steatohepatitis. *World J Gastroenterol*, 18(34): 4651-8.

Aigner, E., Theurl, I., Theurl, M., Lederer, D., Haufe, H., Dietze, O., Strasser, M., Datz, C., & Weiss, G. 2008. Pathways underlying iron accumulation in human nonalcoholic fatty liver disease. *Am J Clin Nutr*, 87(5): 1374-1383.

Albano, E., Mottaran, E., Vidali, M., Reale, E., Saksena, S., Occhino, G., Burt, A. D., & Day, C. P. 2005. Immune response towards lipid peroxidation products as a predictor of progression of non-alcoholic fatty liver disease to advanced fibrosis. *Gut*, 54(7): 987-993.

Angulo, P. 2002. Nonalcoholic fatty liver disease. *N Engl J Med*, 15(16): 7-10.

Anstee, Q. M., & Goldin, R. D. 2006. Mouse models in non-alcoholic fatty liver disease and steatohepatitis research. *Int J Exp Pathol,* 87(1): 1-16.

Argo, C. K., Northup, P. G., Al-Osaimi, A. M. S., & Caldwell, S. H. 2009. Systematic review of risk factors for fibrosis progression in non-alcoholic steatohepatitis. *J Hepatol*, 51(2): 371-379.

Athyros, V. G., Katsiki, N., Karagiannis, A., & Mikhailidis, D. P. 2013. Statins and nonalcoholic fatty liver disease: a bright future? *Expert Opin Investig Drugs*, 22(9): 1089-93.

Attie, A. D., Krauss, R. M., Gray-Keller, M. P., Brownlie, A., Miyazaki, M., Kastelein, J. J., Lusis, A. J., Stalenhoef, A. F. H., Stoehr, J. P., Hayden, M. R., & Ntambi, J. M. 2002. Relationship between stearoyl-CoA desaturase activity and plasma triglycerides in human and mouse hypertriglyceridemia. *J Lipid Res*, 43(11): 1899-1907.

Baeck, C., Wehr, A., Karlmark, K. R., Heymann, F., Vucur, M., Gassler, N., Huss, S., Klussmann, S., Eulberg, D., Luedde, T., Trautwein, C., & Tacke, F. 2011. Pharmacological inhibition of the chemokine CCL2 (MCP-1) diminishes liver macrophage infiltration and steatohepatitis in chronic hepatic injury. *Gut*, 2(3): 1-12.

Barnes, P.J., & Karin, M. 1997. Nuclear factor-κB—a pivotal transcription factor in chronic inflammatory diseases. *N Eng J Med*, 336(15): 1066-1071.

Bauernfeind, F. G., Horvath, G., Stutz, A., Alnemri, E. S., MacDonald, K., Speert, D., Fernandes-Alnemri, T., Wu, J., Monks, B. G., Fitzgerald, K. A., Hornung, V., & Latz, E. 2009. Cutting edge: NF-kappaB activating pattern recognition and cytokine receptors license NLRP3 inflammasome activation by regulating NLRP3 expression. *J Immunol*, 183(2): 787-791.

Bedogni, G., Miglioli, L., Masutti, F., Tiribelli, C., Marchesini, G., & Bellentani, S. 2005. Prevalence of and risk factors for nonalcoholic fatty liver disease: the Dionysos nutrition and liver study. *Hepatology*, 42(1): 44-52.

Bell, J. L., Wächter, K., Mühleck, B., Pazaitis, N., Köhn, M., Lederer, M., & Hüttelmaier, S. 2013. Insulin-like growth factor 2 mRNA-binding proteins (IGF2BPs): post-transcriptional drivers of cancer progression? *Cell Mol Life Sci*, 70(15): 2657-75.

Bilzer, M., Roggel, F., & Gerbes, A. L. 2006. Role of Kupffer cells in host defense and liver disease. *Liver Int,* 26(10): 1175-1186.

Bird, T. G., Lu, W.-Y., Boulter, L., Gordon-Keylock, S., Ridgway, R. A., Williams, M. J., Taube, J., Thomas, J. A., Wojtacha, D., Gambardella, A., Sansom, O. J., Iredale, J. P., & Forbes, S. J. 2013. Bone marrow injection stimulates hepatic ductular reactions in the absence of injury via macrophage-mediated TWEAK signaling. *Proc Natl Acad Sci U S A*, 110(16): 6542-7.

Böcker, R., Estler, C. J., Maywald, M., & Weber, D. 1981. Comparative evaluation of the effects of tetracycline and doxycycline on blood and liver lipids on male and female mice. *Arzneimittelforschung*, 31(12): 2118-20.

Brenner, D. A. 2009. Molecular pathogenesis of liver fibrosis. *Trans Am Clin Climatol Assoc*, 120: 361-368.

Bugianesi, E. 2007. Non-alcoholic steatohepatitis and cancer. *Clin Liver Dis*, 11(1): 191-207.

Burd, C. G., & Dreyfuss, G. 1994. Conserved structures and diversity of functions of RNA-binding proteins. *Science*, 265(5172): 615-621.

Caballero, F., Fernández, A., De Lacy, A. M., Fernández-Checa, J. C., Caballería, J., & García-Ruiz, C. 2009. Enhanced free cholesterol, SREBP-2 and StAR expression in human NASH. *J Hepatol*, 50(4): 789-796.

Caldwell, S. H., Oelsner, D. H., Iezzoni, J. C., Hespenheide, E. E., Battle, E. H., & Driscoll, C. J. 1999. Cryptogenic cirrhosis: clinical characterization and risk factors for underlying disease. *Hepatology*, 29(3): 664-669.

Campbell, S., Michaelson, J., Burkly, L., & Putterman, C. 2004. The role of TWEAK/Fn14 in the pathogenesis of inflammation and systemic autoimmunity. *Front Biosci*, 9: 2273-84.

Chan, D. W., Chan, C.-Y., Yam, J. W. P., Ching, Y.-P., & Ng, I. O. L. 2006. Prickle-1 negatively regulates Wnt/beta-catenin pathway by promoting Dishevelled ubiquitination/degradation in liver cancer. *Gastroenterology*, 131(4): 1218-1227.

Charlton, M. R., Burns, J. M., Pedersen, R. A., Watt, K. D., Heimbach, J. K., & Dierkhising, R. A. 2011. Frequency and Outcomes of Liver Transplantation for Nonalcoholic Steatohepatitis in the United States. *Gastroenterology*, 141(4): 1249-53.

Chen, J.-S., Wang, Q., Fu, X.-H., Huang, X.-H., Chen, X.-L., Cao, L.-Q., Chen, L.-Z., Tan, H.-X., Li, W., Bi, J., & Zhang, L.-J. 2009. Involvement of PI3K/PTEN/AKT/mTOR pathway in invasion and metastasis in hepatocellular carcinoma: Association with MMP-9. *Hepatol Res*, 39(2): 177-186.

Chow, L. M. L., & Baker, S. J. 2006. PTEN function in normal and neoplastic growth. *Cancer Lett*, 241(2): 184-196.

Christiansen, J., Kolte, A. M., Hansen, T. V. O., & Nielsen, F. C. 2009. IGF2 mRNA-binding protein 2: biological function and putative role in type 2 diabetes. *J Mol Endocrinol*, 43(5): 187-95.

Clark, J. 2006. The epidemiology of nonalcoholic fatty liver disease in adults. *J Clin Gastroenterol*, 40(Suppl 1): S5-10.

Cohen, J. C., Horton, J. D., & Hobbs, H. H. 2011. Human fatty liver disease: old questions and new insights. *Science*, 332(6037): 1519-1523.

Crichton, R. R., & Charloteaux-Wauters, M. 1987. Iron transport and storage. *Eur J Biochem*, 164(3): 485-506.

Csak, T., Ganz, M., Pespisa, J., Kodys, K., Dolganiuc, A., & Szabo, G. 2011. Fatty acid and endotoxin activate inflammasomes in mouse hepatocytes that release danger signals to stimulate immune cells. *Hepatology*, 54(1): 133-144.

Czaja, M. J. 2010. JNK regulation of hepatic manifestations of the metabolic syndrome. *Trends Endocrinol Metab*, 21(12): 707-713.

Dai, N., Rapley, J., Angel, M., Yanik, M. F., Blower, M. D., & Avruch, J. 2011. mTOR phosphorylates IMP2 to promote IGF2 mRNA translation by internal ribosomal entry. *Genes Dev*, 25(11): 1159-1172.

Dam-Larsen, S., Franzmann, M., Andersen, I. B., Christoffersen, P., Jensen, L. B., Sørensen, T. I. A., Becker, U., & Bendtsen, F. 2004. Long term prognosis of fatty liver: risk of chronic liver disease and death. *Gut*, 53(5): 750-755.

Day, C. P. 2002. Non-alcoholic steatohepatitis (NASH): where are we now and where are we going? *Gut*, 50(5): 585-588.

Day, C. P., & James, O. F. 1998. Steatohepatitis: a tale of two "hits"? *Gastroenterology*, 114.4: 842-845.

De Lima, V. M. R., Oliveira, C. P. M. S., Alves, V. A. F., Chammas, M. C., Oliveira, E. P., Stefano, J. T., De Mello, E. S., Cerri, G. G., Carrilho, F. J., & Caldwell, S. H. 2008. A rodent model of NASH with cirrhosis, oval cell proliferation and hepatocellular carcinoma. *J Hepatol*, 49(6): 1055-1061.

Dela Peña, A., Leclercq, I., Field, J., George, J., Jones, B., & Farrell, G. 2005. NF-kappaB activation, rather than TNF, mediates hepatic inflammation in a murine dietary model of steatohepatitis. *Gastroenterology*, 129(5): 1663-1674.

Delhaye, M., Louis, H., Degraef, C., Le Moine, O., Devière, J., Gulbis, B., Jacobovitz, D., Adler, M., & Galand, P. 1996. Relationship between hepatocyte proliferative activity and liver functional reserve in human cirrhosis. *Hepatology*, 23(5): 1003-1011.

Dentin, R., Girard, J., & Postic, C. 2005. Carbohydrate responsive element binding protein (ChREBP) and sterol regulatory element binding protein-1c (SREBP-1c): two key regulators of glucose metabolism and lipid synthesis in liver. *Biochimie*, 87(1): 81-86.

Diehl, A. M. 2002. Nonalcoholic steatosis and steatohepatitis IV. Nonalcoholic fatty liver disease abnormalities in macrophage function and cytokines. *Am J Physiol Gastrointest Liver Physiol*, 282(1): G1-G5.

Dobosy, J. R., Fu, V. X., Desotelle, J. A., Srinivasan, R., Kenowski, M. L., Almassi, N., Weindruch, R., Svaren, J., & Jarrard, D. F. 2008. A methyl-deficient diet modifies histone methylation and alters Igf2 and H19 repression in the prostate. *Prostate*, 68(11): 1187-1195.

Dubuquoy, C., Robichon, C., Lasnier, F., Langlois, C., Dugail, I., Foufelle, F., Girard, J., Burnol, A.-F., Postic, C., & Moldes, M. 2011. Distinct regulation of adiponutrin/PNPLA3 gene expression by the transcription factors ChREBP and SREBP1c in mouse and human hepatocytes. *J Hepatol*, 55(1): 145-153.

Eaton, S., Bartlett, K., & Pourfarzam, M. 1996. Mammalian mitochondrial beta-oxidation. *Biochem J*, 320 (Pt 2(Pt 2): 345-357.

El-Serag, H. B. 2011. Current Concepts: Hepatocellular Carcinoma. *New Eng J Med*, 365(365): 1118-27.

El-Serag, H. B., & Rudolph, K. L. 2007. Hepatocellular carcinoma: epidemiology and molecular carcinogenesis. *Gastroenterology*, 132(7): 2557-2576.

Endo, M., Masaki, T., Seike, M., & Yoshimatsu, H. 2007. TNF-alpha induces hepatic steatosis in mice by enhancing gene expression of sterol regulatory element binding protein-1c (SREBP-1c). *Exp Biol Med (Maywood)*, 232(5): 614-621.

Fan, J.-G., & Qiao, L. 2009. Commonly used animal models of non-alcoholic steatohepatitis. *Hepatobiliary Pancreat Dis Int*, 8(3): 233-240.

Farrell, G. C., & Larter, C. Z. 2006. Nonalcoholic fatty liver disease: from steatosis to cirrhosis. *Hepatology*, 43(2 Suppl 1): S99-S112.

Feingold, K. R., Serio, M. K., Adi, S., Moser, A. H., & Grunfeld, C. 1989. Tumor necrosis factor stimulates hepatic lipid synthesis and secretion. *Endocrinology*, 124(5): 2336-2342.

Feldstein, A. E., Canbay, A., Angulo, P., Taniai, M., Burgart, L. J., Lindor, K. D., & Gores, G. J. 2003. Hepatocyte apoptosis and fas expression are prominent features of human nonalcoholic steatohepatitis. *Gastroenterology*, 125(2): 437-443.

Festenstein, R., Tolaini, M., Corbella, P., Mamalaki, C., Parrington, J., Fox, M., Miliou, A., Jones, M., & Kioussis, D. 1996. Locus control region function and heterochromatin-induced position effect variegation. *Science*, 271(5252): 1123-1125.

Frevert, U., Engelmann, S., Zougbede, S., Stange, J., Ng, B., Matuschewski, K., Liebes, L., & Yee, H. 2005. Intravital observation of Plasmodium berghei sporozoite infection of the liver. *PloS Biol*, 3 (6): e192

Friedman, S. L. 2008. Mechanisms of hepatic fibrogenesis. *Gastroenterology*, 134(6): 1655-1669.

Fruchart, J.-C. 2009. Peroxisome proliferator-activated receptor-alpha (PPARalpha): at the crossroads of obesity, diabetes and cardiovascular disease. *Atherosclerosis*, 205(1): 1-8.

Fujita, N., Miyachi, H., Tanaka, H., Takeo, M., Nakagawa, N., Kobayashi, Y., Iwasa, M., Watanabe, S., & Takei, Y. 2009. Iron overload is associated with hepatic oxidative damage to DNA in nonalcoholic steatohepatitis. *Cancer Epidemiol Biomarkers Prev*, 18(2): 424-432.

Furth, P. A., St Onge, L., Böger, H., Gruss, P., Gossen, M., Kistner, A., Bujard, H., & Hennighausen, L. 1994. Temporal control of gene expression in transgenic mice by a tetracycline-responsive promoter. *Proc Natl Acad Sci U S A*, 91(20): 9302-9306.

Gaggini, M., Morelli, M., Buzzigoli, E., Defronzo, R. A., Bugianesi, E., & Gastaldelli, A. 2013. Non-Alcoholic Fatty Liver Disease (NAFLD) and Its Connection with Insulin Resistance, Dyslipidemia, Atherosclerosis and Coronary Heart Disease. *Nutrients*, 5(5): 1544-60.

Ganz, T., & Nemeth, E. 2006. Iron imports. IV. Hepcidin and regulation of body iron metabolism. *Am J Physiol Gastrointest Liver Physiol*, 290(2): G199-203.

Garrick, D., Fiering, S., Martin, D. I., & Whitelaw, E. 1998. Repeat-induced gene silencing in mammals. *Nat Genet*, 18(1): 56-59.

Glosli, H., Gudbrandsen, O. A., Mullen, A. J., Halvorsen, B., Røst, T. H., Wergedahl, H., Prydz, H., Aukrust, P., & Berge, R. K. 2005. Down-regulated expression of PPARalpha target genes, reduced fatty acid oxidation and altered fatty acid composition in the liver of mice transgenic for hTNFalpha. *Biochim Biophys Acta*, 1734(3): 235-246.

Gordon, S., & Taylor, P. R. 2005. Monocyte and macrophage heterogeneity. *Nat Rev Immunol*, 5(12): 953-964.

Gossen, M., Freundlieb, S., Bender, G., Müller, G., Hillen, W., & Bujard, H. 1995. Transcriptional activation by tetracyclines in mammalian cells. *Science*, 268(5218): 1766-1769.

Graham, R. M., Chua, A. C. G., Carter, K. W., Delima, R. D., Johnstone, D., Herbison, C. E., Firth, M. J., O'Leary, R., Milward, E. A., Olynyk, J. K., & Trinder, D. 2010. Hepatic iron loading in mice increases cholesterol biosynthesis. *Hepatology*, 52(2): 462-471.

Gressner, A. M., Weiskirchen, R., Breitkopf, K., & Dooley, S. 2002. Roles of TGF-beta in hepatic fibrosis. *Front Biosci*, 7: d793-d807.

Gressner, O. A., Lahme, B., Demirci, I., Gressner, A. M., & Weiskirchen, R. 2007. Differential effects of TGF-beta on connective tissue growth factor (CTGF/CCN2) expression in hepatic stellate cells and hepatocytes. *J Hepatol*, 47(5): 699-710.

Grotendorst, G. R. 1997. Connective tissue growth factor: a mediator of TGF-beta action on fibroblasts. *Cytokine Growth Factor Rev*, 8(3): 171-179.

Hashimoto, E., & Tokushige, K. 2012. Hepatocellular carcinoma in non-alcoholic steatohepatitis: Growing evidence of an epidemic? *Hepatology Res*, 42(1): 1-14.

He, G., & Karin, M. 2011. NF-κB and STAT3 - key players in liver inflammation and cancer. *Cell Res*, 21(1): 159-168.

Henikoff, S. 1992. Position effect and related phenomena. *Curr Opin Genet Dev*, 2(6): 907-912.

Horie, Y., Suzuki, A., Kataoka, E., Sasaki, T., Hamada, K., Sasaki, J., Mizuno, K., Hasegawa, G., Kishimoto, H., Iizuka, M., Naito, M., Enomoto, K., Watanabe, S., Mak, T. W., & Nakano, T. 2004. Hepatocyte-specific Pten deficiency results in steatohepatitis and hepatocellular carcinomas. *J Clin Invest*, 113(12): 1774-1783.

Hu, T.-H., Huang, C.-C., Lin, P.-R., Chang, H.-W., Ger, L.-P., Lin, Y.-W., Changchien, C.-S., Lee, C.-M., & Tai, M.-H. 2003. Expression and prognostic role of tumor suppressor gene PTEN/MMAC1/TEP1 in hepatocellular carcinoma. *Cancer*, 97(8): 1929-1940.

Hüttelmaier, S., Zenklusen, D., Lederer, M., Dictenberg, J., Lorenz, M., Meng, X., Bassell, G. J., Condeelis, J., & Singer, R. H. 2005. Spatial regulation of beta-actin translation by Src-dependent phosphorylation of ZBP1. *Nature*, 438(7067): 512-515.

Iizuka, K., Bruick, R. K., Liang, G., Horton, J. D., & Uyeda, K. 2004. Deficiency of carbohydrate response element-binding protein (ChREBP) reduces lipogenesis as well as glycolysis. *Proc Natl Acad Sci U S A*, 101(19): 7281-7286.

Iizuka, K., & Horikawa, Y. 2008. ChREBP: a glucose-activated transcription factor involved in the development of metabolic syndrome. *Endocr J*, 55(4): 617-624.

Ioannou, G. N., Haigh, W. G., Thorning, D., & Savard, C. 2013. Hepatic cholesterol crystals and crown-like structures distinguish NASH from simple steatosis. *J Lipid Res*, 54(5): 1326-34.

Ip, E., Farrell, G. C., Robertson, G., Hall, P., Kirsch, R., & Leclercq, I. 2003. Central role of PPARalpha-dependent hepatic lipid turnover in dietary steatohepatitis in mice. *Hepatology*, 38(1): 123-132.

Ip, E., Farrell, G., Hall, P., Robertson, G., & Leclercq, I. 2004. Administration of the potent PPARalpha agonist, Wy-14,643, reverses nutritional fibrosis and steatohepatitis in mice. *Hepatology*, 39(5): 1286-1296.

Isibasi, A., Jimenez, E., & Kumate, J. 1983. Clearance and tissue distribution of intravenously injected Salmonella typhi polysaccharide in rabbits. *Infect Immun*, 42(3): 949-954.

Jakubowski, A., Ambrose, C., Parr, M., Lincecum, J. M., Wang, M. Z., Zheng, T. S., Browning, B., Michaelson, J. S., Baetscher, M., Baestcher, M., Wang, B., Bissell, D. M., & Burkly, L. C. 2005. TWEAK induces liver progenitor cell proliferation. *J Clin Invest*, 115(9): 2330-40.

Jamil, H., Yao, Z. M., & Vance, D. E. 1990. Feedback regulation of CTP:phosphocholine cytidylyltransferase translocation between cytosol and endoplasmic reticulum by phosphatidylcholine. *J Biol Chem*, 265(8): 4332-4339.

Jones, A., Friedrich, K., Rohm, M., Schäfer, M., Algire, C., Kulozik, P., Seibert, O., Müller-Decker, K., Sijmonsma, T., Strzoda, D., Sticht, C., Gretz, N., Dallinga-Thie, G. M., Leuchs, B., Kögl, M., Stremmel, W., Diaz, M. B., & Herzig, S. 2013. TSC22D4 is a molecular output of hepatic wasting metabolism. *EMBO Mol Med*, 5(2): 294-308.

Kawano, Y., & Cohen, D. E. 2013. Mechanisms of hepatic triglyceride accumulation in non-alcoholic fatty liver disease. *J Gastroenterol*. 48(4): 434-441

Kenan, D. J., Query, C. C., & Keene, J. D. 1991. RNA recognition: towards identifying determinants of specificity. *Trends Biochem Sci*, 16(6): 214-220.

Kessler, S. M., Pokorny, J., Zimmer, V., Laggai, S., Lammert, F., Bohle, R. M., & Kiemer, A. K. 2013. IGF2 mRNA binding protein p62/IMP2-2 in hepatocellular carcinoma: antiapoptotic action is independent of IGF2/PI3K signaling. *Am J Physiol Gastrointest Liver Physiol*, 4(304): G328-G336.

Kirsch, R., Clarkson, V., Shephard, E. G., Marais, D. A., Jaffer, M. A., Woodburne, V. E., Kirsch, R. E., & Hall, P. D. L. M. 2003. Rodent nutritional model of non-alcoholic steatohepatitis: species, strain and sex difference studies. *J Gastroenterol Hepatol*, 18(11): 1272-1282.

Kistner, A., Gossen, M., Zimmermann, F., Jerecic, J., Ullmer, C., Lübbert, H., & Bujard, H. 1996. Doxycycline-mediated quantitative and tissue-specific control of gene expression in transgenic mice. *Proc Natl Acad Sci U S A*, 93(20): 10933-10938.

Kleiner, D. E., Brunt, E. M., Van Natta, M., Behling, C., Contos, M. J., Cummings, O. W., Ferrell, L. D., Liu, Y.-C., Torbenson, M. S., Unalp-Arida, A., Yeh, M., McCullough, A. J., & Sanyal, A. J. 2005. Design and validation of a histological scoring system for nonalcoholic fatty liver disease. *Hepatology*, 41(6): 1313-21.

Konopelska, S., Kienitz, T., & Quinkler, M. 2011. Downregulation of hepatic glucose-6-phosphatase-α in patients with hepatic steatosis. *Obesity*, 19(12): 2322-6.

Koruk, M., Savaş, M. C., Yilmaz, O., Tayşi, S., Karakok, M., Gündoğdu, C., & Yilmaz, A. 2003. Serum lipids, lipoproteins and apolipoproteins levels in patients with nonalcoholic steatohepatitis. *J Hum Hypertens*, 9(2): 177-182.

Koteish, A., & Diehl, A. M. 2001. Animal models of steatosis. *Semin Liver Dis*, 21(1): 89-104.

Kramer, B. A., Lemckert, F. A., Alexander, I. E., Gunning, P. W., & McCowage, G. B. 2006. Characterisation of a P140K mutant O6-methylguanine-DNA-methyltransferase (MGMT)-expressing transgenic mouse line with drug-selectable bone marrow. *J Gene Med*, 8(9): 1071-85.

Laggai S., Simon Y., Ranssweiler T., Kiemer A. K., & Kessler S. M. 2013. Rapid chromatographic method to decipher distinct alterations in lipid classes in NAFLD and NASH. *World J Hepatol. in revision*

Larter, C. Z., Yeh, M. M., Haigh, W. G., Williams, J., Brown, S., Bell-Anderson, K. S., Lee, S. P., & Farrell, G. C. 2008. Hepatic free fatty acids accumulate in experimental steatohepatitis: role of adaptive pathways. *J Hepatol*, 48(4): 638-647.

Leclercq, I. A., Farrell, G. C., Field, J., Bell, D. R., Gonzalez, F. J., & Robertson, G. R. 2000. CYP2E1 and CYP4A as microsomal catalysts of lipid peroxides in murine nonalcoholic steatohepatitis. *J Clin Invest*, 105(8): 1067-1075.

Leclercq, I. A., Farrell, G. C., Sempoux, C., Horsmans, Y., & Pen, A. 2004. Curcumin inhibits NF-kB activation and reduces the severity of experimental steatohepatitis in mice. *J Hepatol*, 41(6): 926-934.

Lee, P., Peng, H., Gelbart, T., Wang, L., & Beutler, E. 2005. Regulation of hepcidin transcription by interleukin-1 and interleukin-6. *Proc Natl Acad Sci U S A*, 102(6): 1906-10.

Leroux, A., Ferrere, G., Godie, V., Cailleux, F., Renoud, M.-L., Gaudin, F., Naveau, S., Prévot, S., Makhzami, S., Perlemuter, G., & Cassard-Doulcier, A.-M. 2012. Toxic lipids stored by Kupffer cells correlates with their pro-inflammatory phenotype at an early stage of steatohepatitis. *J Hepatol*, 57(1): 141-9.

Li, J., Wang, L. J., Ying, X., Han, S. X., Bai, E., Zhang, Y., & Zhu, Q. 2012. Immunodiagnostic value of combined detection of autoantibodies to tumor-associated antigens as biomarkers in pancreatic cancer. *Scand J Immunol*, 75(3): 342-9.

Libbrecht, L., & Roskams, T. 2002. Hepatic progenitor cells in human liver diseases. *Semin Cell Dev Biol*, 13(6): 389-396.

Liu, W., Li, Z., Xu, W., Wang, Q., & Yang, S. 2013. Humoral autoimmune response to IGF2 mRNA-binding protein (IMP2/p62) and its tissue-specific expression in colon cancer. *Scand J Immunol*, 77(4): 255-60.

Liu, W., Peng, B., Lu, Y., Xu, W., Qian, W., & Zhang, J.-Y. 2011a. Autoantibodies to tumor-associated antigens as biomarkers in cancer immunodiagnosis. *Autoimmun Rev*, 10(6): 331-5.

Liu, Y., Meyer, C., Müller, A., Herweck, F., Li, Q., Müllenbach, R., Mertens, P. R., Dooley, S., & Weng, H.-L. 2011b. IL-13 Induces Connective Tissue Growth Factor in Rat Hepatic Stellate Cells via TGF-beta-Independent Smad Signaling. *J Immunol*, 187(5): 2814-2823.

Lu, M., Nakamura, R. M., Dent, E. D., Zhang, J.-Y., Nielsen, F. C., Christiansen, J., Chan, E. K. L., & Tan, E. M. 2001. Aberrant expression of fetal RNA-binding protein p62 in liver cancer and liver cirrhosis. *Am J Pathol*, 159(3): 945-953.

Ludwig, J., Viggiano, T. R., McGill, D. B., & Oh, B. J. 1980. Nonalcoholic steatohepatitis: Mayo Clinic experiences with a hitherto unnamed disease. *Mayo Clin Proc*, 55(7): 434-438.

Mandard, S., Müller, M., & Kersten, S. 2004. Peroxisome proliferator-activated receptor alpha target genes. *Cell Mol Life Sci*, 61(4): 393-416.

Marchesini, G., Bugianesi, E., Forlani, G., Cerrelli, F., Lenzi, M., Manini, R., Natale, S., Vanni, E., Villanova, N., Melchionda, N., & Rizzetto, M. 2003. Nonalcoholic fatty liver, steatohepatitis, and the metabolic syndrome. *Hepatology*, 37(4): 917-23.

Martin, D. I., & Whitelaw, E. 1996. The vagaries of variegating transgenes. *Bioessays*, 18(11): 919-23.

Matsuzaka, T., Atsumi, A., Matsumori, R., et al. 2012. Elovl6 promotes nonalcoholic steatohepatitis. *Hepatology*, 56(6): 2199-208.

McKenzie, A. N., Culpepper, J. A., De Waal Malefyt, R., Brière, F., Punnonen, J., Aversa, G., Sato, A., Dang, W., Cocks, B. G., & Menon, S. 1993. Interleukin 13, a T-cell-derived cytokine that regulates human monocyte and B-cell function. *Proc Natl Acad Sci U S A*, 90(8): 3735-3739.

Micsenyi, A., Tan, X., Sneddon, T., Luo, J.-H., Michalopoulos, G. K., & Monga, S. P. S. 2004. Beta-catenin is temporally regulated during normal liver development. *Gastroenterology*, 126(4): 1134-1146.

Milić, S., & Stimac, D. 2012. Nonalcoholic fatty liver disease/steatohepatitis: epidemiology, pathogenesis, clinical presentation and treatment. *Dig Dis*, 30(2): 158-62.

Mims, M. P., & Prchal, J. T. 2005. Divalent metal transporter 1. *Hematology*, 10(4): 339-45.

Min, H.-K., Kapoor, A., Fuchs, M., Mirshahi, F., Zhou, H., Maher, J., Kellum, J., Warnick, R., Contos, M. J., & Sanyal, A. J. 2012. Increased Hepatic Synthesis and Dysregulation of Cholesterol Metabolism Is Associated with the Severity of Nonalcoholic Fatty Liver Disease. *Cell Metab*, 15(5): 665-74.

Mitsui, H., Takuwa, N., Maruyama, T., Maekawa, H., Hirayama, M., Sawatari, T., Hashimoto, N., Takuwa, Y., & Kimura, S. 2001. The MEK1-ERK map kinase pathway and the PI 3-kinase-Akt pathway independently mediate anti-apoptotic signals in HepG2 liver cancer cells. *Int J Cancer*, 92(1): 55-62.

Mittal, S., & El-Serag, H. B. 2013. Epidemiology of Hepatocellular Carcinoma: Consider the Population. *J Clin Gastroenterol*, 47: S2-S6.

Miyazaki, M., Bruggink, S. M., & Ntambi, J. M. 2006. Identification of mouse palmitoyl-coenzyme A Delta9-desaturase. *J Lipid Res*, 47(4): 700-704.

Muir, K., Hazim, A., He, Y., Peyressatre, M., Kim, D.-Y., Song, X., & Beretta, L. 2013. Proteomic and Lipidomic Signatures of Lipid Metabolism in NASH-Associated Hepatocellular Carcinoma. *Cancer Res*, 73(15): 4722-31.

Musso, G., Gambino, R., & Cassader, M. 2013. Cholesterol metabolism and the pathogenesis of non-alcoholic steatohepatitis. *Prog Lipid Res*, 52(1): 175-191.

Nakamuta, M., Kohjima, M., Higuchi, N., Kato, M., Kotoh, K., Yoshimoto, T., Yada, M., Yada, R., Takemoto, R., Fukuizumi, K., Harada, N., Taketomi, A., Maehara, Y., Nakashima, M., & Enjoji, M. 2007. Re-evaluation of fatty acid metabolism-related gene expression in nonalcoholic fatty liver disease. *Int J Mol Med*, 20(3): 663-667.

Nemeth, E., Tuttle, M. S., Powelson, J., Vaughn, M. B., Donovan, A., Ward, D. M., Ganz, T., & Kaplan, J. 2004. Hepcidin regulates cellular iron efflux by binding to ferroportin and inducing its internalization. *Science*, 306(5704): 2090-3.

Neuschwander-Tetri, B. A., & Caldwell, S. H. 2003. Nonalcoholic steatohepatitis: summary of an AASLD Single Topic Conference. *Hepatology,* 37: 1202-1219.

Neyrinck, A. M., Cani, P. D., Dewulf, E. M., De Backer, F., Bindels, L. B., & Delzenne, N. M. 2009. Critical role of Kupffer cells in the management of diet-induced diabetes and obesity. *Biochem Biophys Res Commun,* 385(3): 351-356.

Nielsen, J., Christiansen, J., Lykke-Andersen, J., Johnsen, A. H., Wewer, U. M., & Nielsen, F. C. 1999. A Family of Insulin-Like Growth Factor II mRNA-Binding Proteins Represses Translation in Late Development. *Mol Cell Biol*, 19(2): 1262-1270.

Ntambi, J. M., & Miyazaki, M. 2004. Regulation of stearoyl-CoA desaturases and role in metabolism. *Prog Lipid Res*, 43(2): 91-104.

Odegaard, J. I., Ricardo-Gonzalez, R. R., Red Eagle, A., Vats, D., Morel, C. R., Goforth, M. H., Subramanian, V., Mukundan, L., Ferrante, A. W., & Chawla, A. 2008. Alternative M2 activation of Kupffer cells by PPARdelta ameliorates obesity-induced insulin resistance. *Cell Metab*, 7(6): 496-507.

Ohkawa, H., Ohishi, N., & Yagi, K. 1979. Assay for lipid peroxides in animal tissues by thiobarbituric acid reaction. *Anal Biochem*, 95(2): 351-8.

Okada, T., Furuhashi, N., Kuromori, Y., Miyashita, M., Iwata, F., & Harada, K. 2005. Plasma palmitoleic acid content and obesity in children. *Am J Clin Nutr*, 82(4): 747-750.

Paillard, F., Catheline, D., Duff, F. Le, Bouriel, M., Deugnier, Y., Pouchard, M., Daubert, J.-C., & Legrand, P. 2008. Plasma palmitoleic acid, a product of stearoyl-coA desaturase activity, is an independent marker of triglyceridemia and abdominal adiposity. *Nutr Metab Cardiovasc Dis*, 18(6): 436-440.

Park, E. J., Lee, J. H., Yu, G.-Y., He, G., Ali, S. R., Holzer, R. G., Osterreicher, C. H., Takahashi, H., & Karin, M. 2010. Dietary and genetic obesity promote liver inflammation and tumorigenesis by enhancing IL-6 and TNF expression. *Cell*, 140(2): 197-208.

Pessayre, D., Berson, A., Fromenty, B., & Mansouri, A. 2001. Mitochondria in steatohepatitis. *Semin Liver Dis*, 21(1): 57-69.

Philippe, M.-A., Ruddell, R.-G., & Ramm, G.-A. 2007. Role of iron in hepatic fibrosis: one piece in the puzzle. *World J Gastroenterol*, 13(35): 4746-4754.

Pigeon, C. 2001. Stearoyl coenzyme A desaturase 1 expression and activity are increased in the liver during iron overload. *Biochim Biophys Acta*, 1535(3): 275-284.

Powell, E. E., Cooksley, W. G., Hanson, R., Searle, J., Halliday, J. W., & Powell, L. W. 1990. The natural history of nonalcoholic steatohepatitis: a follow-up study of forty-two patients for up to 21 years. *Hepatology*, 11(1): 74-80.

Qian, H.-L., Peng, X.-X., Chen, S.-H., Ye, H.-M., & Qiu, J.-H. 2005. p62 Expression in primary carcinomas of the digestive system. *World J Gastroenterol*, 11(12): 1788-92.

Ramírez, A., Milot, E., Ponsa, I., Marcos-Gutiérrez, C., Page, A., Santos, M., Jorcano, J., & Vidal, M. 2001. Sequence and chromosomal context effects on variegated expression of keratin 5/lacZ constructs in stratified epithelia of transgenic mice. *Genetics*, 158(1): 341-350.

Razin, A., & Cedar, H. 1991. DNA methylation and gene expression. *Microbiol Mol Biol Rev*, 55(3): 451-458.

Richardson, M. M., Jonsson, J. R., Powell, E. E., Brunt, E. M., Neuschwander-Tetri, B. A., Bhathal, P. S., Dixon, J. B., Weltman, M. D., Tilg, H., Moschen, A. R., Purdie, D. M., Demetris, A. J., & Clouston, A. D. 2007. Progressive fibrosis in nonalcoholic steatohepatitis: association with altered regeneration and a ductular reaction. *Gastroenterology*, 133(1): 80-90.

Rinella, M. E., Elias, M. S., Smolak, R. R., Fu, T., Borensztajn, J., & Green, R. M. 2008. Mechanisms of hepatic steatosis in mice fed a lipogenic methionine choline-deficient diet. *J Lipid Res*, 49(5): 1068-1076.

Rinella, M. E., & Green, R. M. 2004. The methionine-choline deficient dietary model of steatohepatitis does not exhibit insulin resistance. *J Hepatol*, 40(1): 47-51.

Rivera, C. A., Adegboyega, P., van Rooijen, N., Tagalicud, A., Allman, M., & Wallace, M. 2007. Toll-like receptor-4 signaling and Kupffer cells play pivotal roles in the pathogenesis of non-alcoholic steatohepatitis. *J Hepatol*, 47(4): 571-9.

Rizki, G., Arnaboldi, L., Gabrielli, B., Yan, J., Lee, G. S., Ng, R. K., Turner, S. M., Badger, T. M., Pitas, R. E., & Maher, J. J. 2006. Mice fed a lipogenic methionine-choline-deficient diet develop hypermetabolism coincident with hepatic suppression of SCD-1. *J Lipid Res*, 47(10): 2280-2290.

Robinson, S. M., & Mann, D. A. 2010. Role of nuclear factor kappaB in liver health and disease. *Clin Sci (Lond)*, 118(12): 691-705.

Rombouts, K., & Marra, F. 2010. Molecular mechanisms of hepatic fibrosis in non-alcoholic steatohepatitis. *Dig Dis*, 28(1): 229-235.

Roskams, T., Yang, S. Q., Koteish, A., Durnez, A., DeVos, R., Huang, X., Achten, R., Verslype, C., & Diehl, A. M. 2003. Oxidative stress and oval cell accumulation in mice and humans with alcoholic and nonalcoholic fatty liver disease. *Am J Pathol*, 163(4): 1301-11.

Rosmorduc, O., & Fartoux, L. 2012. HCC and NASH: how strong is the clinical demonstration? *Clin Res Hepatol Gastroenterol*, 36(3): 202-8.

Saito, R., Matsuzaka, T., Karasawa, T., Sekiya, M., Okada, N., Igarashi, M., Matsumori, R., Ishii, K., Nakagawa, Y., Iwasaki, H., Kobayashi, K., Yatoh, S., Takahashi, A., Sone, H., Suzuki, H., Yahagi, N., Yamada, N., & Shimano, H. 2011. Macrophage Elovl6 deficiency ameliorates foam cell formation and reduces atherosclerosis in low-density lipoprotein receptor-deficient mice. *Arterioscler Thromb Vasc Biol*, 31(9): 1973-9.

Schönig, K., Bujard, H., & Gossen, M. 2010. The power of reversibility regulating gene activities via tetracycline-controlled transcription. *Methods Enzymol*, 477(10): 429-453.

Seki, S., Kitada, T., Yamada, T., Sakaguchi, H., Nakatani, K., & Wakasa, K. 2002. In situ detection of lipid peroxidation and oxidative DNA damage in non-alcoholic fatty liver diseases. *J Hepatol*, 37(1): 56-62.

Serova, I. A., Andreeva, L. E., Khaidarova, N. V., Dias, L. P. B., Dvoryanchikov, G. A., Burkov, I. A., & Baginskaya, N. V. 2009. Mosaic expression of LacZ reporter gene controlled by 5′-regulatory sequences of alpha-S 1-Casein gene in transgenic mice. *Cell Tissue Biol*, 3(5): 409-416.

Sharif, K. A., Baker, H., & Gudas, L. J. 2004. Differential regulation of laminin b1 transgene expression in the neonatal and adult mouse brain. *Neuroscience*, 126(4): 967-78.

Shimamura, T., Fujisawa, T., Husain, S. R., Kioi, M., Nakajima, A., & Puri, R. K. 2008. Novel role of IL-13 in fibrosis induced by nonalcoholic steatohepatitis and its amelioration by IL-13R-directed cytotoxin in a rat model. *J Immunol*, 181(7): 4656-4665.

Sidossis, L. S., Stuart, C. A., Shulman, G. I., Lopaschuk, G. D., & Wolfe, R. R. 1996. Glucose plus insulin regulate fat oxidation by controlling the rate of fatty acid entry into the mitochondria. *J Clin Invest*, 98(10): 2244-2250.

Smits, M. M., Ioannou. G. N., Boyko. E. J., & Utzschneider. K. M. 2013. Non-alcoholic fatty liver disease as an independent manifestation of the metabolic syndrome: Results of a US national survey in three ethnic groups. *J Gastroenterol Hepatol*, 28 (4): 664-670.

Sorrentino, P., D'Angelo, S., Ferbo, U., Micheli, P., Bracigliano, A., & Vecchione, R. 2009. Liver iron excess in patients with hepatocellular carcinoma developed on non-alcoholic steato-hepatitis. *J Hepatol*, 50(2): 351-357.

Starley, B. Q., Calcagno, C. J., & Harrison, S. A. 2010. Nonalcoholic fatty liver disease and hepatocellular carcinoma: a weighty connection. *Hepatology*, 51(5): 1820-1832.

Stickel, F., & Hellerbrand, C. 2010. Non-alcoholic fatty liver disease as a risk factor for hepatocellular carcinoma: mechanisms and implications. *Gut*, 59(10): 1303-1307.

Stienstra, R., Saudale, F., Duval, C., Keshtkar, S., Groener, J. E. M., Van Rooijen, N., Staels, B., Kersten, S., & Müller, M. 2010. Kupffer cells promote hepatic steatosis via interleukin-1beta-dependent suppression of peroxisome proliferator-activated receptor alpha activity. *Hepatology*, 51(2): 511-522.

Struben, V. M., Hespenheide, E. E., & Caldwell, S. H. 2000. Nonalcoholic steatohepatitis and cryptogenic cirrhosis within kindreds. *Am J Med*, 108(1): 9-13.

Su, Y., Qian, H., Zhang, J., Wang, S., Shi, P., & Peng, X. 2005. The diversity expression of p62 in digestive system cancers. *Clin Immunol*, 116(2): 118-23.

Szabo, G., & Csak, T. 2012. Inflammasomes in liver diseases. *Journal of Hepatology*, 57(3): 642-654.

Taylor, P. R., Martinez-Pomares, L., Stacey, M., Lin, H.-H., Brown, G. D., & Gordon, S. 2005. Macrophage receptors and immune recognition. *Annu Rev Immunol*, 23(1): 901-944.

Teli, M. R., James, O. F., Burt, A. D., Bennett, M. K., & Day, C. P. 1995. The natural history of nonalcoholic fatty liver: a follow-up study. *Hepatology*, 22(6): 1714-1719.

Tilg, H. 2010. The role of cytokines in non-alcoholic fatty liver disease. *Dig Dis*, 28(1): 179-85.

Tomita, K., Tamiya, G., Ando, S., et al. 2006. Tumour necrosis factor alpha signalling through activation of Kupffer cells plays an essential role in liver fibrosis of non-alcoholic steatohepatitis in mice. *Gut*, 55(3): 415-424.

Tschopp, J., & Schroder, K. 2010. NLRP3 inflammasome activation: The convergence of multiple signalling pathways on ROS production? *Nat Rev Immunol*, 10(3): 210-215.

Tybl, E., Shi, F.-D., Kessler, S. M., Tierling, S., Walter, J., Bohle, R. M., Wieland, S., Zhang, J., Tan, E. M., & Kiemer, A. K. 2011. Overexpression of the IGF2-mRNA binding protein p62 in transgenic mice induces a steatotic phenotype. *J Hepatol*, 54(5): 994-1001.

Van Der Poorten, D., Samer, C., Ramezani-Moghadam, M., Coulter, S., Kacevska, M., Schrijnders, D., Wu, L., McLeod, D., Bugianesi, E., Komuta, M., Roskams, T., Liddle, C., Hebbard, L., & George, J. 2013. Hepatic fat loss in advanced nash: Are alterations in serum adiponectin the cause? *Hepatology,* 57(6): 2180-2188.

Van Rooijen, N., & Hendrikx, E. 2010. Liposomes for specific depletion of macrophages from organs and tissues. *Methods Mol Biol*, 605: 189-203.

Van Rooijen, N., Sanders, A., & van den Berg, T. K. 1996. Apoptosis of macrophages induced by liposome-mediated intracellular delivery of clodronate and propamidine. *J Immunol Methods*, 193(1): 93-99.

Van Rooijen, N., Van Nieuwmegen, R., & Kamperdijk, E. W. 1985. Elimination of phagocytic cells in the spleen after intravenous injection of liposome-encapsulated dichloromethylene diphosphonate. Ultrastructural aspects of elimination of marginal zone macrophages. *Cell Tissue Res*, 49(2): 355-358.

Van Thiel, D. H., & Ramadori, G. 2011. Non-Viral Causes of Hepatocellular Carcinoma. *J Gastrointest Cancer*, 42(4): 191-194.

Vance, J. E., & Vance, D. E. 1985. The role of phosphatidylcholine biosynthesis in the secretion of lipoproteins from hepatocytes. *Can J Biochem Cell Biol*, 63(8): 870-881.

Vernon, G., Baranova, A., & Younossi, Z. M. 2011. Systematic review: the epidemiology and natural history of non-alcoholic fatty liver disease and non-alcoholic steatohepatitis in adults. *Aliment Pharmacol Ther*, 34(3): 274-285.

Villanueva, A., Chiang, D. Y., Newell, P., et al. 2008. Pivotal role of mTOR signaling in hepatocellular carcinoma. *Sheng Li Ke Xue Jin Zhan*, 135(6): 1972-1983, 1983.e1-e11.

Vinciguerra, M., Sgroi, A., Veyrat-Durebex, C., Rubbia-Brandt, L., Buhler, L. H., & Foti, M. 2009. Unsaturated fatty acids inhibit the expression of tumor suppressor phosphatase and tensin homolog (PTEN) via microRNA-21 up-regulation in hepatocytes. *Hepatology*, 49(4): 1176-1184.

Vinciguerra, M., Veyrat-Durebex, C., Moukil, M. A., Rubbia-Brandt, L., Rohner-Jeanrenaud, F., & Foti, M. 2008. PTEN down-regulation by unsaturated fatty acids triggers hepatic steatosis via an NF-kappaBp65/mTOR-dependent mechanism. *Gastroenterology*, 134(1): 268-280.

Wang, J., Chen, G., & Pantopoulos, K. 2005a. Inhibition of transferrin receptor 1 transcription by a cell density response element. *Biochem J*, 392(Pt 2): 383-8.

Wang, R.-H., Li, C., Xu, X., Zheng, Y., Xiao, C., Zerfas, P., Cooperman, S., Eckhaus, M., Rouault, T., Mishra, L., & Deng, C.-X. 2005b. A role of SMAD4 in iron metabolism through the positive regulation of hepcidin expression. *Cell Metab,* 2(6): 399-409.

Wasmuth, H. E., Zaldivar, M. M., Beraza, N., & Trautwein, C. 2007. Of mice and NASH - from fat to inflammation and fibrosis. *Drug Discov Today Dis Models*, 4(1): 25-30.

Watanabe, S., Horie, Y., & Suzuki, A. 2005. Hepatocyte-specific Pten-deficient mice as a novel model for nonalcoholic steatohepatitis and hepatocellular carcinoma. *Hepatol Res*, 33(2): 161-166.

Weltman, M. D., Farrell, G. C., & Liddle, C. 1996. Increased hepatocyte CYP2E1 expression in a rat nutritional model of hepatic steatosis with inflammation. *Gastroenterology*, 111(6): 1645-1653.

Weng, H.-L., Liu, Y., Chen, J.-L., Huang, T., Xu, L.-J., Godoy, P., Hu, J.-H., Zhou, C., Stickel, F., Marx, A., Bohle, R. M., Zimmer, V., Lammert, F., Mueller, S., Gigou, M., Samuel, D., Mertens, P. R., Singer, M. V, Seitz, H. K., & Dooley, S. 2009. The etiology of liver damage imparts cytokines transforming growth factor beta1 or interleukin-13 as driving forces in fibrogenesis. *Hepatology*, 50(1): 230-43.

Wynn, T. A. 2004. Fibrotic disease and the TH1/TH2 paradigm. *Nat Rev Immunol*, 4(8): 583-594.

Wynn, T. A., Chawla, A., & Pollard, J. W. 2013. Macrophage biology in development, homeostasis and disease. *Nature*, 496(7446): 445-55.

Yamazaki, Y., Kakizaki, S., Takizawa, D., Ichikawa, T., Sato, K., Takagi, H., & Mori, M. 2008. Interstrain differences in susceptibility to non-alcoholic steatohepatitis. *J Gastroenterol Hepatol*, 23(2): 276-282.

Yang, S., Koteish, A., Lin, H., Huang, J., Roskams, T., Dawson, V., & Diehl, A. M. 2004. Oval cells compensate for damage and replicative senescence of mature hepatocytes in mice with fatty liver disease. *Hepatology*, 39(2): 403-411.

Yang, S. Q., Lin, H. Z., Lane, M. D., Clemens, M., & Diehl, A. M. 1997. Obesity increases sensitivity to endotoxin liver injury: Implications for the pathogenesis of steatohepatitis. *Proc Natl Acad Sci U S A*, 94(6): 2557-2562.

Yao, Z. M., & Vance, D. E. 1988. The active synthesis of phosphatidylcholine is required for very low density lipoprotein secretion from rat hepatocytes. *J Biol Chem*, 263(6): 2998-3004.

Yesilova, Z., Yaman, H., Oktenli, C., Ozcan, A., Uygun, A., Cakir, E., Sanisoglu, S. Y., Erdil, A., Ates, Y., Aslan, M., Musabak, U., Erbil, M. K., Karaeren, N., & Dagalp, K. 2005. Systemic markers of lipid peroxidation and antioxidants in patients with nonalcoholic Fatty liver disease. *Am J Gastroenterol*, 100(4): 850-855.

Yilmaz, Y. 2012. Review article: is non-alcoholic fatty liver disease a spectrum, or are steatosis and non-alcoholic steatohepatitis distinct conditions? *Aliment Pharmacol Ther*, 36(9): 815-23.

Yoshimura, A., Naka, T., & Kubo, M. 2007. SOCS proteins, cytokine signalling and immune regulation. *Nat Rev Immunol*, 7(6): 454-465.

Zhang, J., & Chan, E. K. L. 2002. Autoantibodies to IGF-II mRNA binding protein p62 and overexpression of p62 in human hepatocellular carcinoma. *Autoimmun Rev*, 1(3): 146-53.

Zhang, J. Y., Zhu, W., Imai, H., Kiyosawa, K., Chan, E. K. L., & Tan, E. M. 2001. De-novo humoral immune responses to cancer-associated autoantigens during transition from chronic liver disease to hepatocellular carcinoma. *Clin Exp Immunol*, 125(1): 3-9.

Zhang, J.-Y., Chan, E. K. L., Peng, X.-X., & Tan, E. M. 1999. A Novel Cytoplasmic Protein with RNA-binding Motifs Is an Autoantigen in Human Hepatocellular Carcinoma. *J Exp Med*, 189(7): 1101-1110.

CURRICULUM VITAE

Research experience

since 06/2010 — Ph.D. research work, Department of Pharmaceutical Biology, Group Prof. Dr. A.K. Kiemer, Saarland University, Germany

05/2008 - 06/2008 — Internship, Department of Pharmaceutical Biotechnology, Saarland University, Germany "Gene knockout experiments in *M.xanthus* DK1622"

International research experience

05/2009 - 11/2009 — Diploma in Pharmacy, University of New South Wales, Sydney, Australia in cooperation with the Department of Pharmaceutical Biotechnology, Saarland University, Germany "Isolation of secondary metabolites from marine bacteria and decoding of parts from new gene clusters"

04/2007 - 08/2007 — Erasmus Student exchange, School of Biosciences, Biocatalysis Centre, University of Exeter, Great Britain "Purification of *Pseudomonas putida* 2,5-diketocamphane 1,2-monooxygenase and purification and crystallisation of MsuE"

Professional experience

12/2009 - 05/2010 — Pharmacist, Brunnen-Apotheke, Homburg Saar, Germany

10/2008 - 04/2009 — Internship at Burg-Apotheke, Kirkel, Germany

Education

University Education

11/2009 — Licensed pharmacist (Pharm D, Approbation)

06/2010 — Diploma in Pharmacy

2004 - 2009 — Study of Pharmacy at Saarland University, Germany

PUBLICATIONS

Original publication

Simon Y, Kessler SM, Bohle RM, Haybaeck J, Kiemer AK. The insulin-like growth factor 2 (*IGF2*) mRNA binding protein p62/IGF2BP2-2 as a promoter of NAFLD and HCC? 2013; *Gut*; doi:10.1136/gutjnl-2013-305736

Laggai S, **Simon Y**, Ranssweiler T, Kiemer AK, Kessler SM. Rapid chromatographic method to decipher distinct alterations in lipid classes in NAFLD and NASH. 2013; *World Journal of Hepatology*; *in revision*

Simon Y, Kessler SM, Gemperlein K, Bohle RM, Müller R, Haybaeck J, Kiemer AK. Elevated production of free cholesterol as a hallmark of NASH in p62/IGF2BP2-2 transgenic animals. 2013; *submitted*

Abstracts to poster presentation

Simon Y, Kessler SM, Van Rooijen N, Haybaeck J, Kiemer AK. The insulin-like growth factor 2 (*IGF2*) mRNA binding protein (IMP) p62 accelerates steatosis, inflammation and fibrosis in a dietary model of non-alcoholic steatohepatits. Poster and ePoster presentation at the International Liver Congress 2013 by EASL (48th annual meeting), Amsterdam, Netherlands, *Journal of Hepatology* 2013, 58 Suppl. TOP 10% best abstracts

Kessler SM, **Simon Y**, Kiemer AK. The insulin-like growth factor 2 (IGF2) mRNA binding protein (IMP) p62 promotes an inflammatory response in mouse models of early hepatocarcinogenesis and steatohepatitis. Poster presentation at The Liver Meeting 2011 by AASLD (62nd annual meeting), San Francisco, USA, *Hepatology* 2011; 54 Suppl.

Scholarship

04/2013 EASL Young Investigator´s Full Bursary for the International Liver Congress™ 2013, in Amsterdam, The Netherlands, April 24-28, 2013 offered by BMS, Gliead, MSD and Roche

ACKNOWLEDGMENTS

Und zum Schluss das wohl schwierigste Kapitel: Meine Danksagung!

Zu aller erst möchte ich mich bei **Frau Prof. Alexandra K. Kiemer** für die Möglichkeit bedanken, mit diesem interessanten Thema in ihrer Arbeitsgruppe zu promovieren. Ausdrücklich möchte ich mich für ihr Interesse, Engagement und das entgegengebrachte Vertrauen bedanken. Die fast immer „offene Tür“ zu ihrem Büro hat es ermöglicht, dass viele interessante Diskussionen und Anregungen den Fortschritt meiner Arbeit entscheidend vorangetrieben haben und aus mir eine „echte“ Wissenschaftlerin geworden ist.

Mein besonderer Dank gilt **Herrn Prof. Johannes Haybäck** von der Medizinischen Universität Graz für die Übernahme des Koreferats dieser Arbeit. Insbesondere möchte ich ihm danken, dass er die lange Reise aus Graz auf sich genommen hat, um als Mitglied der Prüfungskommission bei meinem Promotionskolloquium anwesend zu sein und des Weiteren für das schnelle Scoring meiner Leberschnitte, ohne welches ich diese Zeilen wohl noch nicht schreiben könnte.

Herzlich bedanken möchte ich mich bei **Herrn Prof. Claus-Michael Lehr** für die Übernahme des Prüfungsvorsitzes und **Herrn Dr. Matthias Engel** für die Teilnahme als wissenschaftlicher Mitarbeiter in der Prüfungskommission.

Ein ganz fettes Merci geht an meine Betreuerin, **Dr. Sonja M. Kessler**. Ohne sie wäre die Zeit wohl nur halb so toll gewesen. Sie war stets Ansprechpartnerin für alle Belangen, hatte immer einen guten Rat, hat mir bei der einen oder anderen Rechenaufgabe geholfen ;-), hat mich mit der Zellkultur vertraut gemacht und hat nicht zuletzt zusammen mit Herrn Prof. Haybäck die Schnitte gescored. Aber auch die tolle Zusammenarbeit im Mausstall und die unzähligen Korrektur-Lese-Aktionen sollen nicht ungedankt bleiben. Zuletzt bin ich total glücklich, dass aus der guten Zusammenarbeit eine echte Freundschaft entstanden ist. Vielen Dank, Sonja!

Dann möchte ich mich bei meinen Laborpartnern und Leidensgenossen **Rebecca Hahn** und **Stephan Laggai** für die tolle Zusammenarbeit hier im Institut bedanken. Es war eine schöne, abwechslungsreiche und lehrreiche Zeit, die wir schon seit dem 1. Semester des Pharmazie-Studiums gemeinsam verbracht haben.

Bei unserer Tierpflegerin **Eva Dilly** möchte ich mich für die tolle gemeinsame Zeit im Mausstall bedanken. Durch sie habe ich gelernt, gut und sicher mit den Mäusen umzugehen.

Nadja Chomy verdanke ich, dass ich heute in der Lage bin, „echt schöne“ Schnitte am Mikrotom zu schneiden. Sie hat mir Tipps und Tricks gezeigt und mir auch das ein oder andere Mal am Mikrotom unter die Arme gegriffen.

Die vielen schönen bunten mikroskopischen Bilder verdanke ich **Christina Guth** vom INM. Danke, dass ich immer so spontan vorbeikommen konnte!

Bei **Herr Prof. Rolf Müller** und **Katja Gemperlein** möchte ich mich für die Durchführung der GC-MS Messungen bedanken.

Dr. Zapp, Dr. Britta Diesel und **Dr. Ksenia Astanina** möchte ich für die tolle Zusammenarbeit und gemeinsame Zeit danken. **Dr. Jessica Hoppstädter** gilt mein Dank für ihre stete Hilfe bei der Rechnerei ;-) aber auch für das ein oder andere Gespräch vor der Tür mit oder ohne einem Gläschen Sekt! Danke auch an **Susanne Schütz**, die als neue Azubine eine klasse Arbeit macht.

Den Newbies im Doktoranten-Business **Christina Schultheiß** und **Nina Hachenthal** danke ich für die schöne gemeinsame Zeit. Macht so weiter und behaltet eure gute Laune bei! Es macht echt Spaß mit euch! ;-)

Ein Labor würde nicht funktionieren ohne erstklassiges technisches Personal und da geht’s uns echt gut: **Herr Schneider** als PC-Experte, **Klaus Gladel** mit dem wohl besten „grünen Daumen“ (Danke nochmal für die In-Pflege-Nahme meines Kaffeebaums), der Mann im Gelben Trikot, **Theo Ranssweiler**, den man immer um Hilfe fragen kann und natürlich unsere gute **Astrid Decker**, denn wer sonst kennt

sich mit dem universitären Bürokratie-Latein besser aus? Ohne sie wäre ich ein manches Mal aufgeschmissen gewesen.

Ein ganz großes Dankeschön gebührt auch meinen Freunden, denen ich es zu verdanken habe, an den Wochenenden und Abenden die Arbeit einmal komplett vergessen zu können. Um einige zu nennen: Sarah, meine langjährige beste Freundin, die trotz der Entfernung immer für mich da war und ist, die „Alte Forsthaus-Crew um Freed und Frank, mit denen ich schon seit jüngsten Jahren eine tolle Freundschaft verbinde, Markus und Tina mit ihren wunderbaren Kindern, Paul und Lena, die Mittwochs-Squash und Beachvolleyball-Gruppe, Babsi und Flo, Nadine und Christoph, und und und… auch alle, die ich jetzt nicht namentlich erwähne, sind ein Teil meines Lebens geworden, ohne sie wäre es nicht so toll, wie es jetzt ist!

Mein größter Dank gilt meiner Familie, die mich zu dem geformt hat, was ich heute bin: Meine Oma und mein Opa, die wie Eltern für mich waren; mein Bruder Jan-Hendrik, mit dem ich so manche turbulente Zeit hatte, aber im Endeffekt haben wir immer wie Pech und Schwefel zusammengehalten; und meine Mama, DIE ALLERBESTE: Sie hat immer an mich geglaubt und hat mich immer mit allem unterstützt, was in ihrer Macht stand. Gemeinsam haben wir ein dunkles Kapitel überstanden und sind richtig dicke Freundinnen geworden.

Zum guten Schluss gilt mein Dank meiner großen Liebe - Pit. In den vergangen Jahren hast Du mir mit Deiner tollen, so unglaublich positiven Art gezeigt, wie das Leben leichter zu bewältigen ist. Dank Dir war jede Hürde wie eine kleine Bodenwelle und trotz der Fernbeziehung hat es sich angefühlt, als wärst Du immer bei mir gewesen. Ich danke Dir aus tiefsten Herzen für Deine Liebe und kann es nun kaum erwarten, den nächsten Schritt mit Dir in eine gemeinsame Zukunft zu gehen. Ich liebe Dich.